Wind loading of STS cranes

Investigating improved calculation methods

F.L.A. Rasch

Technische Universiteit Delft

TU Delft

Wind loading of STS cranes

Investigating improved calculation methods

by

T.L.A. Rasch

to obtain the degree of Master of Science
at the Delft University of Technology,
to be defended publicly on Wednesday April 8, 2022 at 19:63 CET.

Report number:	2022.MME.8660	
Student number:	4028503	
Project duration:	November 1, 2021 – May 25, 2022	
Thesis committee:	dr. ir. D. Schott,	TU Delft, chair
	ir. W. van den Bos,	TU Delft, daily supervisor
	W. van Cappellen,	Kalmar Netherlands

TU Delft KALMAR

Summary

Wind loading of STS cranes is an important design parameter to be taken into account when designing STS cranes. Wind loads affect both stability of the crane as well as other design parameters such as tie down and brake forces. With ever increasing sizes of cranes, both in new construction as well as in heightening of cranes, accurate calculation of these loads is vital for both safety and cost reasons. A crane may not become unstable or unsafe, and a customer does not want to pay too much.

Based on earlier experience it was noted that standard calculations tend to overestimate wind loads on STS cranes when compared to wind tunnel models. Improving the calculations to be more accurate would be beneficial for designing safe cranes without over-engineering.

This main goal of this research is to find adaptations to current standards to more accurately calculate wind actions on STS cranes. For this wind tunnel tests and computational fluid dynamics are used to gain more insights in the aerodynamic behaviour of cranes and the elements from which the structure is made up.

To fulfil this main research goal several research subquestions have been posed to better understand this problem. Firstly it was investigated how standards work. A general common working principle was found in all standards examined. Each standard has their own interpretation of coefficients, which seem to be based on previous works. As such, the calculation methods do not differ, but the results get iteratively better.

A wind tunnel test was performed in the Open Jet Facility of the Delft University of Technology. A $\frac{1}{150}$ scale model of a STS crane was placed on a six component external balance which was mounted on a turntable to allow for a varying wind angle. The model was tested with 3 different boom configurations (down, intermediate, and up) and 3 different levels of auxiliary (non-structural) elements to investigate the influence of these parameters on the wind loading. A total of 9 different measurements were made. Additionally, smoke trace testing was performed to get qualitative insight in how air flows around the structure.

The results from the wind tunnel test were compared against the standard calculations. Standard calculations were performed for the wind tunnel model using an equivalent wind profile for direct comparison. This confirmed the suspicion that wind tunnel tests yield lower wind loads than standard calculations. However, it was also noted that the aerodynamic load on cranes is biggest at angles which deviate from the right angles typically used in standard calculations. Recognising this behaviour it was found that a difference in wind loads is still present, but smaller than initially thought.

To understand this difference, the use of computational fluid dynamics was explored. Whilst CFD is heavily used in other industries, use of CFD for calculating wind loads on STS cranes is quite novel. Simulations performed showed promising results which were in agreement with the wind tunnel tests.

Using CFD, wind loads per-part were investigated. It was found that shielded elements (i.e., elements placed behind another element) were subjected to lower loads than assumed in standard calculations. This held true for both configurations calculated with standard calculations as well as a third case near the wind angle where wind loads are maximum. Visualisation of the flow around the crane structure as well as evaluation of surface pressure gave better understanding in the principle of shielding. It was found that elements are not only influence by elements in longitudinal direction, but also in lateral direction finding, which is currently unaccounted for in standards.

Ultimately circling back to the main research goal of finding an adaptation to current standards to more accurately calculate wind actions on STS cranes, no such adaptation is proposed. Several recommendations were made which can serve as leads to develop such adaptations and/or further research into the matter.

Samenvatting

Windbelasting van STS-kranen is een belangrijke ontwerpparameter waarmee rekening moet worden gehouden bij het ontwerpen van STS-kranen. Windbelastingen beïnvloeden zowel de stabiliteit van de kraan als andere ontwerpparameters, zoals de trek- en remkrachten. Met steeds groter wordende kranen, zowel bij nieuwbouw als bij het verhogen van kranen, is een nauwkeurige berekening van deze belastingen belangrijk, vanwege de kosten, en nog belangrijker vanwege de veiligheid.

Op basis van eerdere ervaringen werd geconstateerd dat standaarden de windbelasting op STS-kranen te overschatten in vergelijking met windtunnel modellen. Verbetering van de berekeningen door ze nauwkeuriger te maken zou gunstig zijn voor het ontwerpen van veilige kranen zonder over-engineering.

Het hoofddoel van dit onderzoek is het vinden van aanpassingen aan de huidige normen om de windwerking op STS-kranen nauwkeuriger te berekenen. Hiervoor worden windtunneltesten en numerieke stromingsleer gebruikt om meer inzicht te krijgen in het aerodynamische gedrag van kranen en de elementen waaruit de constructie is opgebouwd.

Om de hoofdvraag te beantwoorden, werden verschillende subvragen gesteld om dit probleem beter te begrijpen. Ten eerste werd onderzocht hoe normen werken. Alle onderzochte normen hadden hetzelfde werkingsprincipe, maar hebben een andere uitwerking van coefficienten. Derhalve verschillen de berekeningsmethoden niet, maar worden ze iteratief beter.

Een windtunneltest werd uitgevoerd in de Open Jet Facility van de Technische Universiteit Delft. Een $\frac{1}{150}$ schaalmodel van een STS-kraan werd op een 6-componenten externe balans geplaatst, die op een draaischijf was gemonteerd om een variërende windhoek mogelijk te maken. Het model werd getest met 3 verschillende giekconfiguraties (neer, op, stormstand) en 3 verschillende niveaus van hulpelementen (niet-structurele elementen) om de invloed van deze parameters op de windbelasting te onderzoeken. Zo zijn 9 verschillende metingen verricht. Bovendien werden rookspoortests uitgevoerd om inzicht te krijgen in hoe de lucht rond de constructie stroomt.

De resultaten van de windtunneltest zijn vergeleken met standaardberekeningen. Voor het windtunnelmodel zijn standaardberekeningen uitgevoerd met een equivalent windprofiel voor een directe vergelijking. Dit bevestigde het vermoeden dat windtunneltests lagere windbelastingen opleveren dan standaardberekeningen. Er is ook vastgesteld dat de windbelasting op kranen het grootst is bij hoeken die afwijken van de rechte hoeken die doorgaans in standaardberekeningen worden gebruikt. Dit gedrag werd onderkend en er werd vastgesteld dat er nog steeds een verschil in windbelasting is, maar kleiner dan aanvankelijk werd gedacht.

Om dit verschil te begrijpen, werd het gebruik van computationele vloeistofdynamica onderzocht. Hoewel CFD veel wordt gebruikt in andere industrieën, is het gebruik van CFD voor het berekenen van windbelastingen op STS-kranen vrij nieuw. De uitgevoerde simulaties lieten veelbelovende resultaten zien die overeenkwamen met de windtunneltests.

Met behulp van CFD werd de windbelastingen per onderdeel onderzocht. Gebleken is dat afgeschermde elementen (d.w.z. elementen die achter een ander element staan) lagere belasting ondervinden dan in standaarden wordt aangenomen. Dit gold voor beide configuraties berekend met standaardberekeningen en voor een derde geval in de buurt van de windhoek waar de windbelasting maximaal is. Visualisatie van de stroming rond de kraan, en evaluatie van de oppervlaktedruk gaven een beter inzicht in het principe van afscherming. Gezien is dat elementen elkaar niet alleen in de lengterichting beinvloeden, maar ook in de dwarsrichting, wat momenteel niet in de normen is opgenomen.

Uiteindelijk terugkerend naar het hoofddoel van het onderzoek, namelijk het vinden van een aanpassing van de huidige normen om de windbelasting op STS-kranen nauwkeuriger te berekenen, wordt een dergelijke aanpassing niet voorgesteld. Er zijn verschillende aanbevelingen gedaan die kunnen dienen als aanknopingspunten voor het ontwikkelen van dergelijke aanpassingen en/of verder onderzoek op dit gebied.

Nomenclature

β	Wind angle
Δ	Difference operator
μ	Dynamic viscosity
ν	Kinematic viscosity
ρ	Air density
θ	Rotation angle
A	Area
A_{ref}	Reference area
C_d	Coefficient of drag
CF_i	Force coefficient in direction i
CM_i	Moment coefficient about axis i
d	Characteristic length
F_i	Force in i direction
g	Gravity
H	Model height
l	Reference height
M_i	Moment about i axis
q	Dynamic pressure
q_{ref}	Reference dynamic pressure
Re	Reynolds number
St	Strouhal number
u	Velocity

List of Figures

List of Tables

Contents

1

Introduction

The history of the modern ship-to-shore gantry crane starts with the advent of containerisation in the shipping industry. Shipping containers were first introduced in the 1950's [26]. It was the Ideal-X, a converted T-2 petroleum tanker stemming from the second world war, that started a revolution. Aboard this ship were 58 truck bodies which were detached from their bodies and functionally were the first commercially successfully shipped containers [12]. The first modern ship-to-shore container crane was the PACECO (Pacific Coast Engineering Company) Container Crane, constructed in 1959 [19]. Perhaps unbeknownst in the time before colour television, the shipping container would revolutionise global trade.

Over the next few decades the world container throughput would grow steadily every year, as shown in figure 1.1.

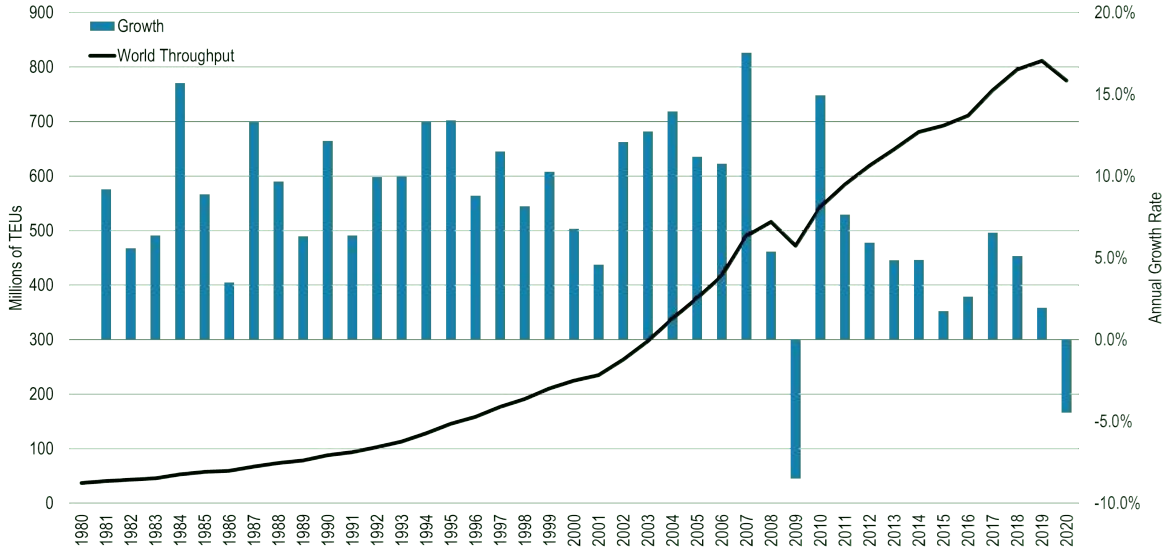

Figure 1.1: Global container throughput and growth per year 1980-2020 [28]

To keep up with our ever growing container transportation needs, container ships grew in size as well. With the first container ships not exceeding a few hundred TEU, this would prove too small facilitate such increased trade numbers. Since drag scales with the wetted surface (see the drag equation eq 2.1), and transported mass with volume, the logical way forward was to increase ship size. And increase they did. Where 12.5kTEU was once thought to be the practical upper limit for container ship size, this limit has since been surpassed and shattered [31] with container ships nearing double the capacity originally thought of as limit [21]. Evolution of the container ship size in both physical dimensions as well as capacity can be seen in figure 1.2.

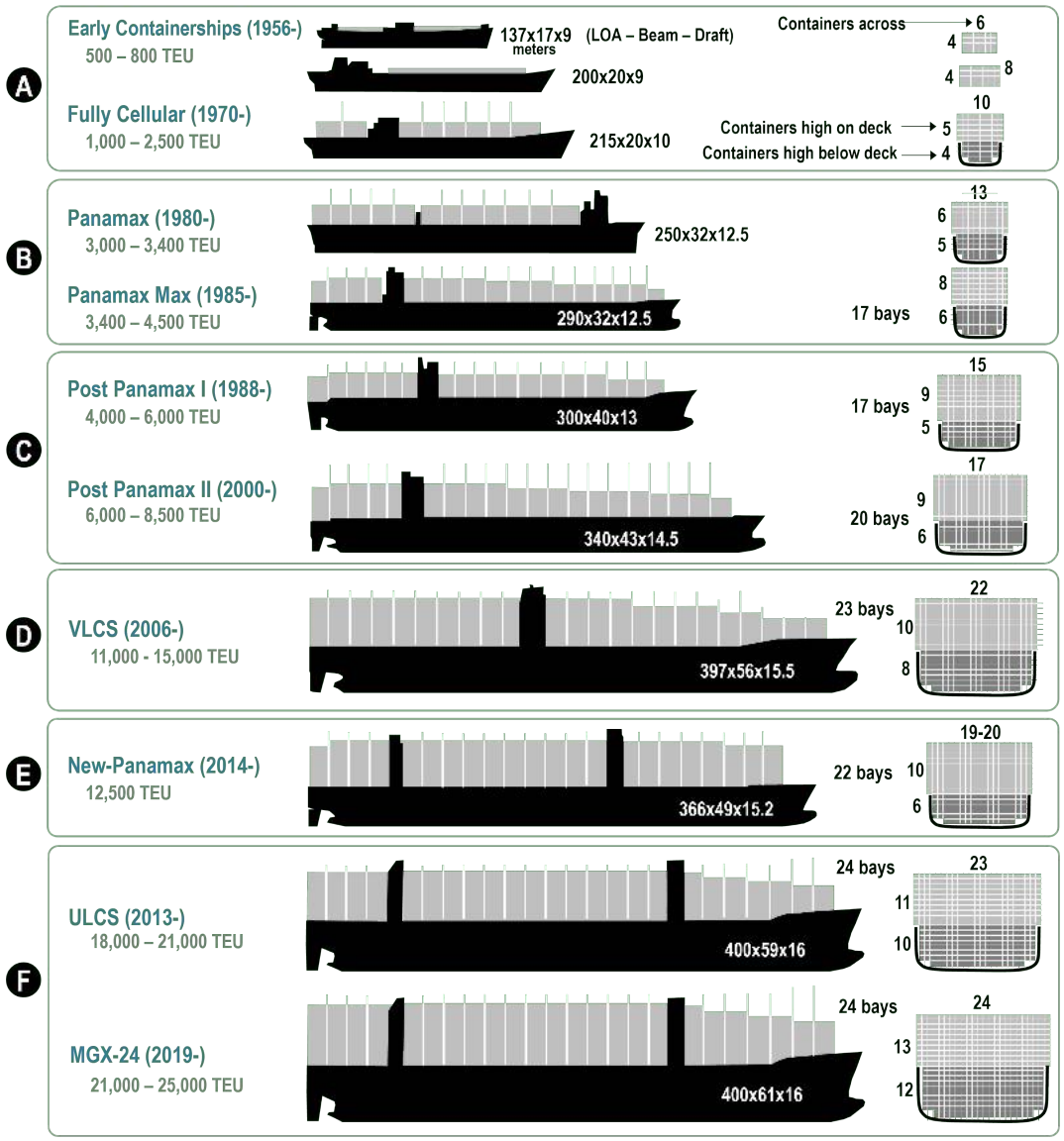

Figure 1.2: Evolution of container ships: 1956-2019 [34]

As ships and world container throughput rose, ship-to-shore cranes from days long gone were no longer enough to handle the ever increasing volume. They were too small for the boats and too slow for the volumes. As ships grew into ever bigger hulks, so did the cranes that tended them. Figure 1.3 shows this trend throughout the years 1970 to 2013. And this increase in sts crane size leads us to the problem at hand which started this research. As cranes became increasingly taller, and their booms increasingly longer, the wind actions on these cranes became ever more problematic.

Wind plays an important factor in the design stage of a sts crane. Whereas in the past, simple conservative wind calculations were sufficient to provide a safe and stable crane design, these calculation methods now put too many constraints on crane design. A need to create ever more accurate methods for calculating wind loads is a natural consequence. Cranes must become taller, lighter, more stable, and all of that at the same time.

	1970	1995	2002	2013	2018
Outreach	37	54	67	72	72
Backreach	15	20	25	25	
Lift Height +	25	38	41	52	55
Lift Height -	10	14	17	17	

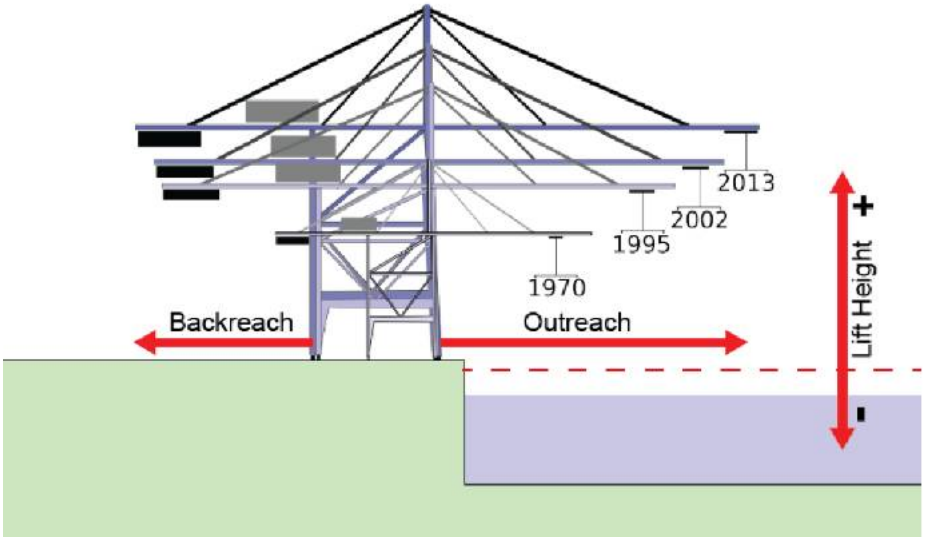

Figure 1.3: Evolution of sts crane size: 1970-2013 [33]

1.1. Research questions

The objective of the present work is to present a method for adapting current calculation standards for calculating wind loads on ship-to-shore cranes to achieve more accurate results. Where cranes are becoming ever increasingly complex feats of engineering, straddling the limits of force and stability constraints, more accurate calculation methods can be used to develop more intricate designs.

With the research objective outlined above, the following research question has been formulated to answer in this study:

How should standards for calculating wind actions on ship-to-shore cranes be adapted to achieve more accurate results with the use of wind tunnel testing and computational fluid dynamics?

To answer this research question, several supporting questions have been posed:

- What is the current state-of-the-art on wind actions on STS cranes?
  Chapter 2
- How do the different standards compare?
  - What are the calculation methods used?
  - What are the main similarities and differences?
  - How do the calculation results compare?

  Chapter 3
- How do different standards compare to wind tunnel test of a ship-to-shore crane?
  Chapter 4
- Can CFD be used to replace wind tunnel tests?
  Chapter 5
- What kind of aerodynamic characteristics can be identified for a ship-to-shore crane?
  Chapter 6
- How do auxiliary elements (e.g., staircases) influence the total wind load?
  Chapter 6

A adaptation to EN 13001-2 will be proposed in section 6.7.

1.2. Research scope

This research is bounded in its breadth and has the following initial assumptions and limitations:

- **General scope**
  - *Single crane geometry*
    For this research, a single crane geometry is considered. This limits the amount of data generated from the wind tunnel and CFD analysis.
  - *Uniform wind profile*
    The wind profile used throughout this research is a uniform wind profile. This was mainly due to wind tunnel limitations. This profile was extended to the CFD analyses to allow direct comparison between measurements.
- **Wind tunnel**
  - *Three crane configurations*
    The physical crane model was constructed in such a way that three different configurations could be set up. This allowed the examination of the influence of these configurations.

  - *Three boom configurations*
    The physical crane model had a movable boom. The effect of the boom position was examined in three typical positions.

- **Computational fluid dynamics**

  - *Single crane configuration*
    The digital crane model will only be examined in a single configuration which can be compared to the wind tunnel model.
  - *Single boom configuration*
    The digital crane model will only be examined in a single boom configuration, namely the boom down configuration.

1.3. Report structure

This report is written such that the questions posed in section 1.1 will be covered in the following chapters:

Chapter 2 - Will provide background information on the research. The current state of the art is presented which frames the research. Additionally, background information will be given on several concepts used throughout this research.

Chapter 3 - Will discuss the setup and execution of the wind tunnel tests. The scope of the wind tunnel tests, the used crane model, the testing setup and the data acquisition will be discussed.

Chapter 4 - Will discuss the setup and execution of the computational fluid dyanmics. The scope of the computational fluid dynamics, the used crane geometry, and the case setup will be discussed.

Chapter 5 - Will present the results from the wind tunnel tests, the computational fluid dynamics, and the standard calculations.

Chapter 6 - Will discuss the results presented in chapter 5. Whereas chapter 5 is intended to present the results, chapter 6 will analyse the results and provide insights into what the results mean and implicate.

Chapter 7 - Will present the conclusion of this research and offer recommendations for both practical implementation as well as further research.

2

Background

2.1. State of the art

Exploring the current state of the art is necessary to identify the working area of this investigation. This section will discuss the current state of the art for determining wind loads on sts cranes, as well as looking at other industries to find relevant literature which can be applicable to sts cranes.

Historically there have been two methods for determining wind loads on STS cranes:

1. Hand calculations according to standards.

2. Wind tunnel tests.

Standard calculations are an industry accepted method of calculating wind loads on cranes [29]. Such standards include but are not limited to: DIN1055, F.E.M. 1.004, Eurocode 1-4, EN 13001-2, among others. These standards are based on experimental studies on aerodynamic drag of crane structures and members which make up different elements [17][32].

Where calculations according to standard offer a cost effective method of determining wind loads according to a industry accepted standard, they often lack the more fine and detailed results of a wind tunnel test. Comparative studies between wind tunnel tests and standard calculations show this deficiency [16][22][43].

Wind tunnel testing offers a more refined result of the effect that wind actions have on STS cranes. Wind tunnel testing allows for evaluation of wind loading through 360 degrees of rotation [23], and in different configurations which are either difficult to calculate by or not covered in standards [10].

Recently, the use of computational fluid dynamics has showed up in the field of ship to shore cranes. A first study appeared in 2006 [3]. Whilst limited in scope and results due to computational limitations of the time, very important first steps were made. They recognised the potential of CFD in calculation of wind loads on STS cranes stating that:

"In the future, it is judged that the wind direction coefficient, which is one of the main causes of wind load, can be calculated based on the wind pressure according tot he wind direction obtained through this study." Additional studies [2][4] by the same authors noted the effect of shielding on elements in series. The conclusion of this study was not seen in any other research. However, this shielding effect was of particular interest in this study.

Since then, CFD analysis in conjecture with wind loads on cranes has been studied relatively sparsely. In 2014, a study was done on a lattice type sts crane which utilised computational fluid dynamics in conjecture with wind tunnel testing to examine the effectiveness of current standards used in quantifying wind induced loading on these detailed engineered structures [20]. Findings from that study were in agreement with those done in 2002 [10], however the conclusion was different. This study did not take into account the rotation of the wind with respect to the construction element.

In 2021 a study was conducted which focused on the application of CFD for use with STS cranes as potential alternative for wind tunnel testing [24]. Whilst this study focused and showed the feasibility of computational fluid dynamics, no comparison was made to current standards.

2.1.1. Literature gap

From the literature study, several gaps were identified:

- The effect of wind rotation on the wind forces acting on the crane
- The discrepancy between wind tunnel tests and standard calculations
- The cause of the discrepancy between wind tunnel tests and standard calculations

The research gaps found are investigated during this research. The effect of wind rotation on the wind forces acting on the crane will be investigated by means of a wind tunnel test. This wind tunnel test will also be used to verify the discrepancy between wind tunnel tests and standard calculations. Computational fluid dynamics will be used to dive deeper into the mechanisms which cause these effects as well as to gain new insights in air flow around a crane structure.

2.2. Aerodynamics

Wind loading of STS cranes is the results of aerodynamic forces. To provide context for the research which was done, the following sections contain several key principles which are behind the theory covered.

The wind load on an object is called drag and can be calculated with the drag equation (section 2.2.1). This equation is dependent on the fluid velocity, the drag coefficient (section 2.2.1, and the Reynolds number (section 2.2.2).

2.2.1. Drag

Drag is a natural phenomenon and which occurs when an object moves through a fluid. Drag is described by a mechanical force acting on this object and is the resultant of the interaction between an object and a fluid, or a fluid and a fluid. This force acts opposite to the relative motion of the object and the fluid. Drag is dependent of the relative velocity of the object and the fluid through which it moves. Drag is typically said to comprise of the form drag and the skin friction drag [6].

Drag is dependent on both the properties of the object in question and the fluid through which it moves. The relationship between these properties and drag are expressed in the drag equation 2.1. The drag equation describes the drag force as equation of the fluid velocity, air density,the reference area of an object, and the drag coefficient of the object. The drag equation is the main equation used in all standard calculations for calculating wind load on STS cranes.

$$F_d = \frac{1}{2}\rho u^2 C_d A \tag{2.1}$$

The drag coefficient is a dimensionless coefficient which describes an objects drag in a fluid. The drag coefficient is dependent on the shape of the object in question, as well as the local flow conditions. A selection of drag coefficients for 2D members (or 3D members of infinite length) can be seen in table 2.1. Drag coefficients are determined empirically from wind tunnel research. When using drag coefficients to determine a force acting on a member, it is important to verify that the drag coefficient holds true for the used flow conditions. A common way of doing this is by calculating the Reynolds number, which will be expanded upon in section 2.2.2, as well as some Reynolds number depended drag.

2.2.2. Reynolds number

The Reynolds number is a dimensionless number typically used to predict whether a flow is turbulent or laminar. Defined by the ratio of the inertial forces and viscous forces in a fluid, the Reynolds number is given by equation 2.2. The Reynolds number helps predict flow patters in different fluid flow situations, regardless of dimensions. Since the Reynolds number is dimensionless, it can also be used to achieve similar or equal flow characteristics under different geometrical dimensions and flow conditions. Using the Reynolds number, it is possible to achieve equal flow characteristics at a different scale by varying parameters such as fluid velocity. This is important when scaling geometry like is done in wind tunnel testing to achieve results which are accurate for the full scale geometry.

$$\mathrm{Re} = \frac{\rho u d}{\mu} \tag{2.2}$$

Type of body		Reference area S (b = length)	Reynolds number Re	Drag coefficient C_D
Square rod		S = b D	Re > 10^4	→ 2.00
		S = b D	Re > 10^4	→ 1.50
Semicircular shell		S = b D	Re > 10^4	→ 1.20 ← 2.30
Semicircular cylinder		S = b D	Re > 10^4	→ 1.15 ← 2.15
Equilateral triangle cylinder		S = b D	Re > 10^4	→ 1.40 ← 2.10
Flat plate		S = b D	Re > 10^4	→ 1.90
T-beam		S = b D	Re > 10^4	→ 1.80 ← 1.65
I-beam		S = b D	Re > 10^4	→ 2.05
Hexagon		S = b D	Re > 10^4	→ 1.00
		S = b D	Re > 10^4	→ 0.70
Circular cylinder		S = b D	Re > 10^4	→ 0.51

Figure 2.1: Typical drag coefficients for regular 2D objects [7]

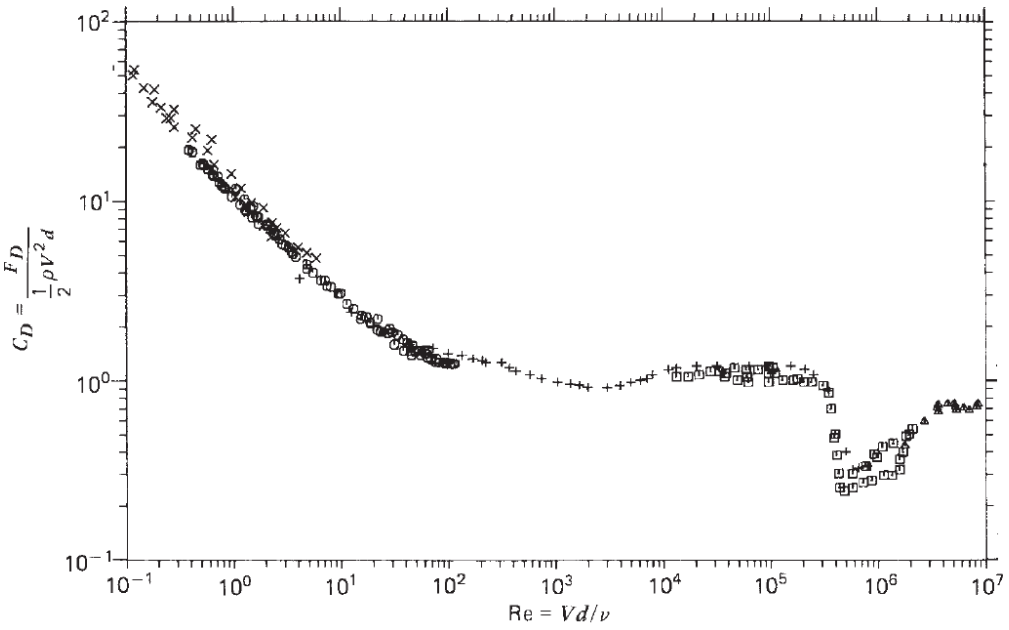

Figure 2.2: Drag coefficient of a cylinder against the Reynolds number. [30]

When a fluid flows past a surface, the fluid will interact with this surface. The region in which this happens is called the boundary layer and is characterised by the fact that viscous forces are dominant.

Fluid at the fluid-surface interface will stick to the surface and will reach a near zero velocity. Fluid in the free stream will have free stream velocity. Between these two points a velocity profile will appear which is dependent on the fluid and conditions in the boundary layer.

The skin friction drag is dependent on the viscous drag in the boundary layer around the object. As such, skin friction is closely tied to the Reynolds number. A prime example of how the drag coefficient of an object can change with the Reynolds number is the drag around a cylinder. In figure 2.2 it can be seen how the drag coefficient of a cylinder can change significantly with the Reynolds number. Two steady regions are identified where the drag coefficient is relatively stable: $100 \leq Re \leq 1x10^5$ and $Re \geq 3.5x10^6$ [8]. For this reason, the Reynolds number is typically used in research and calculations of wind loads on STS cranes. Failure to account for the Reynolds number may lead to incorrect results in calculations, as the wrong drag coefficients are used. Likewise, failure to account for the Reynolds number in wind tunnel testing will lead to differences in forces compared to a full scale crane.

3

Standards for calculating wind loads on crane structures

Wind loads acting on STS cranes are commonly calculated with standards. Several standards have been developed and adopted over time [29]. Whilst all standards follow the same methodology for calculating wind loads, their exact methods are different and thus produce different results.

In this section the general methodology, which is applicable to all standards, for determining wind loads will be covered first. Subsequently the following four different standards will be discussed as well as their distinctive properties. The standards are sorted on their date of introduction.

- DIN 1055 (1986) [14]
- F.E.M. 1.004 (2000) [17]
- EN 1991-1-4 (2005) [36]
- EN 13001-2 (2014) [27]

3.1. General method

Calculation of wind loads on cranes is calculated using the following steps:

1. Determine the constraints of the calculation.
   Constraints are to be understood as design specifications and environmental properties. These will influence wind velocities as a result of base wind speed, storm conditions and exceptional meteorological conditions.

2. Division of structure into basic geometric elements.
   Cranes are complex structures but are mostly constructed from simple geometric shapes such as beams and cylinders. For these elements the aerodynamic properties are known and can be calculated by hand. This allows for the calculation of the individual elements which make up a complex structure.

3. Calculation of aerodynamic properties of construction elements.
   All shapes have basic aerodynamic properties, i.e. properties of the element in free-stream conditions. These aerodynamic properties are dependent on geometric dimensions and the flow conditions as expressed in the Reynolds number.

4. Determining modification coefficients.
   All of the aforementioned standards use coefficients to better simulate reality. Coefficients are used to account for end-effects, shielding from other elements, surface roughness, slenderness, and other factors.

5. Calculation of element specific wind load.
   Combining all basic aerodynamic properties and the coefficients results in the wind load on a specific element. Combining all elements produces the structural wind load.

All aforementioned standards use this same method for calculating wind loads. Differences between standards can be found in specific application of the steps above. These differences will be detailed in the following section.

3.1.1. DIN 1055

This standard is from the German Institute for Standardisation (German: Deutsches Institut für Normung, DIN) and was issued in 1986. It superseded the 1977 edition of the same name.

The scope of this standard are wind loads on structures insusceptible to vibration. Static deformation of members under examination may not exceed 10%.

Wind speeds and dynamic pressure are taken as constant over a height interval. This means that the velocity profile of the wind is a stepped profile. The wind speed is independent of region although notes are made that depending on topological influences, different values may be used. The wind speeds in this standard do not differentiate between out-of-service storm velocities and in-service conditions. The given wind speeds correspond with out-of-service conditions in other standards.
The velocity profile is compared to other standards and shown in figure 3.1.

Reynolds number is only taken into account when calculating circular members and derivatives thereof such as lattice structures. The drag coefficient is presumed constant below Re = 10e5 and is described by a formula above Re = 10e5. This appears to be congruent with experimental research on such cylinders [30].

Shape coefficients are presented for a wide variety of elements, most notably cylinders, angular profiles, bars with a polygonal cross section, and single- and two-plane trusses.

Shielding effects of objects placed in series are taken into account for identical bars, panels, or trusses. The method presented in this standard may be used for similar structural elements in series, provided that the reference area of the largest element is used as reference area. This method adds the area of the individual elements offset with a shielding coefficient where applicable.
This standard notably accounts for spacing ratios up to 25 and solidity ratios from 0 to 1. Values can be read from a simple linear graph.

The DIN 1055 accounts for the position of a structure or element with respect to other elements in the vicinity.

3.1.2. F.E.M. 1.004

The F.E.M. 1.004 is a recommendation rather than an standard issued by a ISO member body. In the light of this research and the implementation of this recommendation it will be treated as a standard. The F.E.M. 1.004 is issued by the European Materials Handling Federation (French: Fédération Européenne de la Manutention, FEM) and replaces earlier publications by the F.E.M. on the same topic.

The 1.004 document is mainly built up from a study written in 1988 by the CETIM (Centre Technique des Industries Mecaniques), at French crane makers' request. Additionally the DIN 1055, and works of Technical Committee CEN/TC147/WG2 were used in the formulation of this standard.

The scope of this standard is specifically constrained to the calculation of wind loads on crane structures.

Wind speeds in the F.E.M. 1.004 are given for both in and out-of-service design conditions. For in-service conditions design wind pressures are given for 3 different use cases. The wind pressures given are constant with the height of the appliance.

The out-of-service wind conditions are determined by the geographical location, the exposure to prevailing winds, and vary with the height above the ground.

Appended to this standard is a map of Europe which roughly indicates different regions in Europe for which different wind conditions apply. For regions A, B, C (non-coastal regions) a stepwise velocity profile may be applied, much akin to DIN 1055. For all regions the velocity and pressure may be calculated based on the geographical position. The calculation of the wind profile is based on the atmospheric boundary layer and accounts for local topology.

Velocity profiles for both in- and out-of-service conditions are compared to the other standards and are shown in figure figure 3.1.

Inclined surfaces are accounted for in this standard by calculating the component of the wind normal to the surface. Surface friction is ommitted.

The F.E.M. 1.004 differentiates between critical and sub-critical flow depending on the Reynolds number. Depending on the flow regime, this standard takes the influence of slenderness, turbulence, and edge radius into account. Shape coefficients may also differ depending on the flow regime, but are constant within a flow regime.

Shape coefficients are presented for rolled, angle, cylindrical, square, rectangular, and rectangular sections for sub-critical flow regimes. For critical flow regimes only the following types are presented: circular, square and rectangular and lattice structures. In both cases, a category is included for all sections which do not fit the other catergories.

For lattice structures an appendix is included which provides more detailed shape coefficients depending on geometry and Reynolds number.

Shielding effects of objects placed in series are taken into account for parallel frames or members. No notion is made of frames or members needing to be identical. Shielding coefficients are multiplied with the wind load for windward frames and members.

This standard considers a spacing ratio from 0.5 to 6.0 and a solidity ratio from 0.1 to 0.6 and on. Shielding coefficients are given in table form with no guidance on interpolation for intermittent values.

3.1.3. EN 1991-1-4

EN 1991-1-4 is part of the Eurocodes which are a set of ten standards which specify how structural design should be conducted within the European Union. Eurocode 1 specifically details the actions on structures, where part 1-4 specifies ”General actions - Wind actions”. The Eurocodes are issued by the European Committee for Standardization (French: Comité Européen de Normalisation, CEN). Member states are expected to make national annexes which specify parameters which are applicable for that country. Localised versions such as NEN-EN 1991-1-4+A1+C2:2011/NB+C1:2020 provide a version of EN 1991-1-4 which is adapted to local conditions, within the rules and space given by the original EN 1991-1-4.

The scope of this standard is to provide guidelines for the determination of natural wind loads for the structural design of buildings and civil engineering works for each of the surfaces to be considered [36]. This standard does not mention cranes specifically but can be applied nonetheless.

Wind speeds in the EN 1991-1-4 are given in both a fundamental value of the basic wind velocity and peak velocity. The basic wind velocity is a characteristic 10 minute mean wind velocity irrespective of wind direction and time of year at a reference height and topography. The peak velocity accounts for both mean velocity as well as short-term velocity fluctuations.

The calculation of the wind profile is based on the atmospheric boundary layer and accounts for local topology. Detailed information on the local terrain and topology can be found in the national annexes, or from the general guidelines in EN 1991-1-4.

Velocity profiles for both basic wind velocities and peak velocities are compared to the other standards and are shown in figure figure 3.1.

The EN 1991-1-4 does take the Reynolds number into account when calculating the shape coefficient of regular polygons, cylinders and derivatives thereof such as lattice structures. For square sections with rounded corners the possible influence of the Reynolds number is mentioned but specifics are defered to national annexes.

Shape coefficients are presented for circular, rectangular, sharp edged, and regular polygonal sections, as well as for lattice structures and scaffoldings.

EN 1991-1-4 does take into account the shielding effect of windward elements on leeward elements, but only on walls, fences, and vertical cylinders in a row. For all other elements, no shielding is accounted for. As a result, almost no shielding effects are accounted for when applying this standard on steel structures such as cranes, truss structures or lattice towers.

As a more general standard, the EN 1991-1-4 has provisions to account for orography. This can be applied when calculating wind loads as a result of headwind (e.g. from the waterside).

3.1.4. EN 13001-2

EN 13001-2 Crane safety - General design - Part 2: Load actions is a standard by CEN, prepared by Technical Committee CEN/TC 147 “Cranes — Safety”. As European Standard, this standard shall be given the status of national standard in all member states. EN 13001-2 is part of the EN 13001 series of standards which all relate to crane design.

The scope of this standard is not specifically limited to wind actions, but to all actions acting on a crane. This is a combination of load actions and load combinations from which the load effects on the crane can be determined which can serve as a proof of competence of the crane and its main components. As such, it extensively covers the aspects of the load actions which act on the crane.

Wind speeds in the EN 13001-2 are given for both in-service as well as out-of-service conditions. The wind force is assumed to be normal to members’ surfaces, where the normal element of the wind is taken should the wind angle deviate from the normal.

For in-service winds the wind is assumed to blow horizontally at a constant mean velocity at all heights. The mean velocity can be found in a table which specifies 3 wind states from which the appropriate one has to be selected for the design conditions. Wind actions resulting from wind velocity are specified in three wind effect levels which are used for different calculations. Level 1 is used for structural calculations whilst levels 2 and 3 are used for operational calculations relating to motor power.

For out-of-service conditions wind is assumed to blow horizontally at a velocity which increases with height. To calculate the velocity profile, values for the storm recurrence interval and the reference storm velocity have to be determined. The resulting wind profile simulates the atmospheric boundary layer.

The EN 13001-2 does differentiate shape coefficients for different Reynolds numbers for circular sections and lattice structures constructed of aforementioned.

Shape coefficients are presented for a wide variety of elements. For circular sections shape coefficients are presented with a dependency on the Reynolds number. Within circular sections differentiation is made between general circular sections, pipes and rods, and ropes, based on the aerodynamic slenderness ratio. For flat sided structural members there is no dependency on the Reynolds number but shape coefficients are given depending on the wind angle [0, ±45, 90] in x- and y-direction. For triangular and rectangular members, no distinction is made based on wind direction or Reynolds number.

Additional coefficients are presented which account for the effect of the aerodynamic slenderness and solidity ratios as well as for the position of the member and obstacle in wind direction.

EN 13001-2 does take shielding into account in the same manner as the DIN 1055 does. The areas of successive members are added with shielding coefficients applied to elements following the most windward member.

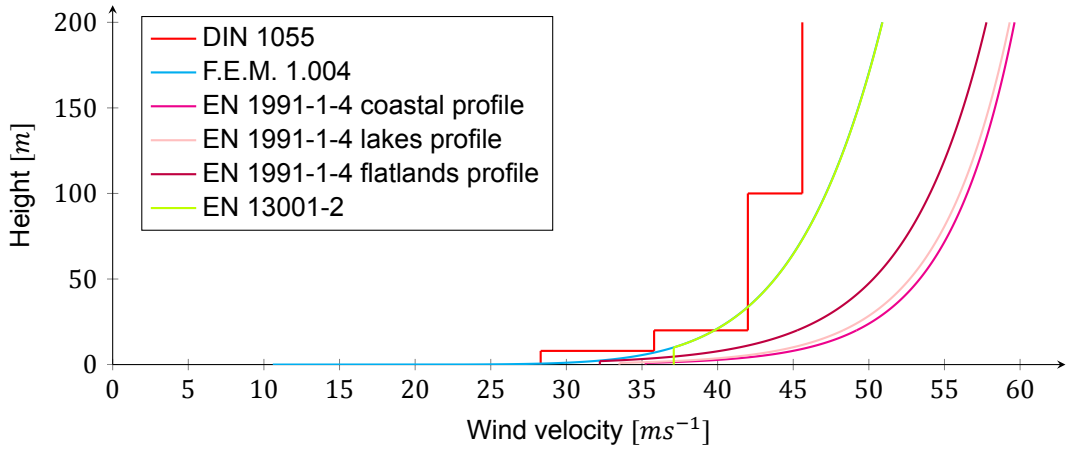

Figure 3.1: Wind profiles according to the four discussed standards. Note that F.E.M. 1.004 and EN 13001-2 overlap for heights over 10m.

3.2. Standard calculations

Standard calculations were performed using the wind tunnel test parameters. This has several consequences:

- Wind profiles, as detailed in section 3.1, are not taken into consideration.
- The model scale is smaller than the typical scope of the crane. This typically does not pose any problems as many calculations are based on dimensionless quantities.
- The Reynolds number is lower than what is typically encountered on cranes. This incurs different flow properties and drag coefficients, however mostly at cylindrical objects. Since this is the case for all standards under consideration, this is presumed to be of non-critical influence.

It is important to note that with standard calculations, only forces and moment in and about crane local x and y directions (see figure 4.6) are typically calculated. Calculation of forces and moments in other directions and about other axes require significantly more effort and time, and will typically encounter situations not covered by standards.

3.2.1. Wind tunnel model and dynamic pressure

The wind tunnel model and conditions were used as a basis for calculation of wind loading according to the 4 standards detailed in section 3. While these standards are not primarily intended for calculations at this scale, the principle theory behind the standards is sound and therefore deemed applicable.

- F_x and M_y are calculated by using the front view of the crane, figure 3.2, a 0° wind angle.
- F_y and M_x are calculated by using the side view of the crane, figure 3.2, a 90° wind angle.

From these forces and moments the reaction forces at the 4 corners are calculated with equations 3.1, 3.2, and 3.3.

$$F_x = \frac{F_x}{4} \tag{3.1}$$

$$F_y = \frac{F_y}{4} \tag{3.2}$$

$$F_z = \frac{M_i}{2d_i}, \text{ where i = x,y} \tag{3.3}$$

3.2.2. Overall forces and moments

The overall forces and moments are compared for the four standards under consideration. These results are used to evaluate their performance against each other. The overall forces and moments are shown in table 3.1.

Comparing standards

When comparing the standards in table 3.1, several observations can be made:

- There appears to be a downward trend where newer standards produce lower calculated wind forces.
- Although the DIN 1055 has the most extensive shielding coefficients, the resultant wind actions are highest of the standards considered.
- The F.E.M. 1.004 is significantly lower than all other standards on all metrics.
- Although the EN 1991-1-4 and the EN 13001-2 are very similar in calculation method, the addition of shielding factors in the EN 13001-2 differentiates it from the EN 1991-1-4.
- In all cases, the force in y direction stays the same regardless of boom position.

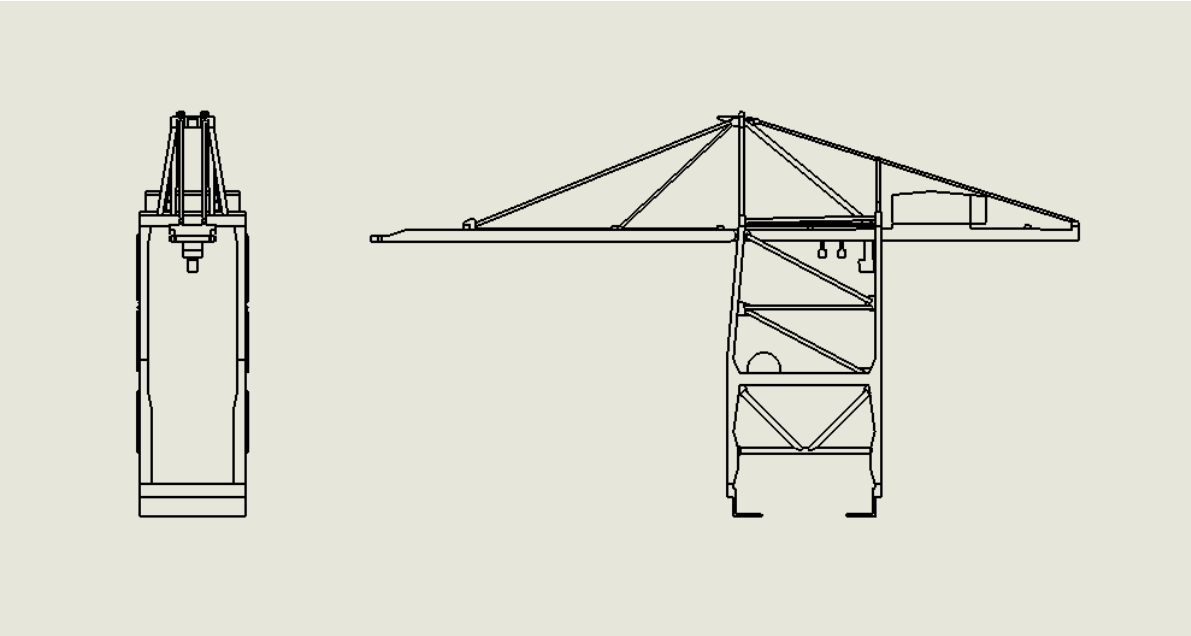

Figure 3.2: Crane front and side view drawing

Table 3.1: Standard calculations: comparison of overall forces and moments.

		DIN 1055	F.E.M. 1.004	EN 1991-1-4	EN 13001-2
Boom down	F_x	26.32	18.10	25.33	22.49
	F_y	34.53	24.99	37.48	32.17
	M_y	11.54	8.50	13.03	10.96
	M_x	7.91	5.21	7.22	6.39
Boom up	F_x	32.04	20.93	29.02	26.64
	F_y	34.53	24.99	37.48	32.30
	M_y	12.92	9.64	14.96	12.46
	M_x	12.24	7.48	10.22	9.67
Boom intermediate	F_x	31.40	19.61	28.40	25.34
	F_y	34.53	24.99	37.48	32.30
	M_y	12.54	9.33	14.43	12.06
	M_x	11.08	6.30	9.31	8.36

Table 3.2: Standard calculations: comparison of reaction forces per corner.

		DIN 1055	F.E.M. 1.004	EN 1991-1-4	EN 13001-2
Boom down	F_x	6.58	4.53	6.33	5.62
	F_y	8.63	6.25	9.37	8.04
	$F_{z,x}$	19.46	12.81	17.77	15.72
	$F_{z,y}$	28.39	20.91	32.05	26.97
Boom up	F_x	8.01	5.23	7.26	6.66
	F_y	8.63	6.25	9.37	8.07
	$F_{z,x}$	30.11	18.41	25.16	23.79
	$F_{z,y}$	31.79	23.71	36.81	30.65
Boom intermediate	F_x	7.85	4.90	7.10	6.34
	F_y	8.63	6.25	9.37	8.07
	$F_{z,x}$	27.27	15.51	22.91	20.57
	$F_{z,y}$	30.85	22.95	35.50	29.69

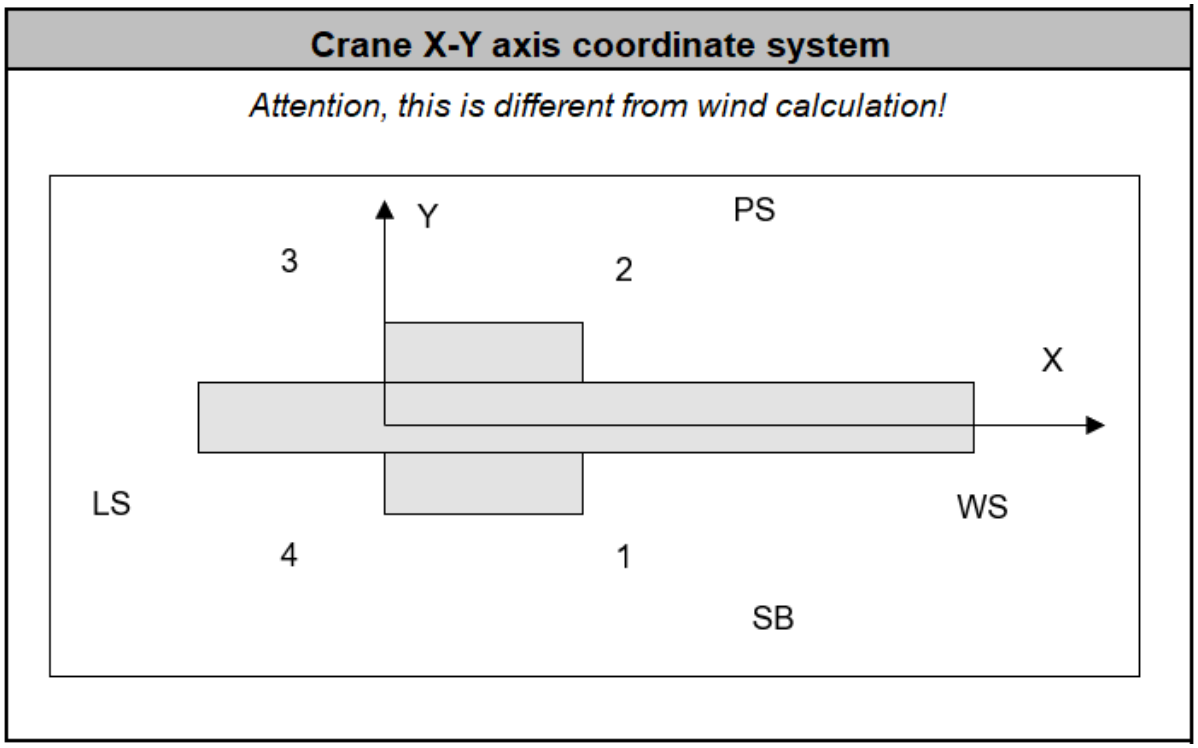

Figure 3.3: Locations of port, starboad, water, and land side

3.2.3. Reaction forces

From the general forces and moments, reaction forces for the four corners can be calculated. The resultant forces are shown in table 3.2. Reaction forces are not split up per corner. Since reaction forces in this table are calculated with equations 3.1, 3.2, and 3.3 it can be seen that no asymmetrical element is introduced and as such that the load is spread evenly over the 4 corners. Furthermore, the reaction forces in z direction are given for both calculation scenarios. That is to say the force in z direction as a result of the wind at 0° which is given as $F_{z,x}$ and the force in z direction as a result of the wind at 90° which is given as $F_{z,y}$. From these calculations several observations can be made:

- Reaction forces in x, y, and z directions follow the same trend as the general force in x and y directions, and moments about x and y.
- Reaction forces in the z direction are an order of magnitude bigger than those in x and y directions.

These observations are unsurprising given the simple equations used to calculate the reaction forces. Since moment is the cross product between a position vector and a force vector, given by: $\tau = r \times F$ (3.4). The arm over which the four corners have to resist the moment is much smaller than the arm where force is applied. This also shows the instability problem where the biggest forces and moments are found in the direction of the smallest footprint.

4

Wind tunnel testing

“Wind tunnel test: A procedure using scale models loaded by fan-driven airflow to predict responses of a structure, structural components, and cladding to actual wind storm conditions.”[25]

Wind tunnel testing has been an important tool in the engineer’s toolbox for determining the aerodynamic behaviour and characteristics of a object in an airflow. Wind tunnel testing is done in a highly controllable environment which allows for studying of specific areas of interest in a design. Historically wind tunnel testing has been used in the aerospace and automotive industries, where aerodynamic performance is paramount. But other industries have also found use for wind tunnel testing finding areas for design improvements and new engineering insights. Even in a time of high-performance computing where CFD is used across many industries [40], wind tunnel testing remains the golden standard [11].

The quality of wind tunnel testing results closely correlates to the controlled environment. A properly scaled model with properly scaled parameters in an accurate testing setup will yield high quality results whilst the inverse holds true for incorrectly scaled models, parameters and setups.

4.1. Scope

Little research is published on wind actions on cranes with respect to wind tunnel testing and the effect of a rotating wind angle. While various standards have been published regarding the wind loading of cranes, and wind tunnel tests have been performed, these effects remain poorly understood. The aim of this wind tunnel test is to gain a better understanding of the effects of wind on a crane. To achieve this goal both quantitative and qualitative measurements will be performed. Quantitative measurements will be done by means of a balance measurements which measure forces and moments on and about the base. Qualitative measurements will be done with smoke traces to visualise airflow around the model.

The scope of this wind tunnel test is limited to the following parameters:

- 1 crane model, 3 configurations
  - Model with cable rails and staircases
  - Model with cable rails and without staircases
  - Model without cable rails and without staircases
- 3 boom configurations
  - Boom down (0°); figure 4.3a
  - Boom intermediate (45°); figure 4.3c
  - Boom up (80°); figure 4.3b
- 360°of rotation
- Uniform wind profile
- Constant velocity

Each of the testing parameters will be discussed in later sections.

4.2. Crane model

The crane model is based on ZPMC gantry cranes as found in the ports of Antwerpen and Tanger. This is a general design which is commonly found worldwide (example in fig. 4.1). The design follows the principle of a crane atop a gantry. The final dimensions are dependent on the requirements set forth by the customer, in this case the terminal, but the overall design of the crane remains virtually the same.

The wind tunnel model was adapted from an existing, earlier used, wind tunnel model. A new gantry was fabricated to evaluate the different characteristics with regards to the original gantry. The original wind tunnel model had a scale of 1:150, and this scale has been maintained.

The new crane wind tunnel model has a girder length of 1m. The model is mainly constructed from wood, with various pieces made from metal. More complex geometrical parts such as the cable rail were 3D-printed. Elements such as hand rails, cable ducting, flanges, and other small elements were either simplified or omitted.

Flights of stairs were modelled by means of a screen with the size, shape, and porosity which is believed to represent the aerodynamic resistance of these elements. This is carried over from the original model on which this model was based.

Figure 4.1: Container crane at APM Terminals Rotterdam

4.2.1. Scaling

Proper scaling of the wind tunnel test would require a similar Reynolds number, as described in equation 2.2 in both cases. From hand calculations it was learned that for the full scale crane the Reynolds number would be in the order of magnitude of 10e5 - 10e7. Since the Reynolds number scales linearly with both fluid velocity and reference dimensions, any change in model scale requires the inverse change in fluid velocity, assuming the fluid remains the same. With a scale of 1:150 this means that with equal air speed the Reynolds number drops 2 orders of magnitude.

As the crane structure consists mostly of sharp edged elements, a low Reynolds dependency is expected. However, since the structure does have a non-insignificant number of round(ed) elements, the potential effect of the Reynolds number has to be taken note of.

The scope of this study focuses solely on the response generated by wind actions on the crane. As such, other aerodynamic properties or the dynamic response of the structure are not taken into account.

4.2.2. Model configurations

As stated previously, the model was tested in 3 model configurations. These configurations represent increasingly simplified models with the reduction of elements. This was done to get a better understanding of how model design choices can influence the results obtained by wind tunnel testing. Suspected

was that the influence of such members can have an influence on the drag which would be bigger than the area of the parts suggests.

The elements under consideration are rails and staircases and are shown in figure 4.2

(a) Cable rail mounted under the girder (highlighted)

(b) Mesh screen representing the lower staircase

(c) Mesh screen representing the upper staircase

Figure 4.2: Crane configurations

4.2.3. Boom configurations

The model was tested with 3 boom configurations. Boom down and boom up configurations represent typical in-service and out-of-service conditions. A third configuration of 45°was tested to gain further insight in how the boom configuration affects stability in storm conditions. The intermediate and up boom positions are very interesting for this study as they change the axis of rotation of the boom from the x-axis to the xz-axis. This has the effect that the cross section and shielding effects change with crane rotation as opposed to the boom down condition where this is not the case.

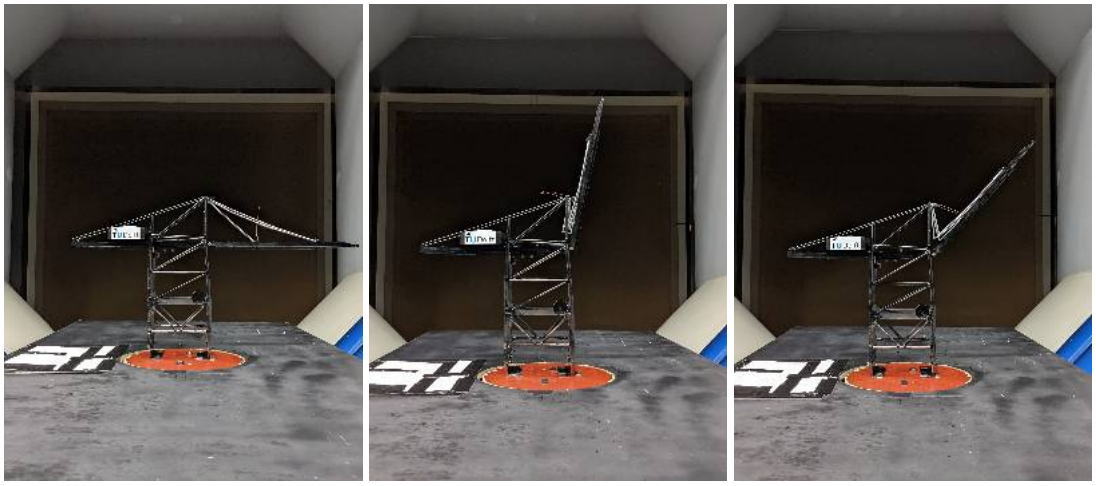

(a) Boom down configuration

(b) Boom up configuration

(c) Boom intermediate configuration

Figure 4.3: Crane boom configurations

4.3. Testing setup

4.3.1. Wind tunnel

Wind tunnel tests were performed in the Open Jet Facility (OJF) of the Delft University of Technology. The OJF is an open section closed-circuit wind tunnel.

“ A large fan powered by a 500 kilowatt electric motor enables it to achieve a maximum speed of around 120 kilometres an hour. Air is rotated 180 degrees through a long diffuser and two rows of corner vanes. It then passes through a short diffuser before entering the ‘settling chamber’. Here, five fine-mesh screens reduce the turbulence and velocity deviations in the airflow. Via a contraction the air is then blown into the test section as an even jet stream and cooled at the end by an enormous cooling radiator and guided back to the fan.” [13]

Due to the constraints of the wind tunnel, only a uniform velocity profile was realisable rather than a power law profile as described in the standards. The differences between these two profiles can be seen in figure 4.4. Due to the difference in profile, the centre of load can shift vertically at an equal overall load. Whilst inconvenient, this is not seen as an insurmountable hurdle since the exact numbers are less relevant than the overall behaviour which can be investigated with this setup. The velocity

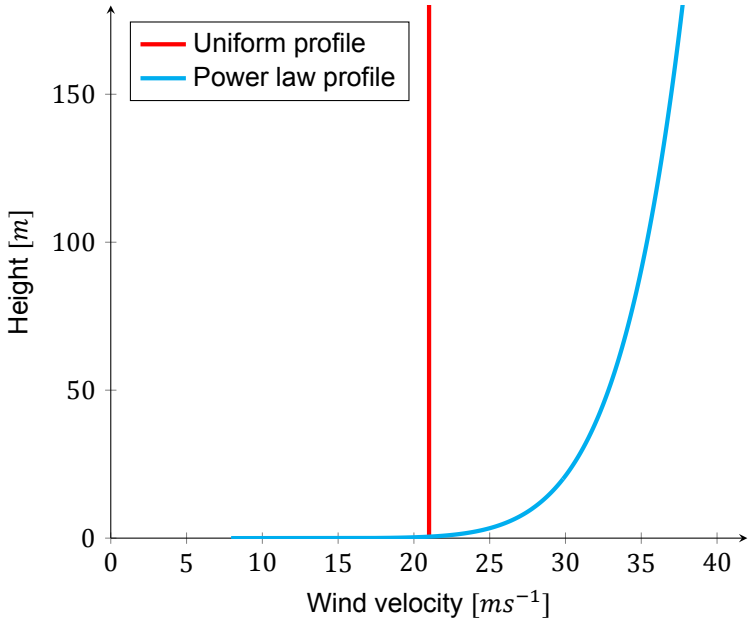

Figure 4.4: Wind profiles according to the four discussed standards. Note that F.E.M. 1.004 and EN 13001-2 overlap for heights over 10m.

was adjustable between 1 and 30 m/s. From this velocity the dynamic pressure could be calculated according to equation 4.1.

$$q = \frac{1}{2}\rho V^2 \tag{4.1}$$

Where q is the dynamic pressure, V is the air speed, and ρ is the air density. The air speed is controllable by the wind tunnel operator, the air density is dependent on several factors including air temperature. As such, this density is measured and calculated from several pitot tubes which are present in the settling chamber of the wind tunnel.

4.3.2. Balance and turntable

The model was mounted to the OJF External Balance B8604, an external 6-component balance which was purchased from the National Aerospace Laboratory (NLR) [5]. This balance has an aluminium model plate on the metric side of the balance on which the test subject can be mounted. The non-metric side of the balance is used to mount the balance to the ”earth”. For mounting, a bolt pattern was specified to which the crane model was made to fit.

To measure forces and moments the balance is equipped with 6 load cells which are are sensitive in only one direction and decoupled from the other directions. Decoupling is done through means of elastic hinges. As a result, this balance can measure forces in x-, y-, and z-directions as well as moments about the x-, y-, and z-axes. The nominal load ranges are specified in table 4.1. Before testing commenced, hand calculations were performed to conservatively estimate the loads the model would incur on the balance. These loads were found to be well under the maximum specified loads, leaving 50-100% safety factor.

Rotation was performed stepwise in steps of 5°. Overlap due to model repositioning at the ±45°, 135°, and 225° positions resulted in 76 measurements per full rotation.

	Component	Simeltaneously	Single load
Force	Axial	±250N	± 250N
	Side	±500N	± 600N
	Vertical	±500N	±3500N
Moment	Rolling	±500N	± 550N
	Pitching	±250N	± 500N
	Yawing	± 50N	± 125N

Table 4.1: Balance load range

To enable variation of wind angles, the balance was mounted on a turntable. This turntable has an angular displacement from -45°to +45°resulting in a total achievable displacement of 90°. To achieve 360°of rotation, the model has to be moved 3 times. To minimise model movement, multiple configurations were tested per setup. This to decrease setup time as well as to reduce the amount of times error can be introduced.

4.3.3. Model setup

The balance and turntable combination were mounted to a height-adjustable movable platform. This platform was then positioned in the opening of the wind tunnel jet opening. The setup can be seen in figure 4.5a. Since the turntable and balance have significant height, it was suspected that this would have significant impact on the balance measurements in an unpredictable and uncorrectable manner. To mediate this, a table was constructed to provide a flat surface for the wind to approach the model setup. This table was placed at such a height that the boundary layer coming from the settling chamber was cut off. The reason for cutting off this boundary layer is that the profile of this boundary layer is unknown and as such is unwanted.

To accommodate the rotation of the turntable, a round cutout was made in the table. The model was then mounted to a round plate which fit the cutout. This allowed for rotation of the model whilst keeping a closed flow plane.

The results for 0° , 90° , and 180° are in agreement whilst the measurements for 270° show deviant behaviour.

4.3.4. Coordinate systems, forces and wind direction

During testing three separate axis systems were used. All systems are right handed, orthogonal systems.

1. Balance local coordinate system
2. Global coordinate system
3. Crane local coordinate system

These systems are shown in figure 4.6.

Balance local coordinate system

The balance local coordinate system is fixed to the balance. This is the reference coordinate system from which the measurements are put out. The x-axis is horizontal and pointed and positive towards

(a) Balance table setup (b) Setup without table (c) Setup with table

Figure 4.5: Balance and table setups

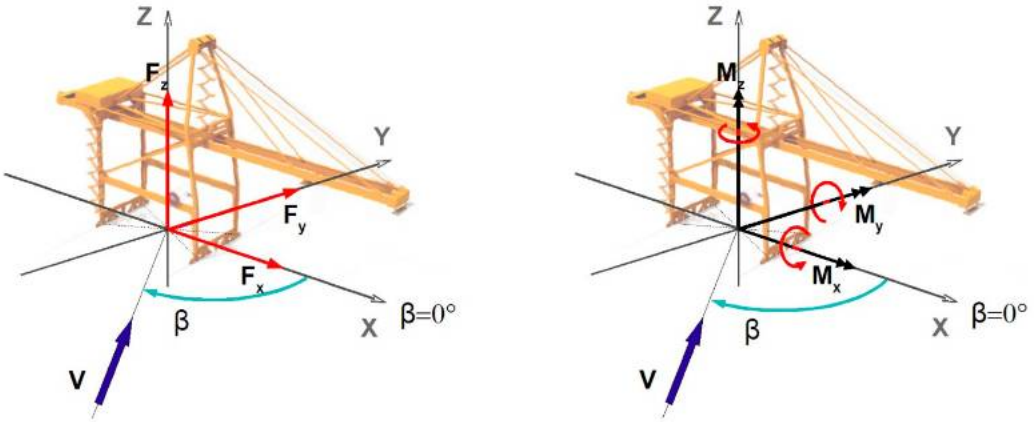

Figure 4.6: Crane local coordinate system with axes, wind direction, forces and moments.

the front of the balance. The z-axis is pointed and positive downwards. This means that wind pressure and lift are registered as positive forces.

The centre of measurement is located below the surface of the balance, this means that moment measurements about the x- and y-axes need to be corrected for this offset.

Global coordinate system

The axes of the global coordinate system are fixed to the wind tunnel. The global coordinate system was used as an intermediate coordinate system when translating from the balance local to the crane local system. In this system the x-axis is pointed and positive towards the wind. The y-axis is pointed and positive in the port side direction relative to the wind and is always perpendicular to the airflow. The z-axis is rotated 180°with regards to the balance local system and is pointed and positive towards the sky.

The main purpose of this intermediate coordinate system is to study the aerodynamic properties of the crane. Secondly it acts as a sanity check to verify all measurements are as expected and no errors are occurring which could otherwise go unnoticed.

To rotate from the balance local to the global system two rotations have to be performed.

1. Rotation about the z-axis of θ°
2. Rotation about the x-axis of 180°

The first rotation aligns the axes with the wind direction, the second rotation flips the y-, and z-axis in direction. These two rotation matrices can be combined in a single rotation matrix, which is given in equation 4.2.

$$R(\theta) = \begin{bmatrix} \cos\theta & \sin\theta & 0 \\ \sin\theta & -\cos\theta & 0 \\ 0 & 0 & -1 \end{bmatrix} = \begin{bmatrix} 1 & 0 & 0 \\ 0 & \cos\theta & -\sin\theta \\ 0 & \sin\theta & \cos\theta \end{bmatrix} \begin{bmatrix} 1 & 0 & 0 \\ 0 & -1 & 0 \\ 0 & 0 & -1 \end{bmatrix} \tag{4.2}$$

The centre of measurements for this coordinate system is placed at the base of the crane. This means that measurements need to be offset in the z-direction. This is done according to equation 4.3 which describes the translation matrix. The offset h_{offset} was measured at 31mm.

$$T = \begin{bmatrix} 1 & 0 & 0 & 0 & 0 & 0 \\ 0 & 1 & 0 & 0 & 0 & 0 \\ 0 & 0 & 1 & 0 & 0 & 0 \\ -h_{offset} & 0 & 0 & 1 & 0 & 0 \\ 0 & h_{offset} & 0 & 0 & 1 & 0 \\ 0 & 0 & 0 & 0 & 0 & 1 \end{bmatrix} \tag{4.3}$$

The transformed forces and moments are then given as described in the equation 4.4. This is achieved by performing the translation followed by the rotation.

$$\begin{bmatrix} F_{x,g} \\ F_{y,g} \\ F_{z,g} \\ M_{x,g} \\ M_{y,g} \\ M_{z,g} \end{bmatrix} = \begin{bmatrix} \cos\theta & \sin\theta & 0 & 0 & 0 & 0 \\ \sin\theta & -\cos\theta & 0 & 0 & 0 & 0 \\ 0 & 0 & -1 & 0 & 0 & 0 \\ -h_{offset}\cos\theta & h_{offset}\sin\theta & 0 & \cos\theta & \sin\theta & 0 \\ -h_{offset}\sin\theta & -h_{offset}\cos\theta & 0 & \sin\theta & -\cos\theta & 0 \\ 0 & 0 & 0 & 0 & 0 & -1 \end{bmatrix} \begin{bmatrix} F_{x,bl} \\ F_{y,bl} \\ F_{z,bl} \\ M_{x,bl} \\ M_{y,bl} \\ M_{z,bl} \end{bmatrix} \tag{4.4}$$

Crane local coordinate system

The crane local coordinate system is fixed to the crane. This coordinate system is used for determining overturning moments and reaction forces. The x-axis is pointed and positive towards the boom. The y-axis is pointed and positive towards the port side of the crane. The z-axis as a result is pointed and positive upwards, towards the sky. The centre of measurements is in the centrally located between the legs and coincides with the centre of measurements of the global coordinate system.

This main purpose of this coordinate system is to study the resultant forces and moments working on the crane. From this the stability and reaction forces can be calculated which are important parameters for crane design.

To transform from the global coordinate system to the crane local coordinate system only a rotation about the z-axis is needed. The wind angle is determined by the rotation angle of the turntable and the position of the crane with respect to the balance. The resulting rotation matrix for this transformation can be found in equation 4.5

$$\begin{bmatrix} F_{x,cl} \\ F_{y,cl} \\ F_{z,cl} \\ M_{x,cl} \\ M_{y,cl} \\ M_{z,cl} \end{bmatrix} = \begin{bmatrix} \cos\theta & -\sin\theta & 0 & 0 & 0 & 0 \\ \sin\theta & \cos\theta & 0 & 0 & 0 & 0 \\ 0 & 0 & 1 & 0 & 0 & 0 \\ 0 & 0 & 0 & \cos\theta & -\sin\theta & 0 \\ 0 & 0 & 0 & \sin\theta & \cos\theta & 0 \\ 0 & 0 & 0 & 0 & 0 & 1 \end{bmatrix} \begin{bmatrix} F_{x,g} \\ F_{y,g} \\ F_{z,g} \\ M_{x,g} \\ M_{y,g} \\ M_{z,g} \end{bmatrix} \tag{4.5}$$

4.4. Measurements and data

Data was collected in 43 runs, of which 38 were balance measurements and 3 were smoke tests. The runs can be found in table 4.2. The first 2 runs were to examine the effect of the Reynolds number, and will be elaborated on in section 4.4.5. The following 36 runs were the result of 9 configurations, as detailed in section 4.1, where each configuration requires 4 runs for the 4 orientations of the crane with respect to the balance to complete 1 full rotation.

	Boom configuration		
Run	Down	Up	Intermediate
Reynolds check	•	•	
Rail, ladders	•	•	•
Rail, no ladders	•	•	•
Smoke testing	•		
No rail, no ladders	•	•	•

Table 4.2: Wind tunnel test program; order as performed

4.4.1. Data acquisition

Data acquisition was done exclusively in a step wise manner. It was decided that the chosen step interval, as detailed in section 4.3.2, was sufficiently small that continuous measurement at continuous rotation was of no added benefit. Also, due to the constraints of the turntable, true continuous rotation would not have been possible during this study as only 90° of rotation could be achieved at a time.

Measurements were done at 2 000Hz and averaged over a time period of 10s. This time step was chosen to act as a low pass filter in the measurements to filter out dynamic behaviour of the crane as result of excitation by the wind. The time averaged data is the result of 20 000 measurements.

4.4.2. Bias and uncertainty

Measurement bias

Due to the construction of the testing table (section 4.3.3) the measurement equipment was suspected to have influence on the measurements. The open bottom would allow airflow under the flow table and could potentially influence the rotation platform and as such the measurements. To eliminate the bias introduced by the measurement setup, measurements were done on the testing setup without the model crane. These measurements were done in the 2 configurations which are the result of the crane placement. These measurements were included in the final balance measurements.

From the measurements done it was seen that this step was essential as a significant bias was removed from the data.

4.4.3. Measurement uncertainty

The balance is calibrated periodically and its maximum error and standard deviation of the errors are presented in percentage of the nominal loads in table 4.3. This error is deemed sufficiently small to not significantly impact measurement data and no additional measures have to be taken to correct errors stemming from this.

	ΔF_x	ΔF_y	ΔF_z	ΔM_x	ΔM_y	ΔM_z
MAX	0.06	0.23	0.16	0.05	0.05	0.25
STDEV	0.02	0.05	0.05	0.01	0.01	0.07

Table 4.3: Measurement uncertainty

4.4.4. Coefficients

To study the aerodynamic properties, behaviour, and reaction of the crane model, it is important to use dimensionless coefficients which are independent of local conditions. Measurements have been taken over the course of 4 days, with varying ambient temperatures and air pressures, as well as small fluctuations in air speed. Differences in dynamic pressure as a result of this can amount up to 5%, which could potentially skew results.

All measured forces and moments have been converted to coefficients according to the drag equation, equation 2.1. This allows for direct comparison of the results between runs. This conversion is done according to:

$$CF_i = \frac{F_i}{q_{ref}A} \quad CM_i = \frac{M_i}{q_{ref}Al} \qquad \text{for} \qquad i = x, y, z \tag{4.6}$$

Where the following parameters were used:

1. F_i: force in i direction
2. M_i: moment about i axis
3. q_{ref}: reference dynamic pressure
4. A: reference area; A reference area of A = $1000/150^2$m^2 was used.
5. l: reference length used to make the CM_i dimensionless; A reference length of $l = 80/150$m was used.

Additionally, derivative coefficients were calculated for the horizontal force, total force, overturning moment: $CF_{hor}, CF_{tot}, CM_{hor}$.

4.4.5. Reynolds check

The first measurements performed were a so called Reynolds check. The aim of these measurement series was to determine if the model showed a behaviour which is dependent on the Reynolds number. To verify this, the model was placed in the wind tunnel and measurements were made with increasing air velocities. As per equation 2.2, this can vary the Reynolds number with 1 order of magnitude.

These measurement series were also necessary to determine at which air velocity the tests should be run. Ideally, the model should show no dependence on the Reynolds number around the test velocity. Should this behaviour occur, any variations during the test can skew the results, which is unwanted.

The checks were performed in 2 boom configurations, with the model rotated 360° at 90° increments. This provided 8 sets of data which was deemed a sufficient amount of data to determine the Reynolds dependency of the model. The results of these checks can be seen in figure 4.7 for the boom down configuration and 4.8 for the boom up configuration.

The results for 0°, 90°, and 180°are showing similar behaviour whilst 270° shows deviant behaviour. This behaviour can not be explained at the present time and is present in both the boom down and boom down situation. Regardless, all measurements show steady behaviour in the [15.0 ,27.5]m/s range. From this data a reference air velocity of 21m/s was chosen.

An additional reason for this speed over a higher speed was that the required power to drive the wind tunnel fan grows exponentially with the air velocity. In light of not wasting too many resources, a lower velocity was preferred.

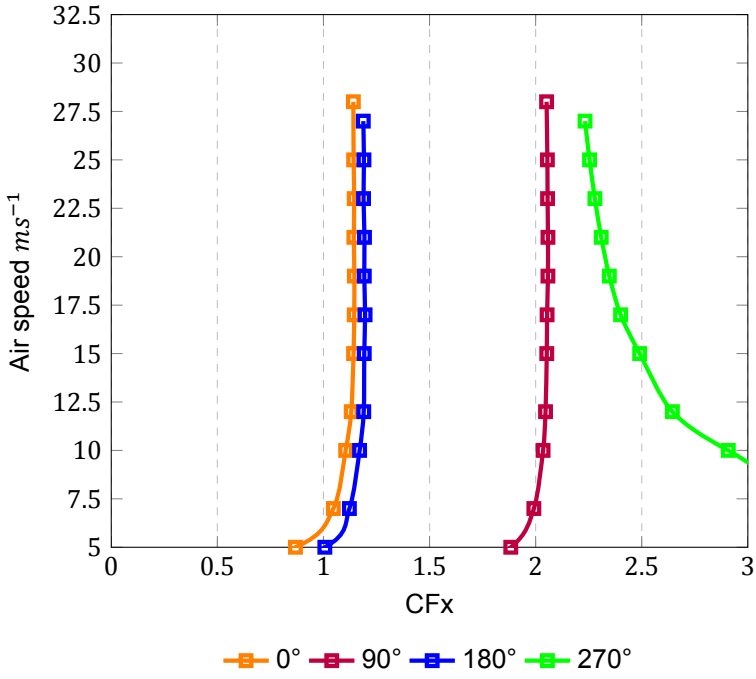

Figure 4.7: Reynolds check with the boom down

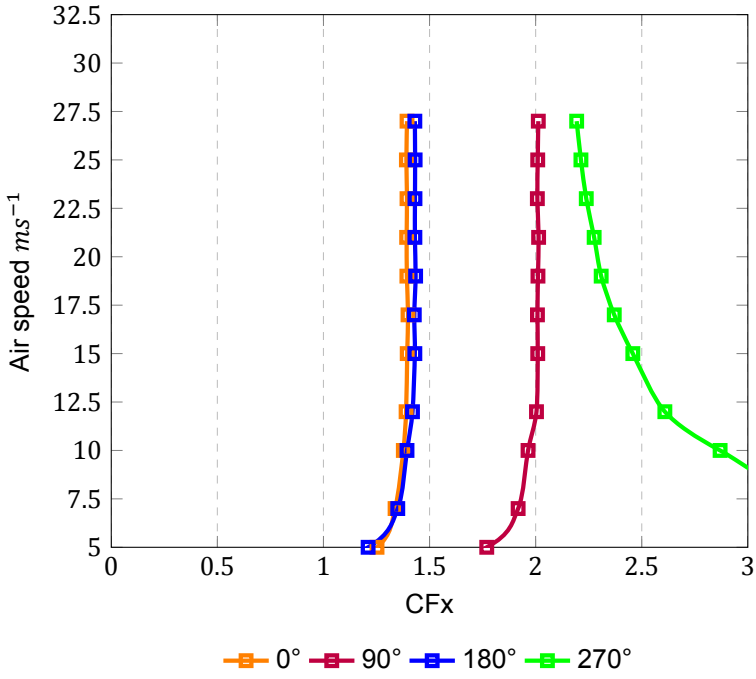

Figure 4.8: Reynolds check with the boom up

4.5. Wind tunnel test results

The results of the wind tunnel tests will be presented in order of how they were performed. First the results of the Reynolds check will be presented and their implications for further testing discussed. The results of the wind tunnel data will be presented over different sections in the following manner:

- Section 4.5.1: General aerodynamic properties
- Section 4.5.2: Effect of asymmetry
- Section 4.5.3 Effect of auxiliary elements
- Section 4.5.4: Effect of boom position
- Section 4.5.5: Reaction forces and stability

4.5.1. General aerodynamic properties

Study of the global forces gives an indication of the general behaviour of the crane as a result of the wind acting upon it. For first impressions it is good to look at the general properties of the model crane in the wind tunnel. This will show the general behaviour of the crane with respect to the direction of the wind. Presented in figure 4.9 is the case for a crane with all aerodynamic elements in the boom down case. This will also serve as the baseline to which other cases will be referenced.

In this section the aerodynamic properties of the crane in the global axes system will be discussed, split out over the different force directions and moment axes.

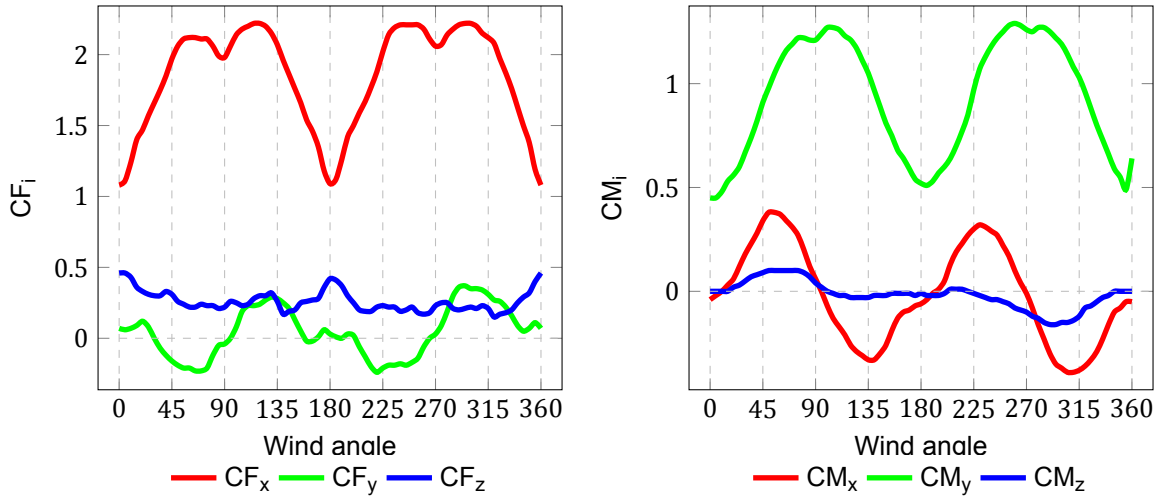

(a) Forces in the standard configuration with the boom down

(b) Moments in the standard configuration with the boom down

Figure 4.9: Forces and moments in the standard configuration with the boom down

Force in x direction

The force in x direction shows 2 local minima at 90° and 270° as well as at 0° and 180°. These points coincide with the four principal crane orientations or wind from the cardinal directions. It is to be noted that these points are local minima and that force in the x direction increases as the wind moves off the cardinal directions.

The force in x direction shows a correlation with the area of the silhouette of the crane projected on a plane normal to the wind direction. This is shown in figure 4.10. Additionally it is shown that the crane shows asymmetric behaviour between the port side and the starboard side, as well as land side and water side.

Force in y direction

The force in y direction shows the lateral force resulting from the wind being deflected by the crane surfaces. The graph passes through 0 several time, the angles at which this happen seem to correlate to wind angles where the wind is perpendicular to most crane surfaces.

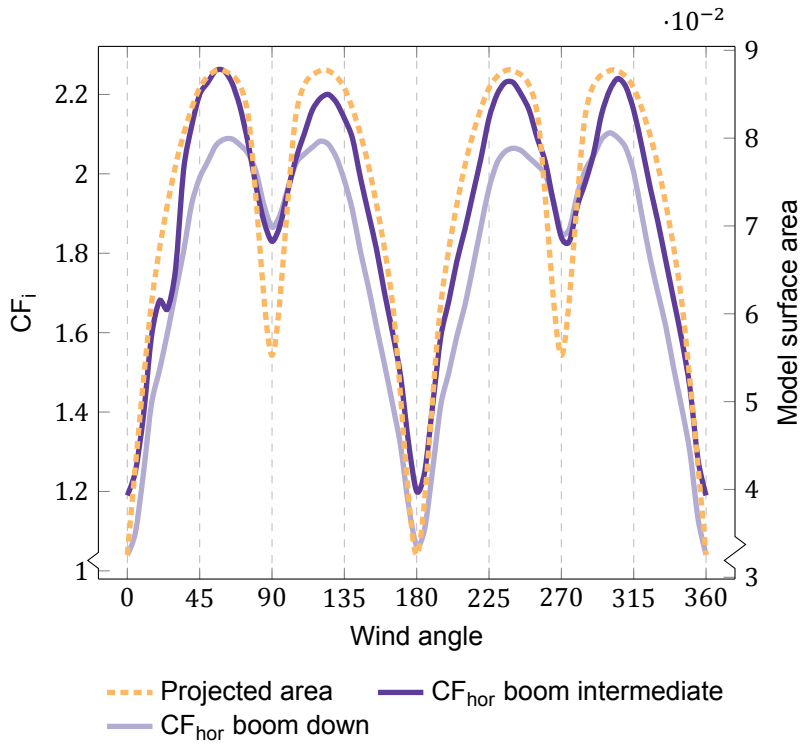

Figure 4.10: Correlation between force and projected surface area

The force in y direction generally tends to be a full order of magnitude lower than the force in x direction. From this we deduce that most force acts in the wind direction.

Force in z direction
The force in z direction shows the lift or downforce generated by the crane. In this case the crane generates lift in all positions. The magnitude of lift is about an order smaller than the magnitude of the drag.

Moment about x axis
The moment about the x axis follows the same trend as the force in y direction.

Moment about y axis
The moment about the y axis follows the same trend as the force in x direction.

Moment about z axis
A small moment, relative to the other moments, was observed about the z axis. This moment will have a small, non-negligible effect, on the reaction forces in x and y direction in the four corners.

4.5.2. Effect of asymmetry and auxiliary elements

As seen in section 4.5.1, the wind angle plays an important role on the wind actions where asymmetrical effects appear.

In section 4.2.2 and figure 4.2 it is shown that one side of the crane was fitted with a mesh screens, to emulate the staircases which are present on real cranes, as well as a cable duct underneath the boom. These auxiliary elements are placed only on the port side of the crane and create an asymmetry in the construction.

The construction of the crane is symmetric with respect to the xz plane. Additional elements such as staircases, cable rails, the HV cable reel, and the asymmetric construction of the machine house introduce asymmetry. The crane is fully asymmetric with respect to the yz plane, from a construction point of view.

xz plane asymmetry
To evaluate the effect of the xz plane asymmetry, the wind actions for wind angle 90° ±90° and 270° ±90° cases are compared. Comparing the port and starboard side winds shows the effect of the placement of auxiliary elements on the overall loads incurred by wind actions.

In figure 4.11a the horizontal force coefficient is compared between port side and starboard side wind. The staircases, represented by mesh, and the cable rail are attached to the port side of the crane. From this graph it is seen that when loaded from the starboard side, the wind load on the crane is generally lower than when loaded from the port side. However, it is to be noted that when loaded with a offshore wind, the port side wind is favourable leading to lower wind loading on the structure.

At 30° the overall wind load is 14% higher on port side with respect to the same wind at starboard side. This is the overall highest difference in wind loading as a result of wind angle. At the 90° wind angle the difference is 4% between a port and starboard side wind.

When evaluating the moment about the x axis in figure 4.11b, it is seen that there is a generally larger overturning moment when the wind is angled of the port side of the crane. Exception to that is when the wind is coming from a 60° to 180° angle. At the 90° wind angle the difference is 3% between a port and starboard side wind. Around the overall maximum overturning moment, which can be found at a 75° port side wind, the difference was found to be as high as 6%.

For both horizontal force and overturning moment the overall trend is the similar showing an M-shaped curve with the dip at 90°. The difference in wind loading behaviour between water side and land side is noted and suspected to be the result of the landward placement of the lower staircase.

When repeating these tests without the mesh screens, the staircases, it is suggested that they have the biggest influence on the asymmetrical behaviour of the crane. This effect can be seen in figures 4.11c 4.11d where the horizontal forces and overturning moments about the x axis are shown.
When further removing asymmetrical elements in the form of the cable rail which is suspended on the port side of the boom and bridge girder, this difference becomes even smaller, which is as expected. This can be seen in figures 4.11e and 4.11f Small asymmetric differences are still observed and are considered the result of asymmetric construction of the machine house and the presence of the HV cable reel.

yz plane asymmetry
To evaluate the effect of the yz plane asymmetry, the influence of the wind is examined in the cases of onshore and offshore wind. For this evaluation, auxiliary elements are not considered as they introduce additional asymmetry which is not under consideration in this case. The yz plane asymmetry is eva by comparing the wind in the 0° ±90° and 180° ±90° cases.

Comparing the horizontal force for onshore and offshore wind, little difference is found. From both the graph, figure 4.12, and the data it is shown that the forces are within ±6% of each other at the most, with the overall difference being 0%. This indicates that both sides are equally unaerodynamic.

When evaluating the moments about the x and y axes, differences show. Regarding moments about the x axis, offshore wind shows a tendency to incur higher moments on the structure than onshore winds. Whilst the percentual difference in CMx is large at a small wind angle deviation from the x axis, the absolute difference is small. Comparing the CMx to the CFhor, it can be seen that whilst the overall force is quite similar, the centre of load is shifted depending on whether the wind is onshore of offshore. Regarding moments about the y axis, the overall trend is similar whilst there being differences between port and starboard side winds. Again, as with the CMx, this variation is not found in the horizontal force coefficient CFhor and as such this means that the centre of load is shifted. Variation about this axis is bigger with respect to the wind angle but this is also expected since the machine house has an xz plane asymmetry which is suspected to influence CMy in this instance.

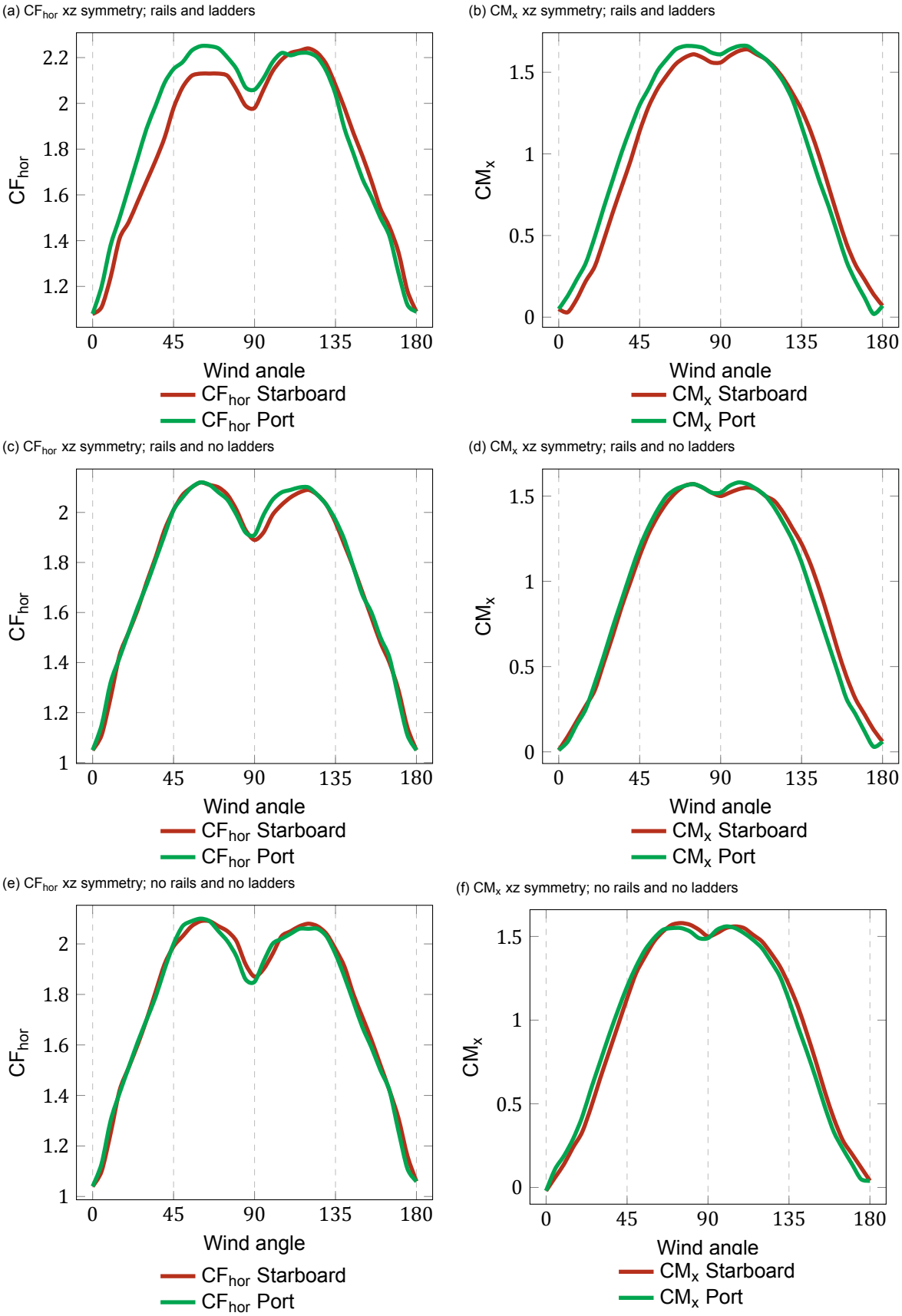

Figure 4.11: Graphs comparing the port side and starboard side of the crane for various levels of auxiliary components.

(a) CF_{hor} yz symmetry

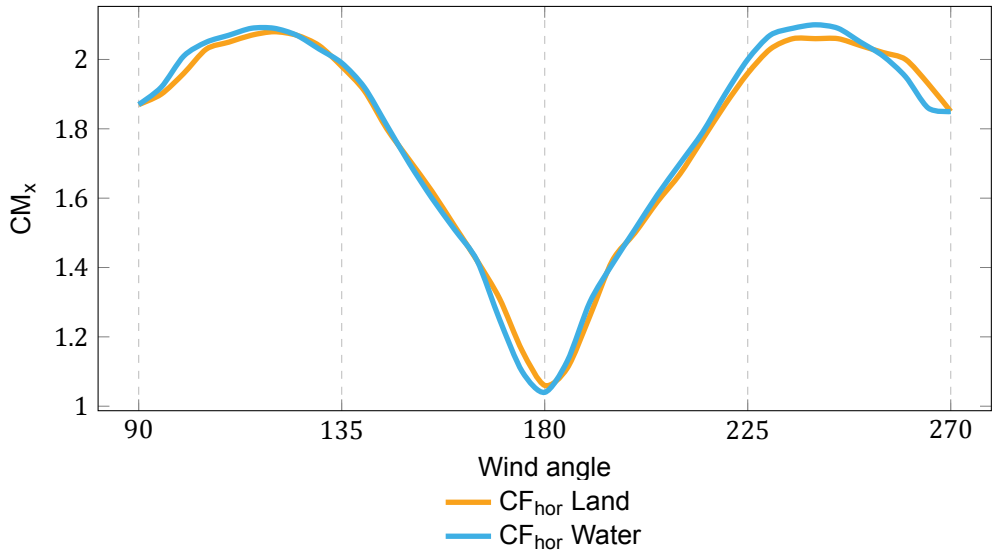

(b) CM_x yz symmetry

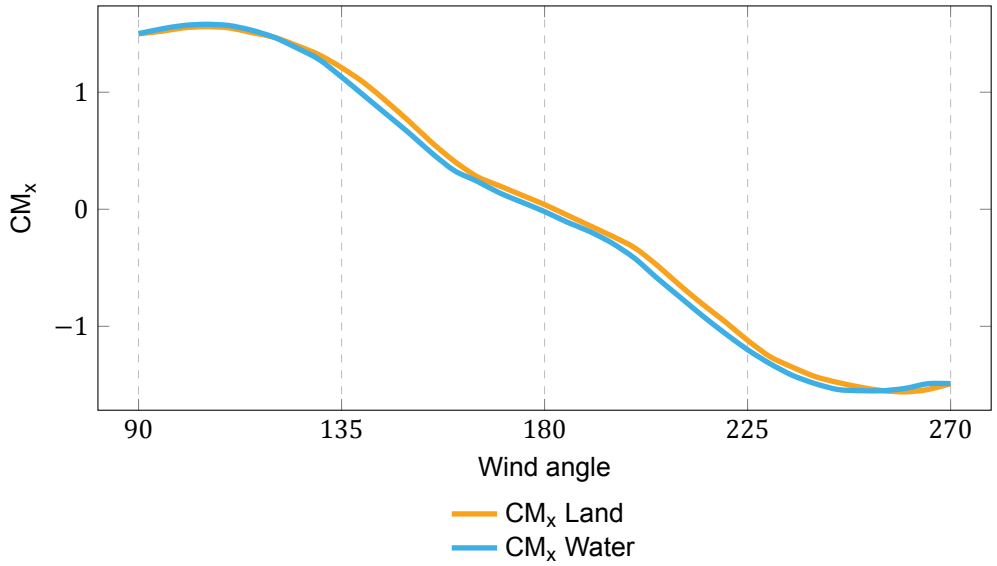

(c) CM_y yz symmetry

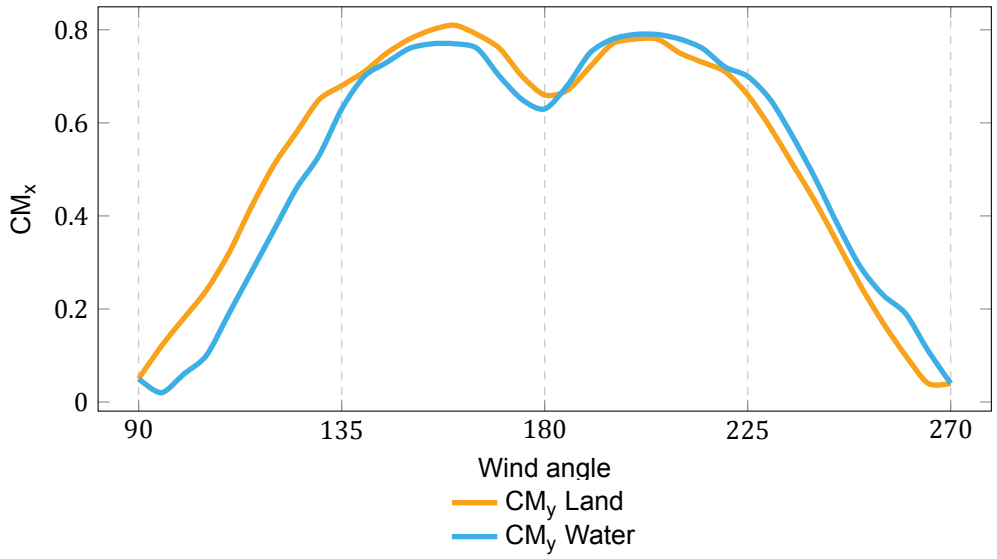

Figure 4.12: Graphs comparing the water side and land side of the crane.

4.5.3. Auxiliary elements

The effect of the auxiliary elements has been shown in the previous sections comparing two sides of the model with and without these elements. In this section the explicit effect of these elements will be presented by comparing the measurements from runs with and without elements.

The forces and moments for the crane in boom down configuration with 3 levels of auxiliary elements, as explained in section 4.2.2, are shown in 4.13. In figure 4.13a a difference in horizontal force can be observed. The mesh staircases cause the biggest difference in force, whilst the cable rail, although spanning a large section, show a smaller difference. In figure 4.13c it can be seen that the this difference is primarily the result of a difference in force in the y direction. When analysing the moments in figure 4.13d the same trend is visible.

The forces and moments for the crane in boom up configuration are shown in figure 4.14, and for the intermediate boom configuration in figure 4.15. The measurements for the boom up configuration series without any auxiliary elements are omitted as they produced unreliable results which could not be properly explained. Both the boom up and intermediate boom configuration show similar trends in forces and moments as the boom down configuration.

From these measurements it is seen that the following differences were found due to auxiliary elements:

- Mesh stair cases:
  - Up to 7% reduction in horizontal force.
  - Average force reduction of 5% between 210° and 340° wind angles.
  - Up to 6% reduction in horizontal moment, where the moment about the x axis has the largest contribution.
  - A relatively large, but absolutely small change moment about the vertical axis, figure 4.13f
- Cable rails:
  - Up to 3% reduction in horizontal force.
  - Average force reduction of 2% between 210° and 300° wind angles.
  - Up to 1% reduction in horizontal moment, where the moment about the x axis has the largest contribution.

4.5.4. Effect of boom position

The effect of the boom position affects the wind actions acting on the crane. The result of this is a change in how forces and stability are affected as a result of rotation.

When the boom is hoisted from its horizontal to a near vertical position, the axis about which the boom rotates changes with respect to the boom. When the boom is hoisted, and the wind angle moves from the cardinal directions, the leeward boom element moves out of the wake of the windward element. As a result the projected area of the crane changes with rotation.

Important: In this section, the crane local coordinate system will be evaluated.

Horizontal force

The effect of the boom position on the horizontal force can be seen in figure 4.16a. From this figure we can see that the general M-shaped trend, as noted in section 4.5.2 is present. The effect of the boom angle can be seen in the variation on the behaviour of this trend.

The effect of the boom angle is that for all cases except ±15° around 90° and 270° the horizontal forces are higher. This is expected behaviour as the silhouetted area of the crane nor the shielding of elements changes with the boom angle. Slight differences are expected and found due to the differences in how elements interact with each other in various boom angles. I.e. the ties and boom are closer together having more interaction in the boom up position than in the boom down position. It is also noted that the height of the arches of the ”M” is more pronounced with increased boom angle. In the boom down scenario the difference between the CFhor at 90° and the highest peak at 120° is 13%. At the intermediate scenario the peak shifts slightly to 125° and the difference with 90° is 21%. At boom up, this difference comes to 26%.

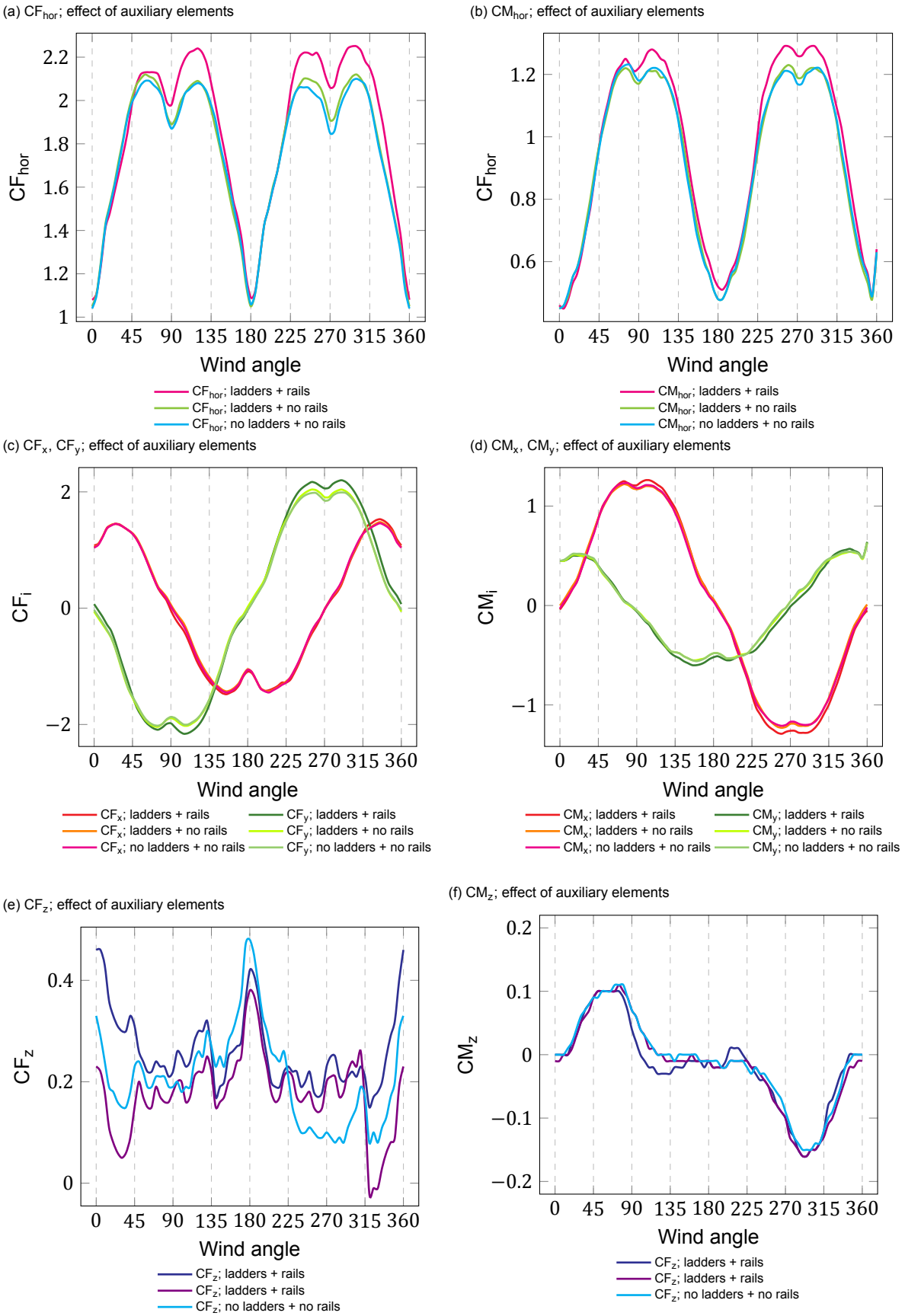

Figure 4.13: Graphs showing the effect of auxiliary components in the boom down configuration.

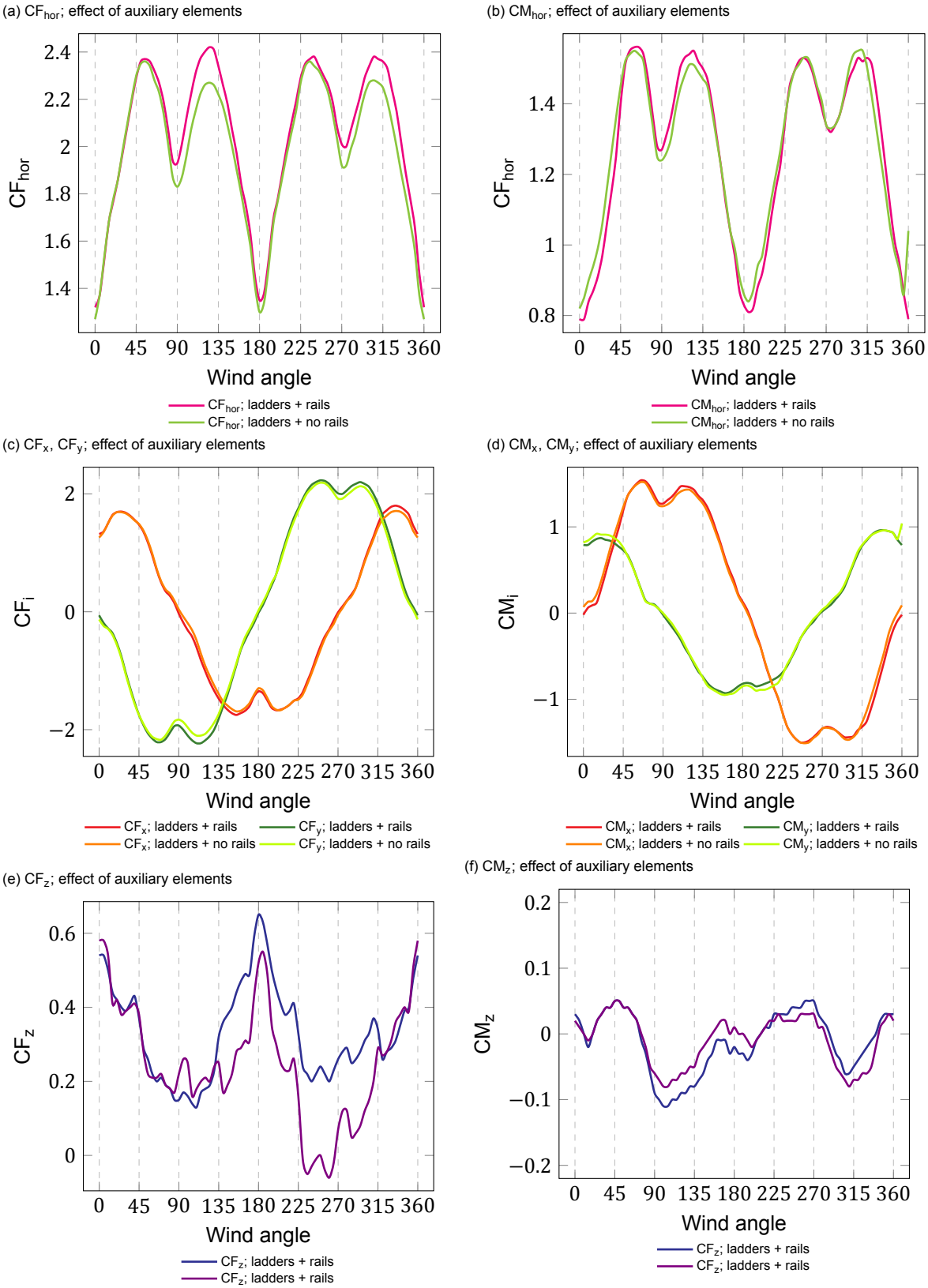

Figure 4.14: Graphs showing the effect of auxiliary components in the boom up configuration.

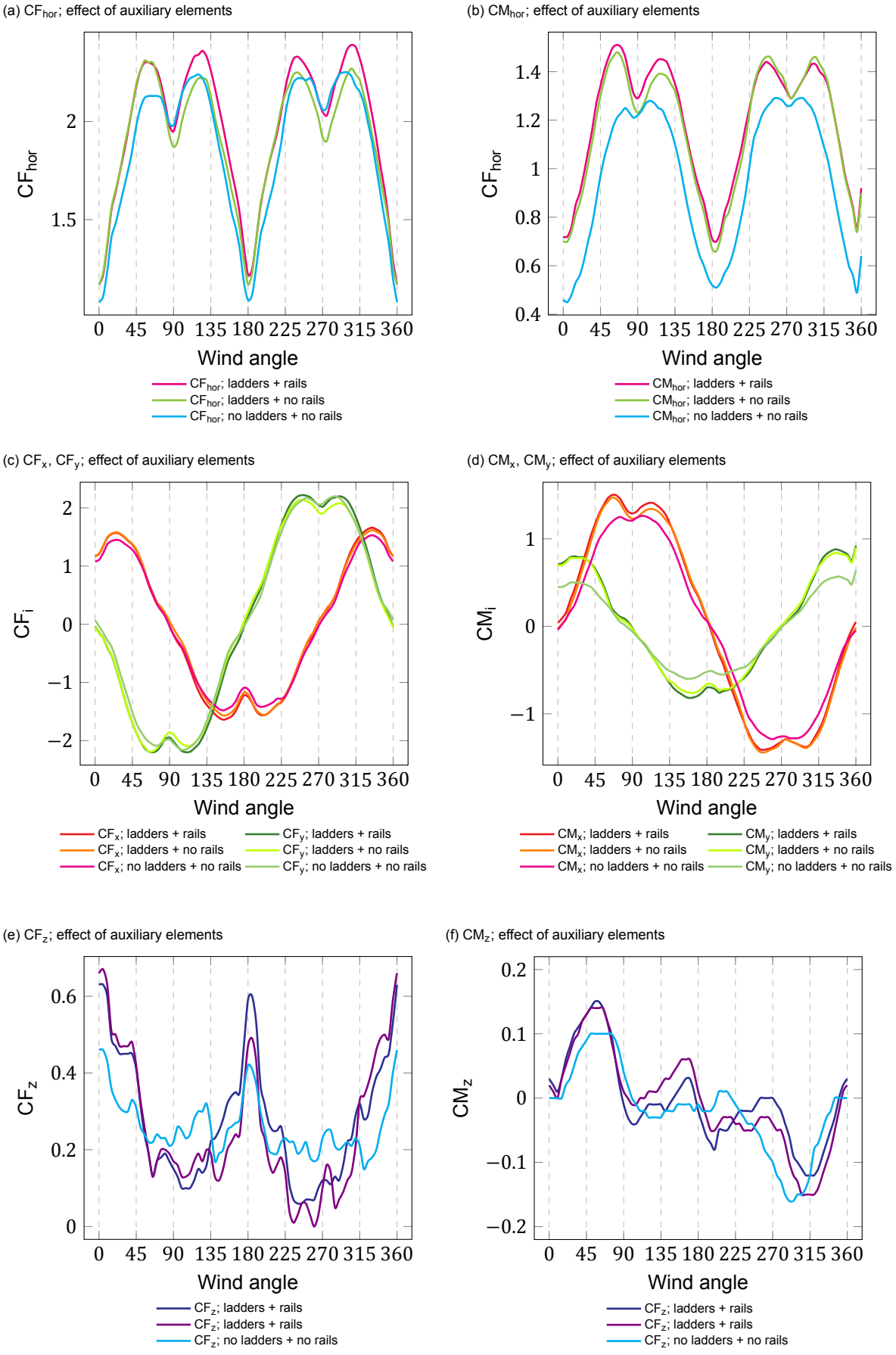

Figure 4.15: Graphs showing the effect of auxiliary components in the boom up configuration.

Moments

In all 3 boom configurations, the horizontal moment increases with the boom angle. This is explained by the fact that the projected area of the boom becomes larger in all wind angles except the 90° and 270° wind angles. Additionally, the centre of load shifts upwards as a result of the hoisting of the boom. This is demonstrated through the higher CMx at the 90° and 270° wind angles. The overall effect of the boom position on the horizontal moment can be seen in figure 4.16b.

When looking at the moment about the x axis in figure 4.16c we can see that whilst the moment about the x axis at 90° and 270° wind angles does not change significantly, a 4% and 5% increase respectively, the maximum moment does change significantly. Where the maximum CMx in the intermediate and up position is 15% and 18% higher respectively. The wing angle for where this maximum occurs shifts from 105° in the boom down position to 70° in the intermediate boom position and 35° in the boom up position.

For the moment about the y axis another trend is observed. The M-shaped trend is visible and is exaggerated with increased boom angle. This effect is mostly observed at wind angles near perpendicular to the yz plane, whilst fading away as the wind turn towards the xz plane. The effect of hoisting the boom is most pronounced at the 0° wind angle, where hoisting the boom leads to a 44% and 59% CMy increase in the intermediate boom and boom up positions respectively.

When evaluating the moment about the z axis, another trend is noticed. In figure 4.16d it can be seen that in the boom down configuration, the moment about the z axis is dominated by the force acting on the boom. In the intermediate boom position the moment about the z axis still seems dominated by the effect of the boom, however a relative flat spot is found between the wind angles of 90° and 270°. In the boom up configuration the effect of the boom is noticeably less and between 75° and 285° the moment about the z axis seems dominated by the machine house.

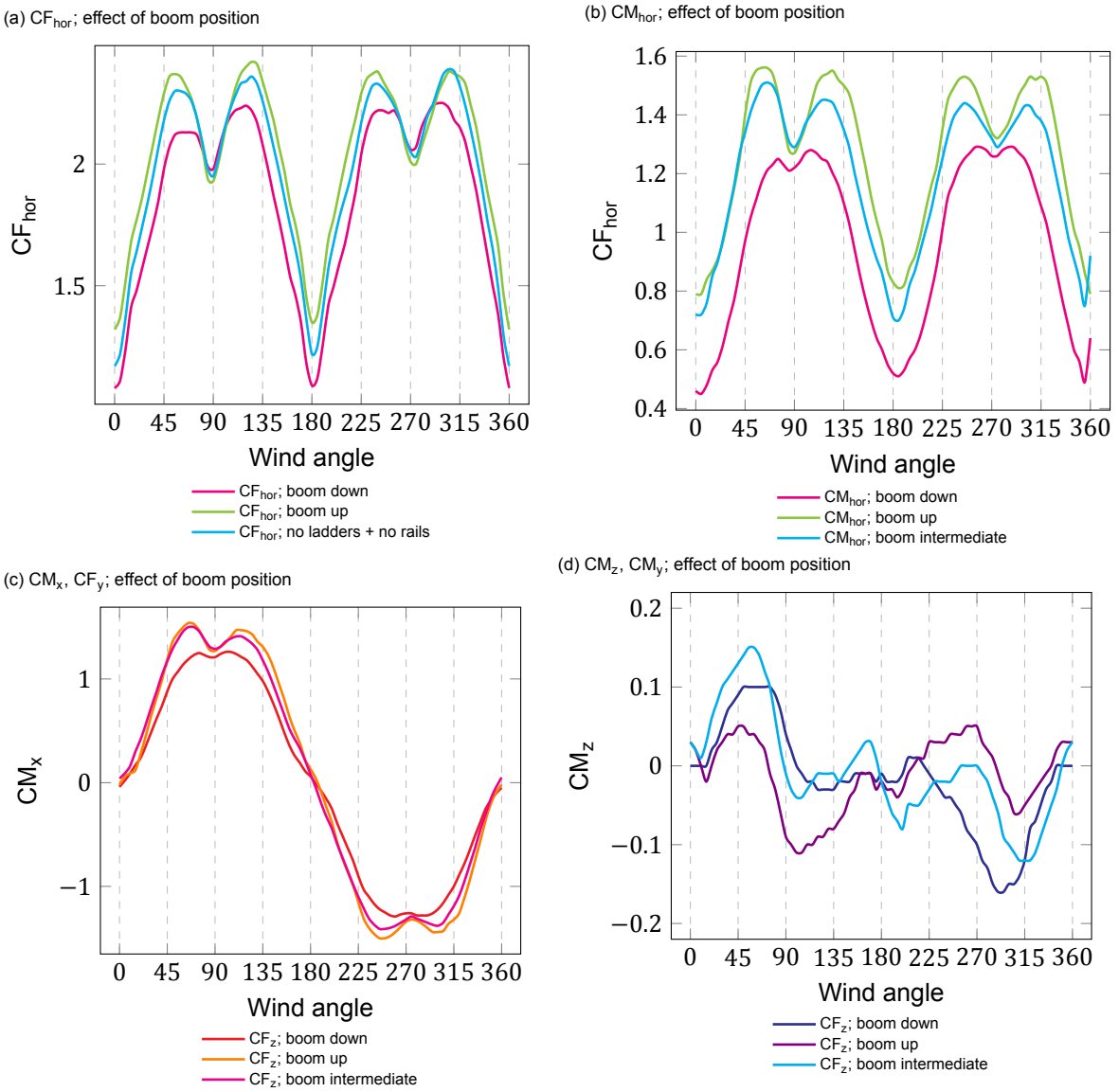

Figure 4.16: Various force and moment graphs for 3 different boom configurations

4.5.5. Reaction forces and stability

The aerodynamic behaviour of the crane has been examined in previous sections. The reaction forces of the crane are evaluated at the points where the bogeys would connect to the frame. This results in four corners in which forces in crane local x, y, and z can be evaluated. Stability is then evaluated by calculating the reaction forces in z direction, where positive z force would indicate leg lift.

Corner forces are calculated as per equations 4.7, 4.8, and 4.9:

$$F_{x,i} = \frac{F_{x,local}}{4} + \frac{M_{z,local}}{4d_{y,i}} \tag{4.7}$$

$$F_{y,i} = \frac{F_{y,local}}{4} + \frac{M_{z,local}}{4d_{x,i}} \tag{4.8}$$

$$F_{z,i} = \frac{F_{z,local}}{4} + \frac{M_{x,local}}{4d_{x,i}} + \frac{M_{y,local}}{4d_{y,i}} \tag{4.9}$$

This calculation does not take into account the construction properties of the frame such as stiffness, i.e. the frame is assumed of infinite stiffness. As such, these are the instantaneous reaction forces. It also assumes that all loads are spread evenly and fully, as well as that no moments are transferred through the corners.

The difference between equations 3.1 & 3.2, and 4.7 & 4.8 is that the moment about the z axis, M_z is not accounted for. For equation 3.3 and 4.9 is that only the moment about either the x or y axis is accounted for, depending on which configuration is calculated. This is a simplified calculation and is thought to contribute to the variation found in wind tunnel corner loads, which is absent in the standard calculations.

Reaction forces in x direction

The reaction forces in x direction are the reaction forces which act perpendicular to the rails, in the xy plane, and result in sideward loading of the rail. This force is a combination of the overal wind force in x direction and a moment about the z axis.

In figure 4.17a it is seen that both legs on the port side show equal reaction forces as well as both legs on the starboard side. It is noted that the water side and land side have different reaction forces, it is thought that this is the result of the asymmetrical construction of the crane about the yz plane, as discussed in section 4.5.2. This asymmetry results in a moment about the z axis which results in different reaction forces between the two sides.

Hoisting of the boom results in a change in x direction reaction forces. This stems from two reasons:

1. The overall force acting on the crane is higher (section 4.5.4).
2. The moment about the z axis changes as a result of a different boom position which changes the forces resulting from the moment about the z axis.

There seems to be no clear trend or correlation between boom angle and reaction forces in the x direction, as was seen in the overall horizontal force in figure 4.13a and moment about the z axis in figure 4.13f.

In line with earlier findings, the maximum reaction forces are not found at the right wind angles. Rather, maximum reaction forces are found at angles that diverge about 30° from the 90° and 180° wind angles to either side. Some key points from the reaction force measurements and calculations:

- Boom down, figure 4.17a
  - Starboard side reaction forces are 150% higher at 310° when compared to 0°.
  - Port side reaction forces are 96% higher at 45° when compared to 0°.
  - Offshore winds result in lower reaction forces in x direction than onshore winds.
- Boom up, figure 4.17b
  - Starboard side reaction forces are 96% higher at 325° when compared to 0°.
  - Port side reaction forces are 28% higher at 35° when compared to 0°.

  - There is a lower spread in reaction forces between right wind angles and off wind angles.
  - In contrast to the boom down situation, onshore winds and offshore winds produce similar reaction forces.

- Boom intermediate, figure 4.17c
  - Starboard side reaction forces are 229% higher at 320° when compared to 0°.
  - Port side reaction forces are 88% higher at 45° when compared to 0°.
  - Onshore wind causes a high variation in x reaction forces both between port and starboard sides as well as in absolute numbers.

(a) Reaction forces in x direction per corner, boom down configuration

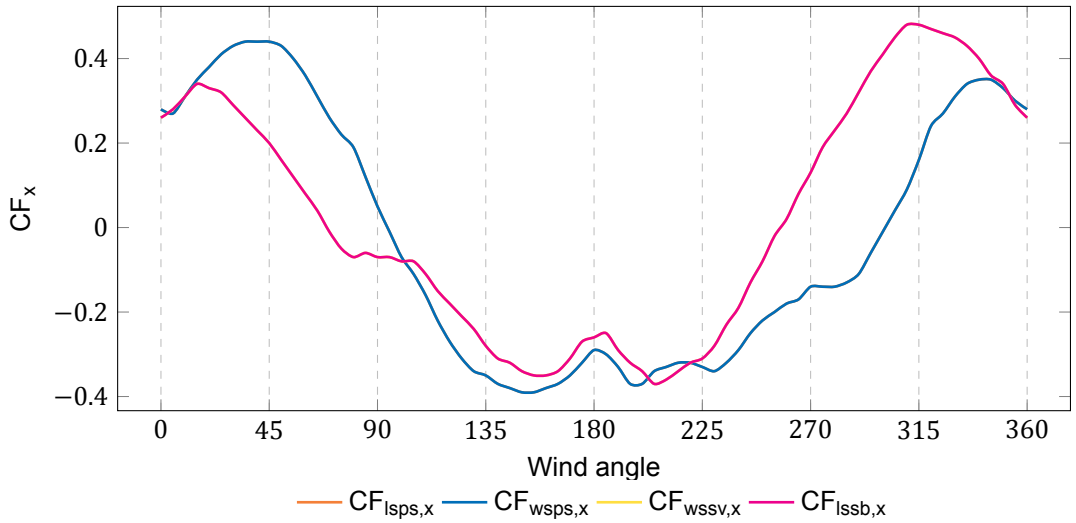

(b) Reaction forces in x direction per corner, boom up configuration

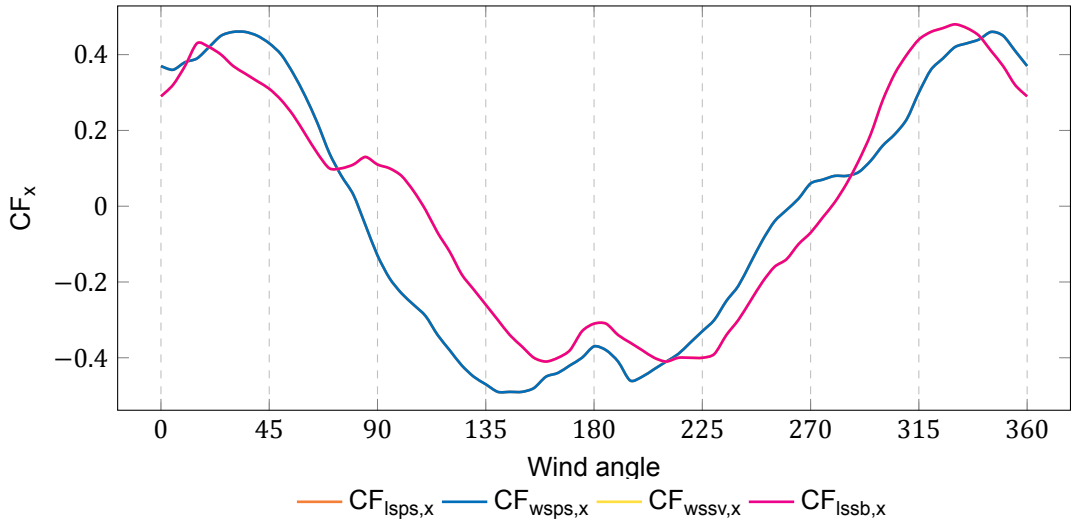

(c) Reaction forces in x direction per corner, boom intermediate configuration

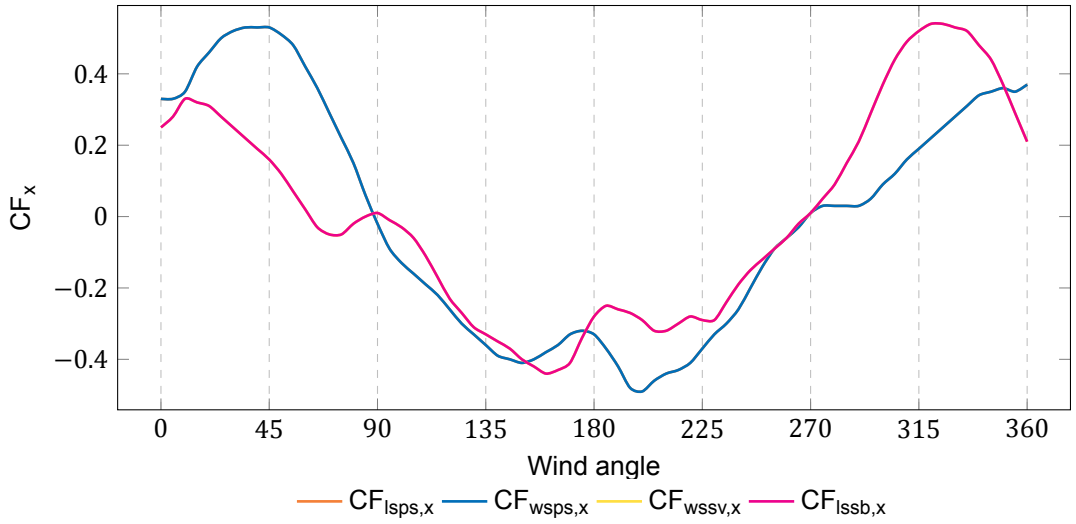

Figure 4.17: Corner reaction forces in x direction for different boom configurations

Reaction force in y direction
The reaction forces in y direction act parallel to the rails in the quay. These forces determine the driving and importantly braking forces required on the crane during storm condition. This force is the result of the overall wind force in y direction and a moment about the z axis.

In figure 4.18a it is seen that reaction forces on the water side, as well as the land side are equal. Similar behaviour was noted in the reaction forces in x direction in section 4.5.5.

Reaction forces in the y direction vary substantially less with both wind direction and boom configuration when compared to reaction forces in the x direction.
Some key points from the reaction force measurements and calculations:

- Boom down, figure 4.18a
  - Water side reaction forces are 17% higher at 75° when compared to 90°.
  - Land side reaction forces are 27% higher at 110° when compared to 90°.
  - The disparity between the reaction forces on the land side as opposed to the water side is larger at 90° than at 270°. The difference between port side and starboard side wind is in line with the wind actions measured in section 4.5.2.
- Boom up, figure 4.18b
  - Water side reaction forces are 59% higher at 65° when compared to 90°.
  - Land side reaction forces are 17% higher at 35° when compared to 90°.
  - There is a lower min-max spread at port side compared to starboard side.
- Boom intermediate, figure 4.18c
  - Water side reaction forces are 50% higher at 65° when compared to 90°.
  - Land side reaction forces are 18% higher at 105° when compared to 0°.
  - There is a lower min-max spread at port side compared to starboard side.

(a) Reaction forces in y direction per corner, boom down configuration

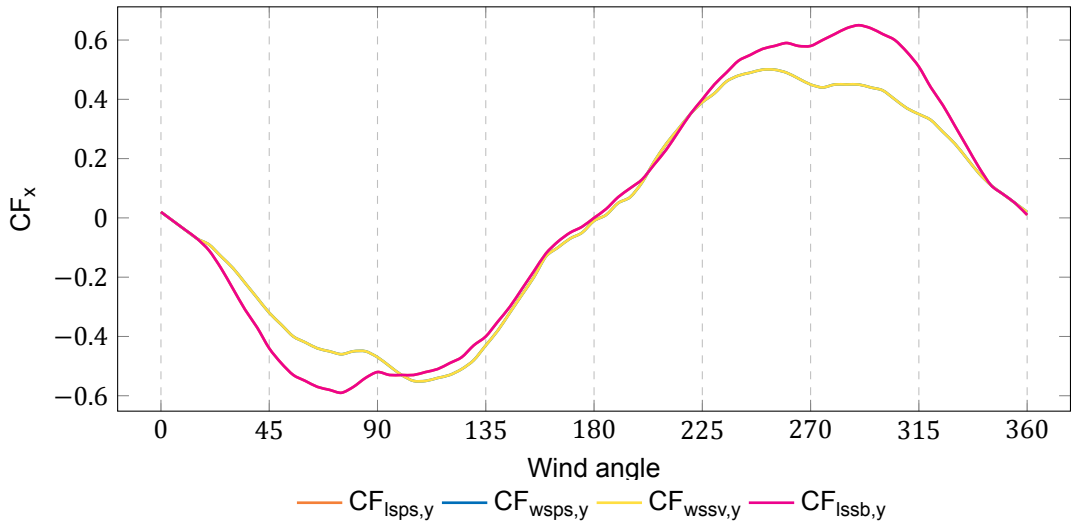

(b) Reaction forces iy x direction per corner, boom up configuration

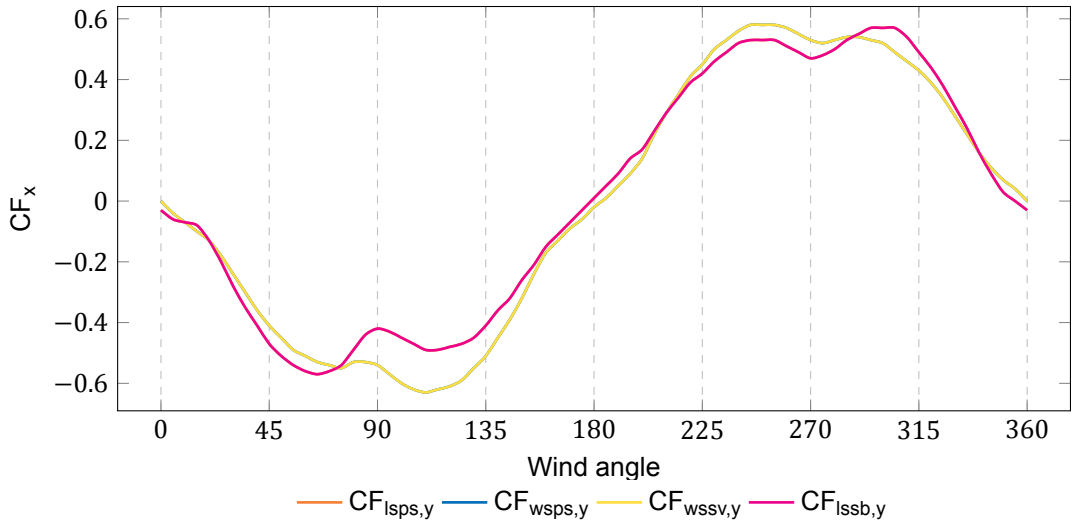

(c) Reaction forces in y direction per corner, boom intermediate configuration

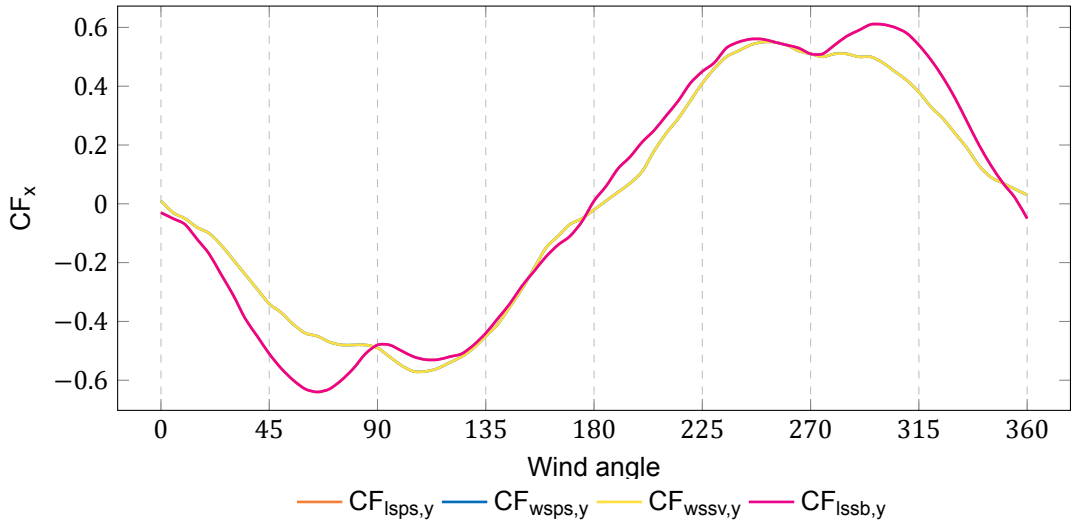

Figure 4.18: Corner reaction forces in y direction for different boom configurations

Reaction force in z direction

The reaction forces in the z direction act perpendicular to the rail and the xy plane. These forces are paramount for determining stability of the crane as well as calculating forces on tie downs and corner loads. This force is the result of the overall force in z direction, i.e. lift or down force, and the moments about the x and y axis.

The reaction forces in z direction globally follow the same trends as the moments about the x and y axis, showing peaks and valleys at similar points. It was expected that the reaction forces from overturning moments would be greater than that of lift or down force.

For all investigated boom configurations it holds true that the most lift and down force were found at sidewards wind, i.e. wind from either port side or starboard side, with individual peaks found at angles that deviate between 20° and 30° from the right angles. This is in line with forces and moments earlier discussed in sections 4.5.1. The footprint of the crane is larger in the x direction than in the y direction, which also contributes to the explanation of this phenomenon. Some key points from the reaction force measurements and calculations:

- Boom down, figure 4.19a
  - The maximum lift on a corner is typically 10% to 13% higher at winds coming from 90°±25° and 270°±25° angles.
  - The maximum downwards force on a corner is typically 10% to 12% higher at winds coming from 90°±25° and 270°±25° angles.
- Boom up, figure 4.19b
  - The maximum lift on a corner is typically 24% to 35% higher at winds coming from 90°±25° and 270°±35° angles.
  - The maximum downwards force on a corner is typically 25% to 35% higher at winds coming from 90°±25° and 270°±25° angles.
  - The min-max differences are more pronounced with the boom up compared to the boom down position. Similar behaviour was seen with the forces and moments.
- Boom intermediate, figure 4.19c
  - The maximum lift on a corner is typically 19% to 26% higher at winds coming from 90°±30° and 270°±35° angles.
  - The maximum downwards force on a corner is typically 20% to 26% higher at winds coming from 90°±25° and 270°±25° angles.
  - The min-max differences are less pronounced with the boom in the intermediate position compared to the boom up position, however still significantly more pronounced than in the boom down position.

(a) Reaction forces in z direction per corner, boom down configuration

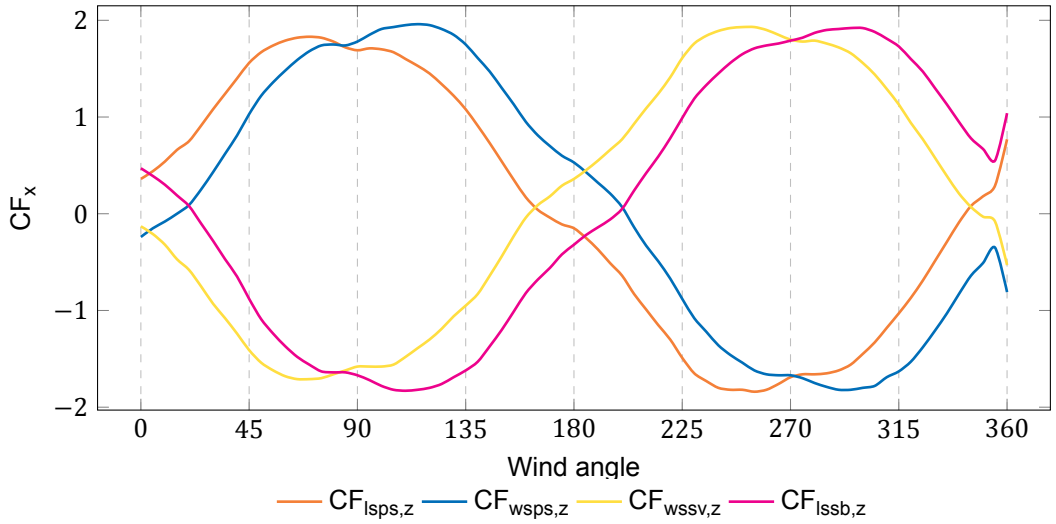

(b) Reaction forces in z direction per corner, boom up configuration

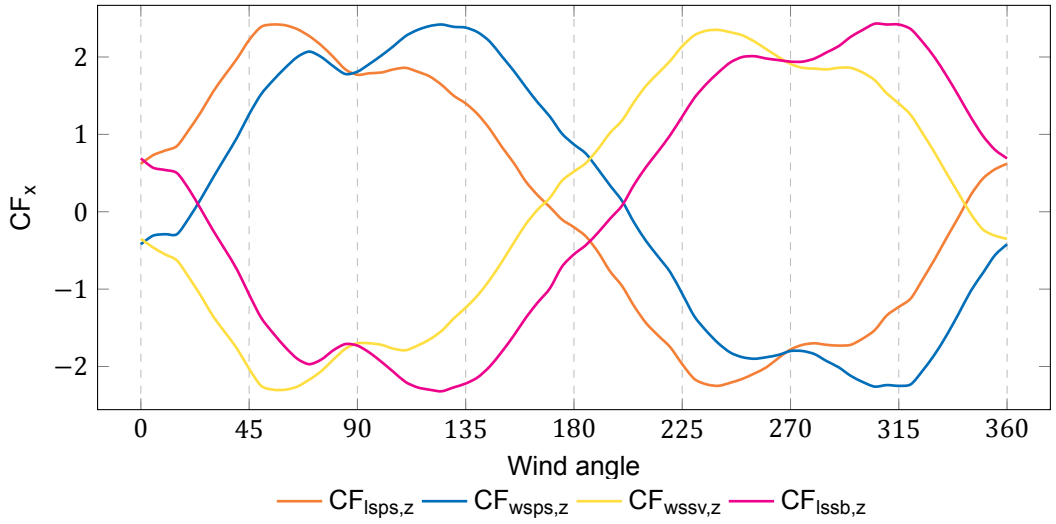

(c) Reaction forces in z direction per corner, boom intermediate configuration

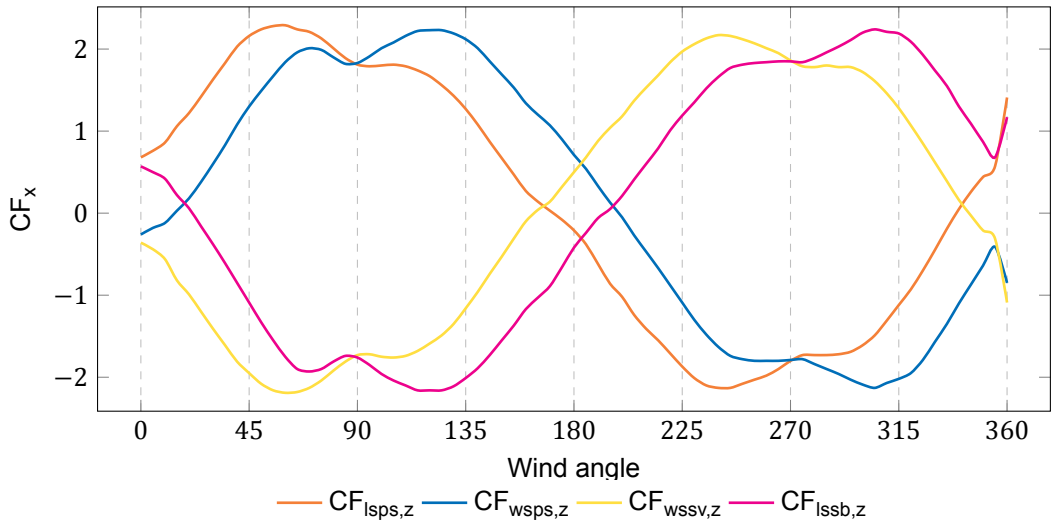

Figure 4.19: Corner reaction forces in z direction for different boom configurations

4.6. Comparing to standards

Wind tunnel testing is the golden standard regarding the determination of wind actions on STS cranes. As such all calculations are to be compared and examined against these measurements. For these comparisons only the EN 13001-2 will be considered. This European Standard is the most recent of the four considered and as such deemed the most representable.

4.6.1. General forces and moments

The general forces in x and y direction, as well as the general moments about the x and y axis, are presented in table 4.4 for the following cases:

- Wind tunnel at 0° and 90°
- Maximum forces and moments found in the wind tunnel
- EN 13001-2 calculations

For the wind tunnel 0° wind angle case, the highest value was selected from the 0° and 180° cases. Likewise, the highest value of the 90°, 270° pair was chosen for the 90° case.

The values for the boom up position in the wind tunnel are absent due to a measurement error and are therefore omitted from this overview.

From these results there are a few key observations:

- Comparing standard calculations according to the EN 13001-2 to the wind tunnel measurements at 0° and 90° yields a big difference between calculated force and wind tunnel measurement.
- Comparing standard calculations according to the EN 13001-2 to the maximum values found in the wind tunnel reduces this difference significantly.

From these observations it is clear that when evaluating standard calculations against wind tunnel measurements, care should be taken to evaluate not only the right angles, but also the maximum values.

		EN 13001-2	Wind tunnel 0°/90°	difference %	Wind tunnel maximum	difference %
Boom up	F_x	22.49	13.01	72.9%	17.86	25.9%
	F_y	32.17	22.85	40.8%	24.77	29.9%
	M_y	6.39	3.11	105.4%	4.15	54.1%
	M_x	10.96	7.70	42.3%	8.04	36.3%
Boom intermediate	F_x	26.64	14.73	80.9%	19.76	34.8%
	F_y	32.30	22.48	43.7%	25.89	24.8%
	M_y	9.67	4.59	110.5%	5.95	62.5%
	M_x	12.46	8.23	51.3%	9.30	34.0%

Table 4.4: Comparison of the EN 13001-2 standard and wind tunnel measurements

4.6.2. Reaction forces

The reaction forces per corner for the EN 13001-2 standard calculation and wind tunnel measurements are shown in tables 4.5, 4.6, and 4.7 for the forces in the x, y, and z directions respectively.

Comparing the equations for calculating the reaction forces in standard calculations (eq. 3.1,3.1, and 3.2) to those used for the wind tunnel measurements (eq. 4.7,4.7, and 4.8) it can be seen that the reaction forces calculated with the wind tunnel data are comprised of more components. From section 4.5.5 it was seen that these extra components have an influence on the reaction forces and introduce asymmetry. For this reason the following data is presented:

- Reaction forces calculated from EN 13001-2
- Reaction forces calculated from the wind tunnel measurements at cardinal wind angles (0°, 90°, 180°, and 270°)
- Reaction forces calculated from maximum values obtained in the wind tunnel measurements

The wind tunnel values are presented as both their maximum and minimum values. For the z direction especially this is of importance since the maximum and minimum values represent downwards pressure and lift respectively, which are different design considerations.

Reaction forces in x direction

For cardinal angles, the reaction forces in the x direction are found to behave similarly to the general forces in the x direction. However, when considering the maximum and minimum force measured in the wind tunnel, the results are closer together.

Some key points from the reaction force calculations and comparisons:

- Reaction forces from wind tunnel measurements in cardinal directions are substantially lower than the maximums found.
- Reaction forces from the maximum wind tunnel values are much closer to the standard calculations.

It is thought that at maximum loads, the force is a combination of force in the x direction, y direction as well as moment about the z axis. The latter two of which are not accounted for in the standard calculations.

Reaction forces in y direction

The behaviour in the y direction is similar to the general forces. In all cases, forces measured are lower than those calculated from the standard. The effect of the boom is clearly visible in the asymmetry in reaction forces as the boom generates a moment about the z direction.

Some key points from the reaction force calculations and comparisons:

- The difference between the reaction forces from wind tunnel measurements in the cardinal directions and the maximum values is less pronounced than in the x direction.
- Standards do not differentiate between the boom positions for the force in y direction and this shows in the reaction forces in y direction.

Where the calculated reaction forces in the x direction were in certain cases higher than the maximums found in the wind tunnel, no such thing was seen in the y direction. The effect of the boom and boom position was clearly observed.

Reaction forces in z direction

The reaction forces in the z direction show the most variance in the wind tunnel results. All four corners show different results for the same wind angle. In all cases, the EN 13001-2 is conservative when calculating these loads.

Some key points from the reaction force calculations and comparisons:

- EN 13001-2 is conservative in all cases considered.

- Since the maximum values measured in the wind tunnel do not occur at once, stability is never considered an issue.

In all cases the reaction forces calculated from the wind tunnel measurements were below the values calculated with the EN 13001-2 standard. This is postive from a safety point of view but also leaves room for improvement.

		EN 13001-2	Wind tunnel cardinal +	diff %	Wind tunnel cardinal -	diff %	Wind tunnel maximum +	diff %	Wind tunnel maximum -	diff %
Boom down	$F_{LSPS,x}$	±5.62	3.20	-43%	-3.44	-39%	5.49	-2%	-4.66	-17%
	$F_{WSPS,x}$	±5.62	3.20	-43%	-3.44	-39%	5.49	-2%	-4.66	-17%
	$F_{WSSB,x}$	±5.62	3.17	-44%	-3.07	-45%	5.98	6%	-4.41	-21%
	$F_{LSSB,x}$	±5.62	3.17	-44%	-3.07	-45%	5.98	6%	-4.41	-21%
Boom intermediate	$F_{LSPS,x}$	±6.34	3.87	-39%	-3.92	-38%	6.23	-2%	-6.07	-4%
	$F_{WSPS,x}$	±6.34	3.87	-39%	-3.92	-38%	6.23	-2%	-6.07	-4%
	$F_{WSSB,x}$	±6.34	3.42	-46%	-3.45	-46%	6.80	7%	-5.63	-11%
	$F_{LSSB,x}$	±6.34	3.42	-46%	-3.45	-46%	6.80	7%	-5.63	-11%

Table 4.5: Comparison of reaction forces per corner in the x direction

		EN 13001-2	Wind tunnel cardinal +	diff %	Wind tunnel cardinal -	diff %	Wind tunnel maximum +	diff %	Wind tunnel maximum -	diff %
Boom down	$F_{LSPS,y}$	±8.04	6.40	-20%	-6.29	-22%	7.32	-9%	-7.08	-12%
	$F_{WSPS,y}$	±8.04	4.94	-39%	-5.13	-36%	5.68	-29%	-5.96	-26%
	$F_{WSSB,y}$	±8.04	4.94	-39%	-5.13	-36%	5.68	-29%	-5.96	-26%
	$F_{LSSB,y}$	±8.04	6.40	-20%	-6.29	-22%	7.32	-9%	-7.08	-12%
Boom intermediate	$F_{LSPS,y}$	±8.07	5.79	-28%	-5.59	-31%	7.50	-7%	-7.39	-8%
	$F_{WSPS,y}$	±8.07	5.44	-33%	-5.63	-30%	6.09	-25%	-6.35	-21%
	$F_{WSSB,y}$	±8.07	5.44	-33%	-5.63	-30%	6.09	-25%	-6.35	-21%
	$F_{LSSB,y}$	±8.07	5.79	-28%	-5.59	-31%	7.50	-7%	-7.39	-8%

Table 4.6: Comparison of reaction forces per corner in the y direction

		EN 13001-2	Wind tunnel cardinal +	diff %	Wind tunnel cardinal -	diff %	Wind tunnel maximum +	diff %	Wind tunnel maximum -	diff %
Boom down	$F_{LSPS,z}$	±26.97	20.12	-25%	-19.18	-29%	22.06	-18%	-20.96	-22%
	$F_{WSPS,z}$	±26.97	20.98	-22%	-19.86	-26%	22.97	-15%	-22.02	-18%
	$F_{WSSB,z}$	±26.97	19.80	-27%	-18.99	-30%	21.59	-20%	-20.81	-23%
	$F_{LSSB,z}$	±26.97	20.47	-24%	-19.84	-26%	22.72	-16%	-21.70	-20%
Boom intermediate	$F_{LSPS,z}$	±29.69	20.75	-30%	-21.14	-29%	26.63	-10%	-26.13	-12%
	$F_{WSPS,z}$	±29.69	20.87	-30%	-21.33	-28%	26.08	-12%	-26.62	-10%
	$F_{WSSB,z}$	±29.69	21.39	-28%	-20.34	-31%	26.11	-12%	-25.96	-13%
	$F_{LSSB,z}$	±29.69	21.58	-27%	-20.46	-31%	27.51	-7%	-25.51	-14%

Table 4.7: Comparison of reaction forces per corner in the z direction

4.7. Wind tunnel smoke tests

During the wind tunnel testing, smoke tests were performed with a smoke generator with the air velocity set to 6m/s. The aim of these experiments was to visualise the air-crane interaction.

Figure 4.20a shows a typical scene from the smoke testing. In this figure, it can be seen how the model was placed in the open jet stream and a smoke trace was trailing from the smoke generator. The chosen air velocity of 6 m/s was selected based on several criteria.

- Air velocity must be sufficiently high to produce a neat smoke trace.
  - When the air velocity is too low, the smoke will diffuse too fast making it more difficult to produce neat smoke trails.
- Air velocity must not be so high as to create a dangerous working environment.
  - As seen in figures 4.20a and 4.20b various cameras were setup around and about the crane. These cameras were not secured and a too high air velocity would pose the risk of flying objects, which was unwanted since that would not produce useful footage.
  - As seen in figure 4.20a manual operation of the smoke generator was required. This required a person near or in the jet stream. To ensure safety of the smoke generator operator, the air velocity was also kept to a minimum.

The smoke generator works by vaporising and heating theatre smoke which creates a thick, white smoke. Whilst the smoke produced is not buoyancy neutral, for visualising the flow patters it was deemed sufficient.

Deflection of the smoke trail was observed around multiple sections as seen in figure 4.21 This deflection of the smoke trail indicates that air flows around members and how it returns to an original position. In figure 4.21a is is visible how the smoke trail ducks under the cross girder and only returns to the original height after passing the second cross girder. This visualises how the first member influences the second member. The distance between the members is $7.5d$ where d is the breath of the cross girder across the wind font. In figure 4.21b similar deflection of the wind can be seen around the machine house. Note that the smoke traces cleaner around the machine house than it does around the cross girder.

(a) Testing with the smoke generator, several cameras used for capturing the smoke trail are also visible in this photo.

(b) Closeup of the camera setup used for the top-down footage

Figure 4.20: Smoke testing and setup.

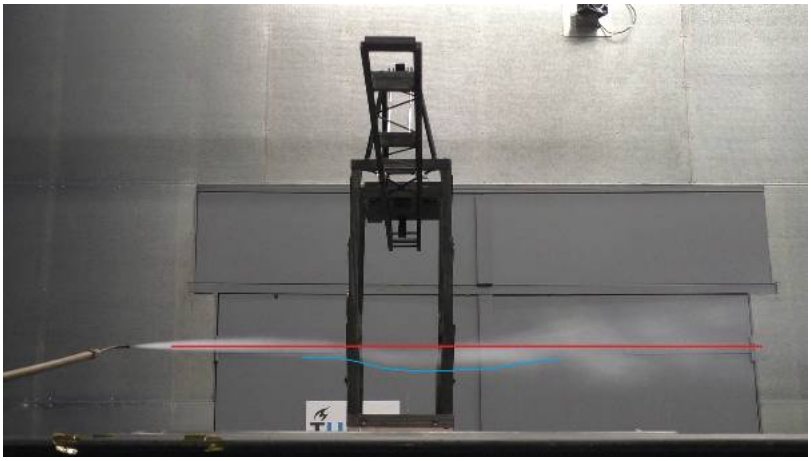

(a) Smoke deflection due to the cross girder at 90° wind.

(b) Smoke deflection due to the machine house at 315° wind.

Figure 4.21: Smoke testing and setup.

5

Computational Fluid Dynamics

“Nevertheless, the basic question remains: what is actually computational fluid dynamics? In retrospect, it has certainly become a new branch integrating the disciplines of fluid mechanics not only with mathematics but also with computer science [...]”[39]

“CFD (computational fluid dynamics) is a set of numerical methods applied to obtain approximate solutions of problems of fluid dynamics and heat transfer.” [44]

Computational fluid dynamics focuses on analysing and solving problems involving fluid flow. To accomplish this, computers are used to solve an incomprehensible amount of calculations from which fluid characteristics and properties can be evaluated. The fundamental basis for (almost) all CFD calculations are the Navier-Stokes equations, which define many single-phase fluid flows. With this in mind, computational fluid dynamics are a very interesting and promising tool for calculating accurate wind loads on STS cranes without the use of expensive wind tunnel testing, as well as gaining new insights in air flow around to crane structure for design optimisation.

This chapter will focus on the methods used for the computational fluid dynamics. This will be done in two parts: the geometry section and the case section.

The geometry section will detail the creation of the 3D model of the crane, based on the wind tunnel model. The section will cover the practical creation with design choices as well as the preparation of the model for the CFD software.

The case section will detail the setup of the simulation case. The simulation settings and setup will be discussed which was used to run the simulations presented in this thesis.

5.1. Scope

The scope of the CFD analysis is mainly to support the wind tunnel tests performed and standard calculations made. The scope outlined in section 1.2 will be further explained in this section.

- **Single crane geometry**
  As with the wind tunnel test, a single crane geometry will be considered. This is for two reasons:

  1. Direct comparison to the wind tunnel tests is only possible if identical geometries are used.
  2. Investigating more geometries was prohibitively expensive computationally speaking. As such, the scope was limited to only the most useful geometries.

  The chosen geometry is the crane geometry without cable rails or mesh screens which represent staircases. These elements were found to add relatively many cells to the mesh, which would greatly increase computation time whilst offering no real benefit over simpler geometry data wise.

- **Single boom configuration**
  No specific preference was expressed regarding boom configuration in CFD. The boom down configuration was chosen. As CFD is computationally expensive, no other configurations were examined. Boom down (0°) configuration was chosen for this purpose.

- **Three angles of rotation**
  - 0°
  - 60 °
  - 90 °

  The three chosen angles are deemed to deliver the most relevant data. The 0° and 90° wind angles yield data which can be compared to the wind tunnel tests and the standards. The latter being especially of interest since it allows comparison on a part level. The 60° wind angle is the approximate angle of most wind resistance.

- **Uniform wind profile**
  The uniform wind profile with constant velocity was chosen in line with the wind tunnel tests and standard calculations allowing for direct comparison.

Compared to the scope of the wind tunnel test the scope for the CFD analysis is rather limited. This is due to the time constraint of this thesis and the computational resources required to run a single simulation.

Regardless, the selected scope should provide enough relevant data which can be used to achieve the following goals:

- Compare CFD analyses with standard calculations
  - Overall
  - On selected parts comparing drag coefficients calculated by the standards against those found using CFD.
- Compare CFD analyses with wind tunnel tests
- Visualise the flow around the crane structure to gain additional insights.

5.2. Geometry setup

For the CFD analyses, the crane model without aerodynamic elements such as the cable rails and mesh screens which represent the staircases was selected. Furthermore, only the boom down position was evaluated. Since wind tunnel data was obtained for this model setup, the CFD analyses can be validated against real world data.

A good 3D model is necessary to produce quality results. For the setup of the model, a list of requirements was formulated which would serve as a guideline whilst creating the model and as a checklist to verify if the geometry creation was successful. This list is the following:

- Digital model must replicate physical model
- Digital model must be not incur unnecessary mesh elements
- Digital model must be manifold
- Digital model must be solid containing no enclosed volumes

The geometry was created in SOLIDWORKS. The choice for SOLIDWORKS was made based on the following arguments:

- SOLIDWORKS is a widely used 3D CAD software package with an extensive user and support base.
- The author has previous experience with SOLIDWORKS.
- The built-in CAD tool in Star CCM+ sucked balls.

The 3D model created can be seen in figure B.1, with detailed parts in appendix B.

Since the 3D model was to be a digital twin of the physical model, direct measurements could be and were taken from the physical model. The model was then split up in parts and built in a part-by-part manner. Working in this manner had the advantage of being able to edit parts on a by-part basis rather than having to edit the entire geometry.

As one of the requirements was for the model not to incur unnecessary mesh elements, some design details were altered. Most notably, the cable rails and mesh screens which represented the staircases were removed. Early tests revealed that these elements incur a lot of mesh elements while wind tunnel tests show they are not essential for this part of the research. As such, they are omitted.
The physical model contained several other small design elements which were omitted as they would require a high mesh density, whilst it was thought that their influence on the overall measurement accuracy was small. Such elements are screws, nuts and bolts which hinge the boom, and hinges in the forestay. Examples of these design elements and how they are modelled can be found in appendix B. While the influence of these elements is thought to be small, their potential effect is noted and is thought to be in part responsible for the differences found between the CFD analysis and the wind tunnel tests.

The digital model had to be manifold in order for the CFD software to be able to run an analysis. This is unsurprising as a non-manifold geometry cannot exist in the real world. Non-manifold geometry errors commonly found are zero-thickness planes, edges shared by ≠2 faces, and disconnected edges. Due to the in-part construction of the crane assembly, several wrongly shared edges were created but this was subsequently fixed.

No enclosed volumes were created due to all parts being constructed as solids. The problem with this specific criterion arises from the fact that the geometry is subtracted from the virtual wind tunnel to create a flow domain. Any enclosed volumes would result in disconnected volumes in the flow domain leading to computational errors and problems such as instability. No enclosed volumes were created.

To simulate different wind angles, the geometry was to be rotated with respect to the flow domain.

5.3. Case setup

In this section the computational domain definition, the mesh, the solver models, and boundary conditions will be described. These elements together make up the case which were used for the CFD analyses. All settings and models discussed and used can also be found in Annex C.

5.3.1. Computational domain

The computational domain is also referred to as the virtual wind tunnel. Proper sizing of the computational domain is important as an improperly sized computational domain can be the source of errors. As such, several best practice guidelines are formulated which compare the issues found in computational domain restrictions similar to those in wind tunnel testing. Finding comparable issues such as blockage and venturi effects [9][18][38]. For the computational domain there are 4 main dimensions to consider [1]:

- Upstream length
- Downstream length
- Domain width
- Domain height

Upstream length

The upstream length of the domain is important to limit the magnitude of wind-blocking errors [1]. Guidelines [18] often specify upstream lengths in the order of 10H (where H is the model height), these guidelines are formulated for buildings which typically have high solidity ratios. In early experimental phase, this was found to be overly conservative. It is thought that the relatively low solidity ratio of an STS crane, and therefore the lower blockage ratio, has a big influence on the required upstream length.

Downstream length
The downstream length of the domain is important since many complex flow features take place in this region. Turbulence, vortex shedding and wake forming happen downstream from the crane. Since all these features influence the flow around the model, it is important to allow for enough downstream computational domain to fully calculate these effects. The downstream length greatly influences the cells in the resulting volume mesh since wake refinements cast from the geometry is typically 2 to 8 times smaller than the base mesh size.

Similar to upstream length, it was found that a downstream length of 10H [38] to 15H [18] was conservative for the type of geometry being evaluated. The value of 3H [1] was more suitable for this geometry.

Domain height and width
Domain height and width must be chosen sufficiently large as that outwash from geometric members can fully develop. If the domain height and width are not sufficiently large, local venturi effects may occur between the geometry and the walls of the computational domain. Conservative values for the domain height and width were found to be less detrimental for calculation performance as the mesh needs to be less refined in this area.

Virtual wind tunnel
The resulting computational domain was chosen based on the geometry in both a 0° and 90° wind angle configuration such that the model can be rotated without needing adjustments of the computational domain. The domain can be seen in figure 5.1, with two crane orientations.

5.3.2. Volume mesh

The volume mesh was generated with the polyhedral mesher incorporated in Star CCM+. The main advantage of the polyhedral mesher over the trimmed cell mesher is that it more economical in terms of computational resources whilst still maintaining an acceptable degree of accuracy [42].

To tailor the volume mesh to the crane, several custom meshing controls were implemented to fine tune the mesh around areas of interest. Surface controls were used to generate a wake refinement area downstream from the surfaces of the crane. This was done in both a short reaching fine refinement and a longer reaching but coarser refinement. Surface controls were used to dictate cell size at the virtual wind tunnel floor and at the crane geometry surface.

To accurately capture the boundary layer around objects, prism layers were used to control the wall functions. Prism layers are essential for creating a mesh which can accurately capture this phenomenon [35]. For various parts of the geometry, the prism layers were used to control the y^+ keeping it either below 1 or above 30. This is preferred since the buffer layer, the layer between the viscous sublayer and the logarithmic are, is complex to model correctly [35].

For the virtual wind tunnel walls and ceiling, no prism layer was used. The slip condition at those boundaries cause no boundary layer to form, and as such render a prism layers obsolete.

Mesh quality
For a good simulation, a good quality mesh is paramount. Star CCM+ offers the mesh diagnostics tool to check various mesh metrics. These metrics [35] and values are:

- Face validity, table 5.2
  "The face validity is an area-weighted measure of the correctness of the face normals relative to their attached cell centroid."
  Values below 1.0 are considered bad.
- Cell Quality, figure 5.2
  "The cell quality metric algorithm is based on a hybrid of the Gauss and least-squares methods for cell gradient calculation methods."
  Values of 1.0 are considered perfect, below 1.0e-5 are considered bad.
- Volume Change, figure 5.2
  "The volume change metric describes the ratio of the volume of a cell to that of its largest neighbor."
  Values below 0.01 are considered bad.

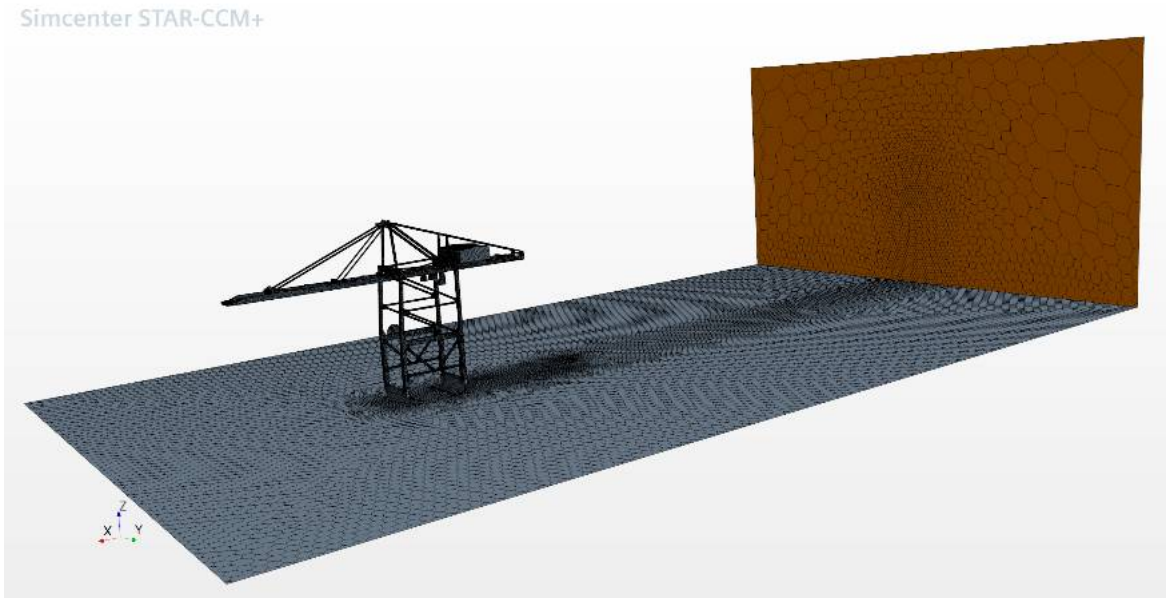

(a) Mesh scene 0° wind.

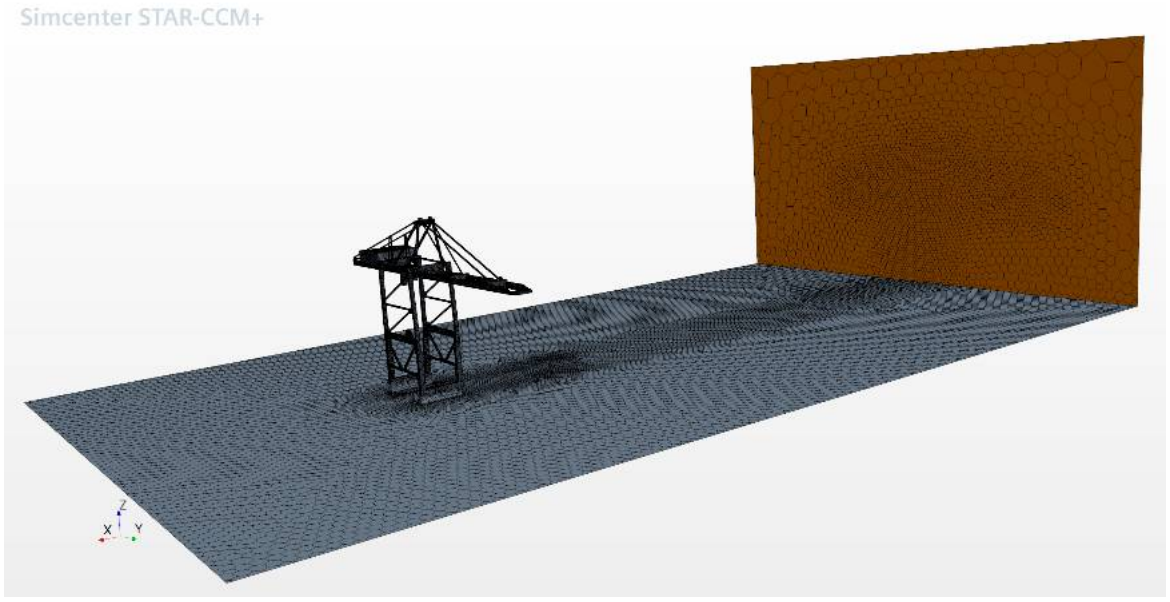

(b) Mesh scene 90° wind.

Figure 5.1: Mesh scenes for 2 wind angles.

- Cell Skewness Angle 5.2
  "This skewness measure is designed to reflect whether the cells on either side of a face are formed in such a way as to permit diffusion of quantities without these quantities becoming unbounded."
  Values over 85° are considered bad.

- Chevron cells 5.2
  "Chevron cells are pairs of thin slender cells which meet at a common face at an angle such that the line joining the cell centers does not pass through the common face."
  Values of 1 indicated chevron cells and are considered bad.

- Least Squares Quality 5.2 *"This field function is an indicator of the quality of a cell, using the physical location of a cell centroid relative to the cell centroid locations of its face-neighbors."*
  Values below 1E-3 are considered bad.

- Cell Warpage Quality 5.2
  "Cell warpage quality identifies thin and warped cells. These types of cells can cause issues for the flow solver, especially for high fidelity simulations such as LES/DES and acoustics, where minimal dissipation is required."
  Values below 0.15 are considered bad.

In all cases considered, bad cells were present. However, this is not necessarily detrimental for the analyses if the number of bad cells are low and the solver stays stable throughout the simulation. This was the case and as such, the mesh was deemed acceptable.

		Mesh			
		0		90	
Cells		4540915		5238091	
Faces		23458207		28657348	
Verts		16552183		21203083	
Face Validit	Min	0.987		0.994	
	Max	1		1	
	0.95 <= Face Validity < 1.00	17	0.0%	14	0
	1.00 = Face Validity	4540898	100.0%	5238077	100
Cell quality	Min	0.001		0.000	
	Max	0.992		1.000	
	Cell Quality < 0.50	1705200	10.3%	916415	17.5%
	0.50 <= Cell Quality < 0.60	3171824	19.2%	1360304	26.0%
	0.60 <= Cell Quality < 0.70	3573351	21.6%	1065350	20.3%
	0.70 <= Cell Quality < 0.80	5860227	35.4%	903928	17.3%
	0.80 <= Cell Quality < 0.90	2205191	13.3%	752537	14.4%
	0.90 <= Cell Quality < 0.95	35145	0.2%	159046	3.0%
	0.95 <= Cell Quality < 1.00	1245	0.0%	80511	1.5%
Volume cha	Min	0.007		0.003	
	Max	1		1	
	1.0e-03 <= Volume Change < 1.0e-0	3	0.0%	9	0
	1.0e-02 <= Volume Change < 1.0e-0	54119	1.2%	60859	1.2%
	1.0e-01 <= Volume Change <= 1.0e+	4486793	98.8%	5177223	98.8%
Cell skewne	Min	0.110		0.087	
	Max	121.170		122.010	
	Skewness Angle < 15	1457241	32%	1446435	28%
	15 <= Skewness Angle < 45	2780488	61%	3453000	66%
	45 <= Skewness Angle < 75	272688	6%	317623	6%
	75 <= Skewness Angle < 80	14296	0%	12234	0%
	80 <= Skewness Angle < 85	15973	0%	8774	0%
	85 <= Skewness Angle < 90	217	0%	15	0%
	90 <= Skewness Angle < 100	4	0%	0	0%
	100 <= Skewness Angle	8	0%	10	0%
Chevron qu	Min	< 1e-3		< 1e-3	
	Max	1		1	
	Chevron quality < 1e-3	4539683	100%	5236958	100%
	Chevron quality = 1	1232	0%	1133	0%
Least squar	Min	3.12E-04		5.48E-05	
	Max	0.91		1.00	
	LSQ < 1e-3	1	0%	52	0%
	1e-1 <= LSQ < 0.6	3453945	21%	2276667	44%
	0.60 <= LSQ < 0.70	4702096	28%	1065350	21%
	0.70 <= LSQ < 0.80	7937967	48%	903928	18%
	0.80 <= LSQ < 0.90	458167	3%	752537	15%
	0.90 <= LSQ < 0.95	7	0%	159046	3%
Cell warpag	Min	0.54		0.00	
	Max	1.00		1.00	
	Cell Warpage Quality < 0.50	0	0%	916415	17%
	0.50 <= Cell Warpage Quality < 0.6	7	0%	1360304	26%
	0.60 <= Cell Warpage Quality < 0.7	104	0%	1065350	20%
	0.70 <= Cell Warpage Quality < 0.8	8809	0%	903928	17%
	0.80 <= Cell Warpage Quality < 0.9	930679	6%	752537	14%
	0.90 <= Cell Warpage Quality < 0.9	792845	5%	159046	3%
	0.95 <= Cell Warpage Quality < 1.00	14819739	90%	80511	2%

Figure 5.2: Mesh quality report

5.3.3. Physics models

In Star CCM+ there are different physics models available which define how physical phenomenons in a continuum are represented. Physics models define what mathematical formulation is used to generate a solution, as well as defining primary variables for the simulation. Selecting the proper models and variables is important for getting a quality simulation.
The following models were selected for this case:

- **Space** - Three-dimensional
  Since the geometry is three-dimensional, the physics continuum is as well.
- **Material** - Gas
  The working fluid is air.
- **Flow** - Coupled flow
  A choice has to be made between coupled flow and segregated flow. Segregated flow solves equations for pressure and velocity separately and links these equations together through a predictor-corrector approach. The coupled flow solver solves the conservation equations for mass and momentum simultaneously using a pseudo-time-marching approach.

  The coupled flow solver tends to yield better results [15], at the cost of greater computational expense.
- **Equation of state** - Constant density
  Due to the low mach number of 0.0063, the fluid can be considered incompressible and of constant density.
- **Time**
  - Steady
    A steady solver was used for the initialisation of the flow in the flow domain. Using a 500 steps as initialisation phase ensures that the basic flow around the crane is captured which will lead to a faster simulation in the implicit unsteady phase.
  - Implicit unsteady
    An implicit unsteady solver was used to capture transient effects in the flow. Transient effects are expected due to potential vortex shedding and buffeting. These effects can affect the forces acting on the crane and as such are deemed important to simulate.
- **Viscous regime** - Turbulent
  The expected Reynolds number numbers are in the order of $10E3$ to $10E5$. Local flow may accelerate leading to higher numbers. The high Reynolds numbers in combination with the in places complex geometry led to the selection of the turbulent viscous regime. Additionally the following models were selected for turbulence:
  - RANS (Reynolds-Averaged Navier-Stokes)
  - k-ω Turbulence

  The combination of RANS and k-ω is typically used in such simulations [24].
- **Optional model** - Cell quality remediation
  The cell quality remediation identifies poor-quality cells and modifies the computed gradients to improve robustness of the solution [35]. This option was chosen to remedy potentially problematic areas which could arise in complex mesh areas.

5.3.4. Boundary conditions

The case was setup with the following boundaries and their respective conditions:

- **Inlet** - Velocity inlet
  The inlet was setup as a velocity inlet with a uniform velocity profile of 21m/s of the entire inlet boundary. This to match the conditions of the wind tunnel tests.

- **Outlet** - Pressure inlet
  The outlet was setup as a pressure outlet with a reference pressure of 0 Pa over ambient.
- **Floor** - No-slip wall
  The floor of the virtual wind tunnel was setup as a wall boundary with a no-slip condition. This condition was chosen to capture the boundary layer along the wind tunnel floor surface.
- **Walls** - Slip wall
  The virtual wind tunnel walls including the roof were chosen as a slip wall. In a slip condition the viscous effects at the boundary are omitted and thus show no boundary layer. The boundary layer along these boundaries isn't of interest and as such could be omitted from the case.
- **Crane** - No-slip wall
  The surface of the crane was selected as a no-slip wall. Boundary layer effects are important at this surface.

5.3.5. Simulation

The simulation was performed following the following steps:

1. Generate mesh
2. Initial steady simulation to initialise flow around the geometry;
3. Unsteady simulation to calculate flow around the geometry including transient flow effects;

Generally, 500 steps of steady simulation proved sufficient to initialise the flow to a point where unsteady simulation could be started. From that point on the solver would be changed to a transient solver. Depending on the flow development, runtime was then selected. It was generally found that after 0.5s flow would have fully developed, although simulation was left to run for longer if required. Depending on the results of the simulation, the time step could be refined in an attempt to get a more accurate result, although this was based on experience and data feedback.

After calculations were completed, the results were averaged over a time of 1 second. With a flow velocity of 21m/s and a domain length of 3.5 meters, this would mean that the entire flow volume was replaced 6 times in this time span. Based on the Strouhal number, vortex shedding was expected to have a frequency of >10Hz, and thus to be sufficiently captured in the chosen time span.

5.3.6. Measurements

The report summaries are useful for post-processing, and enable engineering quantities such as drag, lift, torque, or mass flow to be computed [35]. With reports it is possible to get insights in forces in a way which is not possible through conventional tests such as wind tunnel tests.

Reports were set up for both the entire crane geometry, as well as individual parts. The reports which report on the overall crane geometry allow for direct comparison with the wind tunnel tests. The per part reports offer insights otherwise unobtainable allowing the actual force coefficients acting on parts to be measured.

The combination of reports and parts are presented in table 5.1. It is to be noted that for all parts, reports were generated for both the port side and the starboard side elements, or land side and water side, where applicable. For the global geometry two reports are made. The first one, ”global”, reports the force coefficients as a function of the measured frontal area. The second, ”global WT”, uses a reference area of $\frac{1000}{150^2}m^2$ which is the same as used in the wind tunnel measurements. This allows easy comparison between the wind tunnel and CFD data.

Additional reports were generated to track the simulation performance for back end administration. These reports are listed below but will otherwise not be elaborated on:

- Solver iteration elapsed time
- Mean solver iteration elapsed time
- Maximum memory usage

Part	CFx	CFy	CFz	CMx	CMy	CMz	Fx	Fy	Frontal area
Global	•	•	•	•	•	•	•	•	•
Global WT	•	•	•	•	•	•			
A-frame pylons	•	•							•
Back stay	•	•							•
Back stay verticals	•	•							•
Forestay: inner	•	•							•
Forestay: outer	•	•							•
Bogies	•	•							•
Girder: Boom	•	•							•
Girder: Bridge	•	•							•
Diagonal above girder	•	•							•
Frame	•	•							•
K-frame	•	•							•
Pipe above girder	•	•							•
Apex beam	•	•							•
Machine house	•	•							•

Table 5.1: Reports per part.

5.4. Computational fluid dynamics

CFD offers exceptional flexibility with regards to data collection. Results are computed for the overall forces acting on the crane, as well as per-part force results. The latter offers the benefit of having a detailed force breakdown per part. This offers new insights in the interaction between elements. Furthermore, the surface pressure can be evaluated which helps in the understanding of the shielding effects.

The quantitative results of the computational fluid dynamics are presented in a few ways:

- Comparison of overall forces between CFD, wind tunnel tests, and the standard calculations
- Comparison of per-part forces to those in standard calculations.

5.4.1. Overall results

The overall results will be presented in this section. The results will be presented as a comparison of drag coefficients. The comparison of drag coefficients rather than forces is beneficial because it removes flow conditions from the results. As seen in section 4.5, flow conditions in the wind tunnel can differ between runs, leading to differences in forces up to a few percent.

The force and moment coefficients will be calculated for a standardised reference surface area of $\frac{1000}{150^2}m^2$, and a reference height of $\frac{80}{150}m$. Since the different standards use different methods of calculating the reference area, there is no authoritative method for determining reference area. As such for sake of simplicity, a reference area of $1000m^2$ and height of $80m$ are chosen, scaled down to the crane scale by a factor of 150.

Table 5.2 presents the results of the CFD analysis for the evaluated wind angles in the global reference frame. The results are compared to the equivalent wind tunnel test runs. The difference between the wind tunnel runs and the CFD analysis is given as both a absolute as well as a relative percentual difference. For all CFD analyses the force coefficient in the principle direction, CFx, as well as the corresponding moment, CMy, match quite well. The force coefficients for the other two directions however show differences. While the differences are relatively big, the absolute difference is a lot smaller. This shows the effect of small differences at low CF and CM values. The reason for this difference will be discussed in section 6.

	0 °				90 °				60 °			
	CFD	**WT**	**diff abs**	**diff %**	**CFD**	**WT**	**diff abs**	**diff %**	**CFD**	**WT**	**diff abs**	**diff %**
CFx	0.98	1.04	0.06	6%	1.88	1.87	0.01	-1%	2.15	2.08	0.07	-3%
CFy	0.00	-0.03	0.03	96%	0.01	0.03	0.02	80%	-0.31	-0.19	0.11	-58%
CFz	0.15	0.33	0.18	55%	0.11	0.19	0.08	43%	0.17	0.19	0.02	10%
CMx	0.00	-0.02	0.02	104%	0.01	0.05	0.04	82%	0.33	0.25	0.08	-33%
CMy	0.49	0.45	0.04	-8%	0.94	1.18	0.24	20%	1.18	1.17	0.01	-1%
CMz	0.00	0.00	0.00	58%	0.06	0.07	0.01	14%	0.11	0.10	0.01	-13%

Table 5.2: Results of the CFD analysis in the global reference frame

5.4.2. Per-part results

The per-part results will be presented in this section. The results will be presented as a comparison of force coefficients as well as a comparison of actual forces. For the comparison, the EN 13001-2 standard will be selected as this is the most recent and current standard.

Table 5.4 presents a comparison of forces on selected members between the CFD analysis and the EN 13001-2 for the 0° and 90° wind angles in the global reference frame. Table 5.3 presents a comparison of force coefficients in the global x direction between the CFD analysis and the EN 13001-2 for the 0° and 90° wind angles in the global reference frame. the results of the CFD analysis for the evaluated wind angles in the global reference frame.

Several observations can be made from these tables:

- Several members show negative forces and drag coefficients in CFD.
  This is believed to be the effect of the low pressure wake which forms behind upstream elements. Since these elements do not experience any dynamic pressure, the static pressure creates a negative force.
- EN 13001-2 both over- and underestimates forces on certain members.
- Elements slanted in the wind direction, such as the forestays in the 0° wind, experience a much lower drag than calculated with the standard.
- Elements in close vicinity to each other, but not coaxial with regards to the wind angle still show mutual influence. For example, the windward vertical stay on the backstay experiences a higher than calculated load.

	0° wind angle			90° wind angle		
	0 deg	**EN 13001-2**	**% diff**	**90 deg**	**EN 13001-2**	**% diff**
A-frame PS	8.87E-01	8.16E-01	-8%	6.24E-01	8.70E-01	40%
A-frame SB	9.02E-01	8.16E-01	-9%	9.46E-01	8.70E-01	-8%
Back tie PS	1.20E-01	9.90E-01	726%	9.75E-01	1.14E+00	17%
Back tie SB	1.15E-01	9.90E-01	757%	1.09E+00	1.14E+00	5%
Back tie vertical PS	5.60E-01	7.92E-01	42%	7.00E-01	1.14E+00	63%
Back tie vertical SB	5.35E-01	7.92E-01	48%	1.59E+00	1.14E+00	-28%
Boom girder PS	6.47E-01	6.00E-01	-7%	-1.73E-01	1.80E+00	N/A
Boom girder SB	6.44E-01	6.00E-01	-7%	1.48E+00	1.80E+00	22%
Bracing PS	1.28E-01	8.75E-01	586%	9.11E-01	1.01E+00	11%
Bracing SB	1.45E-01	8.75E-01	502%	1.12E+00	1.01E+00	-9%
Bridge girder PS	4.58E-01	N/A	N/A	-1.10E-01	1.78E+00	N/A
Bridge girder SB	4.54E-01	N/A	N/A	1.19E+00	1.78E+00	50%
Diagonal above girder PS	2.65E-01	7.75E-01	193%	5.45E-01	9.72E-01	78%
Diagonal above girder SB	1.67E-01	7.75E-01	365%	9.60E-01	9.72E-01	1%
Frame PS	2.24E+00	1.45E+00	-35%	4.96E-01	4.70E+00	847%
Frame SB	2.20E+00	1.46E+00	-34%	1.42E+00	5.11E+00	261%
Head	8.62E-01	1.32E+00	53%	1.04E+00	6.75E-01	-35%
K-frame PS	7.32E-02	8.15E-01	1014%	7.55E-01	1.50E+00	99%
K-frame SB	1.49E-01	8.15E-01	449%	1.09E+00	1.49E+00	37%
Long tie PS	1.95E-01	1.20E+00	516%	5.88E-01	1.12E+00	90%
Long tie SB	1.94E-01	1.20E+00	519%	1.09E+00	1.12E+00	2%
Machine House	1.39E-01	1.20E+00	765%	1.21E+00	1.20E+00	-1%
Pipe above girder PS	1.19E-01	7.75E-01	550%	2.61E-01	9.84E-01	277%
Pipe above girder SB	1.45E-01	7.75E-01	433%	8.58E-01	9.84E-01	15%
Short tie PS	3.88E-01	1.14E+00	194%	8.58E-01	1.02E+00	19%
Short tie SB	3.82E-01	1.14E+00	199%	1.39E+00	1.02E+00	-27%

Table 5.3: Comparison of force coefficients on selected members between CFD and the EN 13001-2

	0° wind angle			90° wind angle		
	CFD	**EN 13001-2**	**% diff**	**CFD**	**EN 13001-2**	**% diff**
A-frame PS	2.45E-01	2.28E-01	-7%	1.70E-01	2.39E-01	41%
A-frame SB	2.49E-01	2.28E-01	-8%	2.57E-01	2.39E-01	-7%
Back tie PS	1.82E-02	1.54E-01	748%	4.69E-01	5.91E-01	26%
Back tie SB	1.75E-02	1.54E-01	780%	5.23E-01	5.91E-01	13%
Back tie vertical PS	5.03E-02	7.28E-02	45%	5.88E-02	5.48E-02	-7%
Back tie vertical SB	4.81E-02	7.28E-02	51%	1.34E-01	5.48E-02	-59%
Boom girder PS	2.51E-02	1.69E-02	-33%	-4.04E-01	1.69E+00	N/A
Boom girder SB	2.50E-02	1.69E-02	-32%	3.45E+00	3.76E+00	9%
Bracing PS	3.99E-02	2.82E-01	607%	9.67E-01	1.08E+00	11%
Bracing SB	4.55E-02	2.82E-01	520%	1.19E+00	1.08E+00	-9%
Bridge girder PS	2.49E-02	N/A	N/A	-2.59E-01	1.33E+00	N/A
Bridge girder SB	2.47E-02	N/A	N/A	2.78E+00	4.28E+00	54%
Diagonal above girder PS	8.76E-02	2.56E-01	193%	2.90E-01	5.03E-01	74%
Diagonal above girder SB	5.51E-02	2.56E-01	365%	5.11E-01	5.03E-01	-1%
Frame PS	3.04E+00	3.85E+00	27%	1.55E+00	4.70E+00	203%
Frame SB	2.97E+00	3.82E+00	29%	4.85E+00	5.11E+00	5%
Apex beam	2.36E-01	3.61E-01	53%	1.20E-01	9.81E-02	-18%
K-frame PS	1.41E-02	3.10E-01	2105%	7.20E-01	8.45E-01	17%
K-frame SB	2.86E-02	3.10E-01	986%	1.04E+00	8.45E-01	-19%
Long tie PS	3.93E-02	2.14E-01	445%	3.02E-01	4.10E-01	36%
Long tie SB	3.90E-02	2.14E-01	448%	5.61E-01	5.95E-01	6%
Machine House	2.29E-01	1.98E+00	883%	1.85E+00	1.79E+00	-3%
Pipe above girder PS	1.57E-03	N/A	N/A	7.75E-02	2.99E-01	286%
Pipe above girder SB	1.92E-03	N/A	N/A	2.55E-01	2.99E-01	18%
Short tie PS	6.07E-02	1.63E-01	168%	1.88E-01	2.41E-01	28%
Short tie SB	5.88E-02	1.63E-01	177%	3.05E-01	2.41E-01	-21%
SUM	**9.49E+00**	**1.34E+01**	**41.2%**	**2.22E+01**	**3.15E+01**	**41.5%**

Table 5.4: Comparison of forces on selected members between CFD and the EN 13001-2-2

5.5. Computational fluid dynamics visual results

Since the results of the computational fluid dynamics simulation was assumed to be valid in section 5.4, the visualisation of the results can be used for qualitative interpretation. As such, computational fluid dynamics do not only provide to be a useful tool for calculation of forces and moments, but also to gain insight in the behaviour of winds around a crane.

5.5.1. Velocity field

The first visualisation under scrutiny is the velocity field around the crane. The velocity field is an important tool to see why dynamic pressure at certain points is low. Combined with streamlines, the flow can be visualised giving a better understanding of flow around the geometry. This is visualised for two cases, namely the 0° and 90° cases. In both cases the flow will be visualised on 3 main planes namely:

- **xz-plane** with the normal pointing in the y-direction. This plane will be located through the centre of the crane between the legs.
- **yz-plane** with the normal pointing in the x-direction. This plane will be located through the centre of the crane between the legs.
- **xy-plane** with the normal pointing in the z-direction. This plane will be located at 0.3m above the floor of the tunnel to intersect the crane's legs.

0° case
The 0° case can be seen in figure 5.5.
What can be seen is that the the tip of the boom influences all members behind it. From figure 5.3a it can be seen that a wake is formed starting at the tip of the boom extending en encompassing all girder elements behind it. It can also be seen that around the inner forestay, the flow becomes unstable. During the unsteady simulation, it was seen that the this flow would fluctuate and vortices would appear. This unsteady behaviour was eminent in the force measurements on the elements which showed periodic behaviour fluctuating between a minimum and maximum value.

From this figure we can also see the effect of the angled sections which represent the bogeys. Whilst there is a lower velocity in the direct vicinity of the bogeys, a higher velocity can be observed in the portal, showing a significant increase around the height of the k-frame.

Interesting to note is a small jet of accelerated flow near the hinge of the boom. This jet would fluctuate in direction and would impact the surrounding flow.

In this view, many small eddy currents can be observed in the boom area. These eddies required siginifcant computational power to compute and may impact calculation accuracy.

In the top view, in figure 5.4a, vortex shedding from the water side legs is immediately evident in both the velocity profile as well as the streamlines. A more steady wake can be observed coming from the land side legs.

Although not very clear, it appears that the high voltage cable real has an effect in the downstream wake.

From the frontal view, in figure 5.5a, it can be seen that the velocity profile and the silhouette of the crane not quite match. Showing effects caused by elements both before and after the plane on which the velocities are projected.

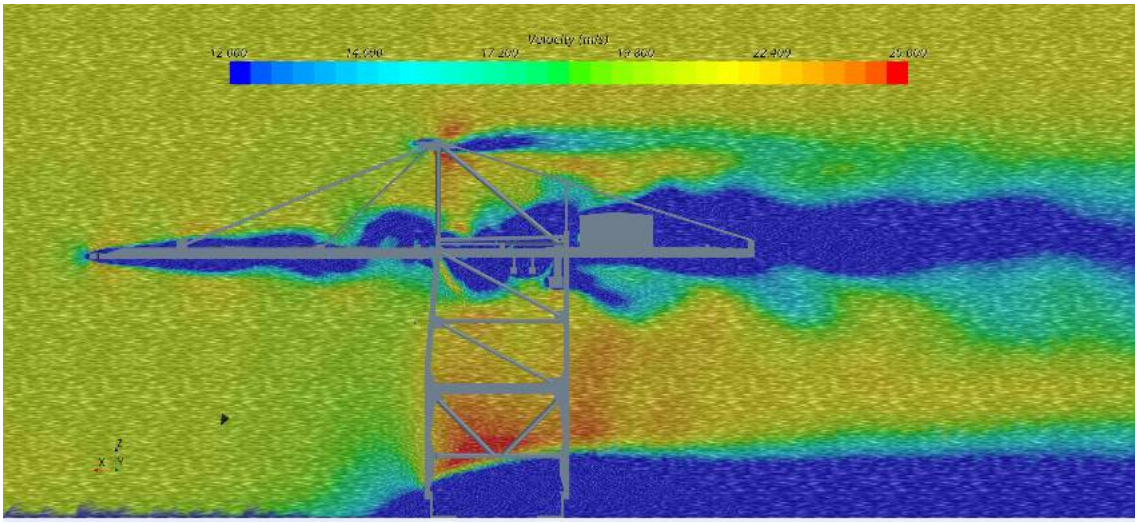

(a) Side view velocity field; 0° wind angle

Figure 5.3: Velocity fields with streamlines; 0° wind angle.

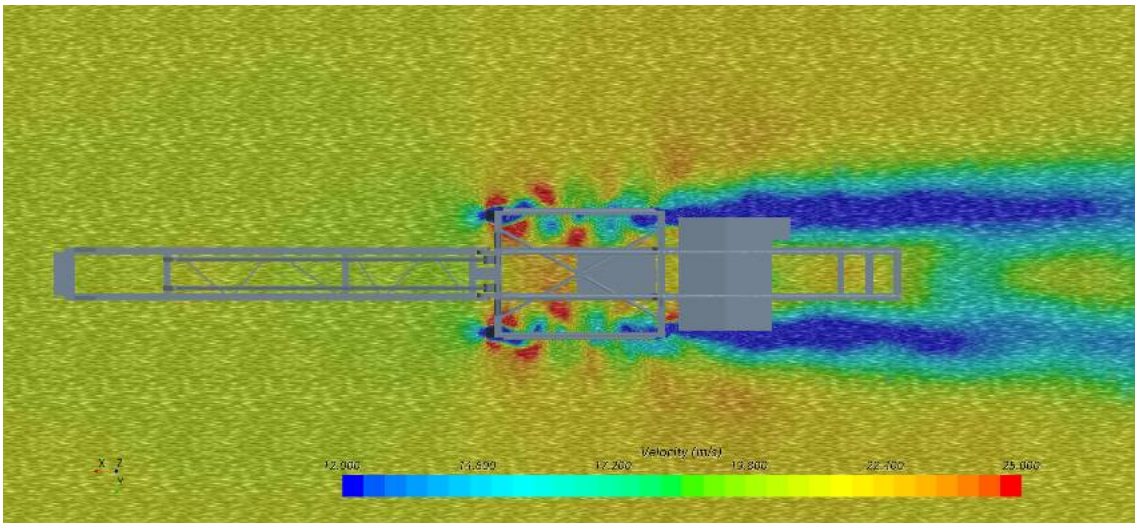

(a) Top view velocity field; 0° wind angle

Figure 5.4: Velocity fields with streamlines; 0° wind angle.

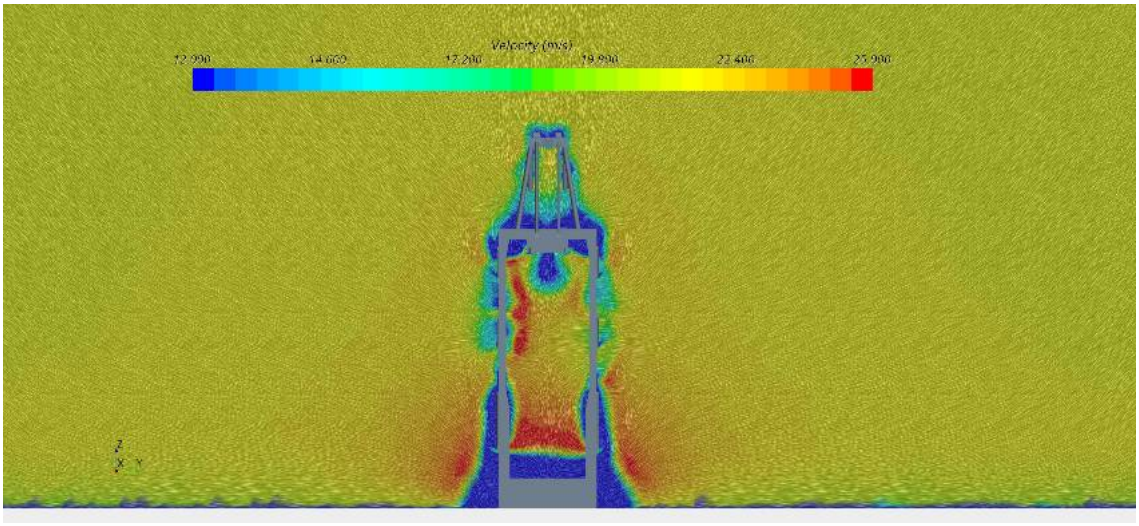

(a) Front view velocity field; 0° wind angle

Figure 5.5: Velocity fields with streamlines; 0° wind angle.

90° case

The 90° case can be seen in figure 5.8.

When evaluating the front view in figure 5.6a, it can be seen that all leeward frame members are in the wake of the windward frame members. Furthermore a relatively large wake can be observed from the girders. These girders also incur significant turbulence in the air flow which can be seen as unsteady behaviour. This is not observed in the other members such as the round frame members.

A similar trend can be observed in figure 5.7a as was observed in 5.3a. The port side legs are affected by the starboard side legs' wake. The wake of the combined legs lasts the entire flow domain. Again local increase of flow velocity is observed which is thought to be caused by the venturi effect.

In the front view, in figure 5.8a, it is again visible how the silhouette of the crane does not match the velocity profile. Interestingly, a higher velocity is observed around the silhouette of the crane which contrasts that seen in figure 5.5a. This could be possible due to the higher blockage factor in this orientation.

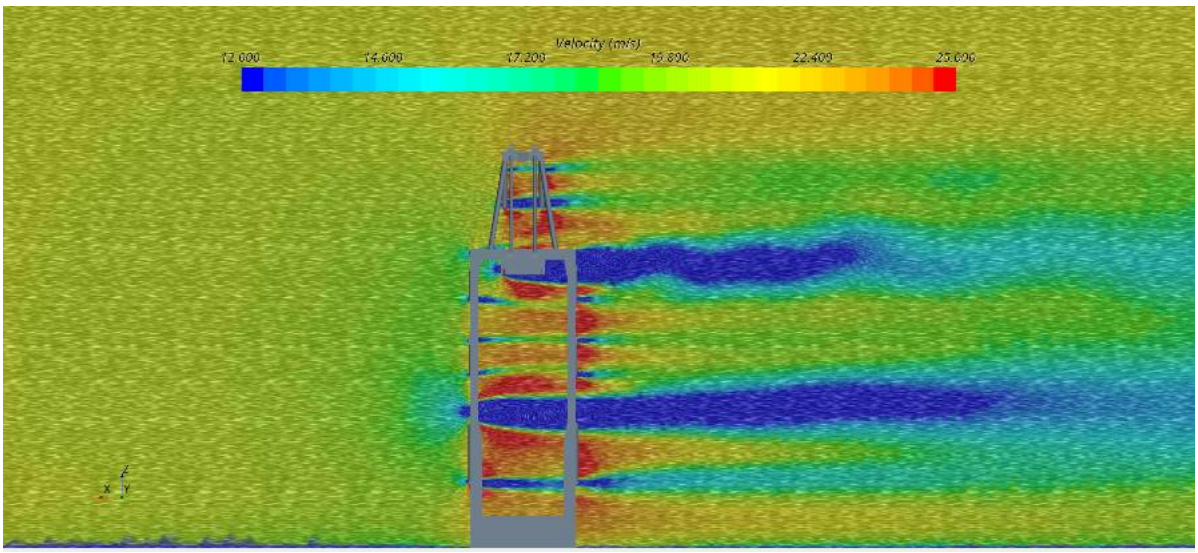

(a) Side view velocity field; 90° wind angle

Figure 5.6: Velocity fields with streamlines; 90° wind angle

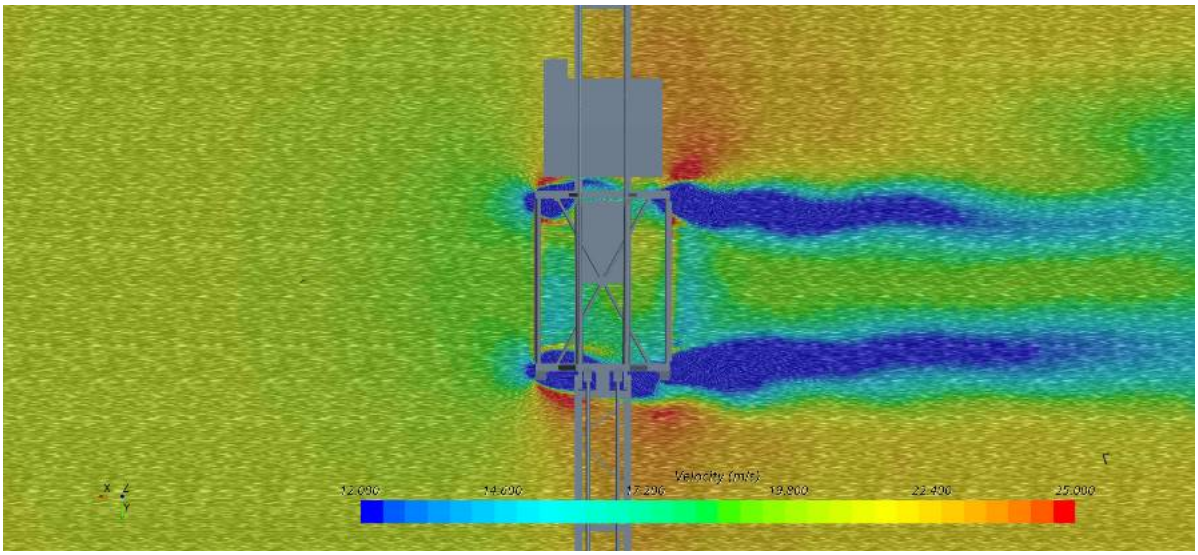

(a) Top view velocity field; 90° wind angle

Figure 5.7: Velocity fields with streamlines; 90° wind angle

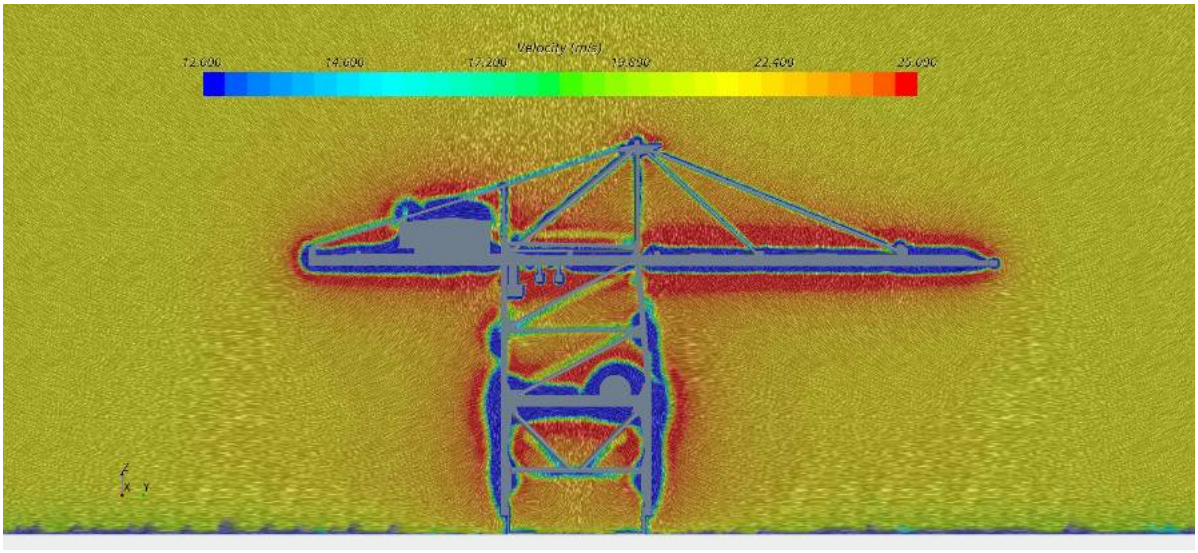

(a) Front view velocity field; 90° wind angle

Figure 5.8: Velocity fields with streamlines; 90° wind angle

5.5.2. Surface pressure

The surface pressure on the surface of the crane is shown for 3 different wind angles:

- **0°** - figure 5.9a
- **60°** - figure 5.10a
- **90°** - figure 5.11a

Where he 60° angle was chosen as additional angle as explained in chapter 5.

What can be seen in all figures is that windward elements experiences a higher overall wind pressure than the leeward elements. This seems congruent with the results from section 5.5.1 which showed a generally lower wind velocity at the leeward elements.

Another thing to be noted from the pressure scenes is that the pressure is typically not evenly distributed on the leeward elements. This finding is to be attributed to two things. Firstly the transient and turbulent nature of the air flow around the structure. The depicted scene is a snapshot in time rather than a time average. This could explain some spottiness on elements. Secondly, certain hot spots can be identified in all images (e.g. machine house upper corners in figure 5.9a) which are the result of airflow being disturbed by elements which are in front of the element under consideration, but also off axis.

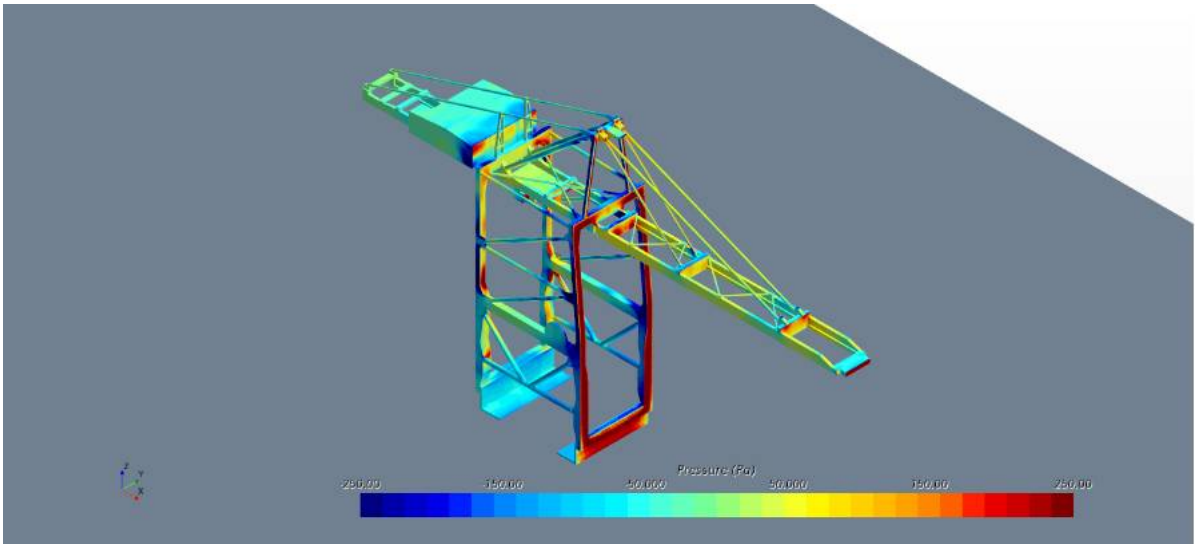

(a) Surface pressure; 0° wind angle

Figure 5.9: Surface pressure for various wind angles

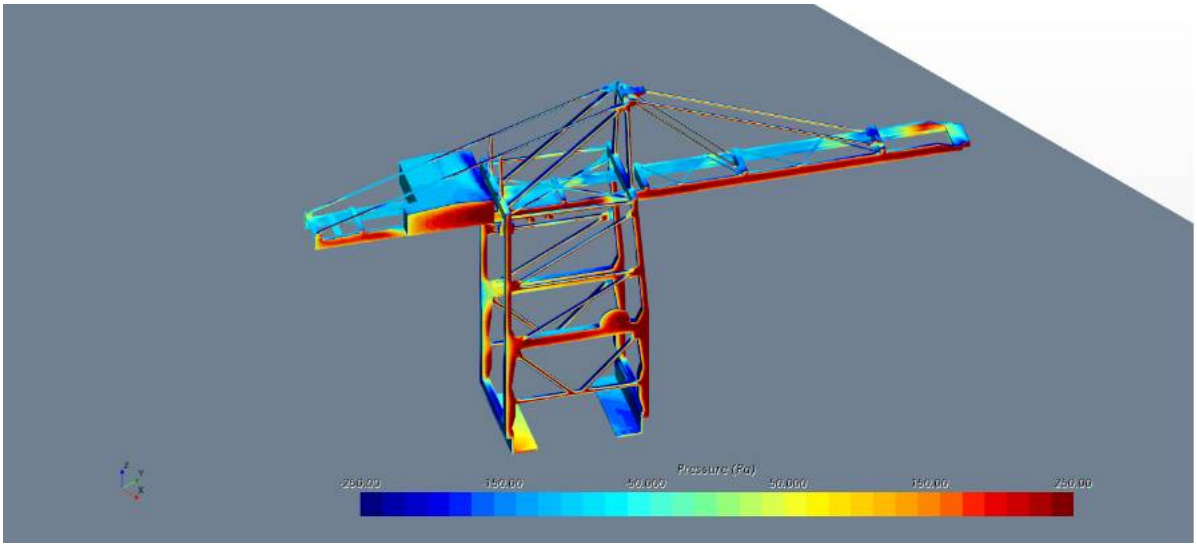

(a) Surface pressure; 60° wind angle

Figure 5.10: Surface pressure for various wind angles

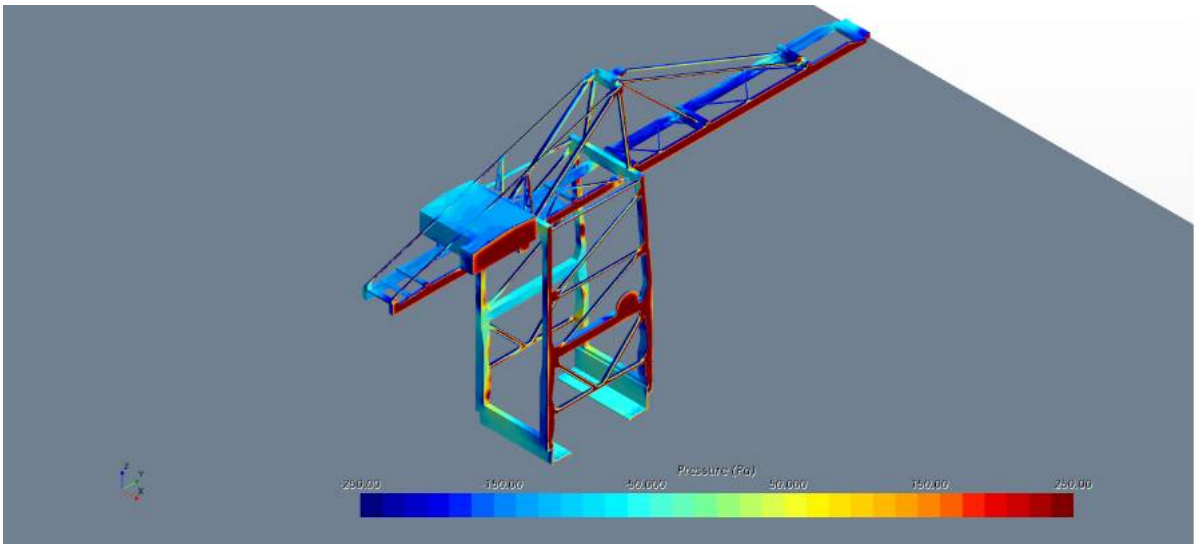

(a) Surface pressure; 90° wind angle

Figure 5.11: Surface pressure for various wind angles

6

Results discussion

The results presented in previous chapters will be explained and discussed in this chapter. This chapter follows the structure set out by previous chapters as a guideline and will add where necessary.

6.1. General aerodynamic properties

In the general aerodynamic properties section the general behaviour of the crane was presented.

The main findings were:

- The maximum forces and moments are not found at right angles, i.e. the cardinal wind directions with respect to the crane.
- The area of the projected silhouette of the crane shows correlation with the measured forces and moments.

These two findings implicate that the angles at which the standards are typically applied, that is the right angles of 0°, 90°, 180°, and 270° are not the dominant angles for determining the wind actions on cranes. It was found that the highest forces and moments were rather found at angles between 20° and 40° off the cardinal angles, for example between 50° and 70°.

This is not unexpected when looking at the standards and how they are applied; see also 3. All standards, except for the Eurocode 1-4, include a form of shielding effect which is to account for the shielding effect windward elements have on leeward elements. However, as mentioned, this shielding effect is only applicable in select circumstances.

As a result, it is thought that the effect of shielding is not fully accounted for in the standards, and that is shown in the general aerodynamic characteristics.

6.2. Effect of asymmetry and aerodynamic elements

6.2.1. Asymmetry

The effect of asymmetry in the construction is of considerable but perhaps not significant influence on the overall wind loading on the crane.

xz asymmetry

The horizontal force on the crane can be as much as 14% higher between the port and starboard side, however this effect does not show in the overturning moment. The overturning moment differs up to 6% between port and starboard side. It is suspected that the centre of load of the asymmetry is relatively low compared to the rest of the crane, having a smaller impact than the force percentually. When looking at the physical crane model, this seems reasonable as at this specific angle, the mesh screen representing the staircases on the lower frame has the biggest surface perpendicular to the wind.

Looking at the effect overall, it seems wise as a general rule of thumb to place asymmetric aerodynamic elements on the leeward side of the crane, relative to the dominant winds in storm conditions.

yz asymmetry
The yz plane symmetry is considered of less importance as there is a smaller degree of design freedom in this plane. Nonetheless a difference in horizontal forces was found of up to 6%. Whilst not insignificant, no clear trends were found.

6.3. Auxiliary elements

The aerodynamic elements were found to have a profound effect on overall force and moment as a result of the wind action. Whilst unsurprisingly, it is a matter for discussion.

When calculating the wind loads using any of the standards, small details such as flanges, ridges, railings and other aerodynamic elements are often omitted. In the same manner that when creating a scaled wind tunnel model, the original crane structure is simplified by omitting such elements. Since none of the standards offer guidance in simplifying such elements, testing the influence of such elements was thought to be of relevance.

The results from these tests indicate that, for the tested elements on the tested crane, both the presence and the positioning of these elements can have non-insignificant impact on the measured results.

6.3.1. Effect of boom position

Since the boom is the only moving structural part, its influence on the overall wind loads is an interesting effect to investigate.

Commonly the boom is raised during out-of-operation storm conditions. When looking at the results this might seem counter-intuitive as the resulting forces and moments increase. However, in real life raising the boom also raises and more importantly moves in the centre of gravity. By moving in the centre of gravity towards the middle of the lower structure, the contribution of the dead weight to the overturning moment is reduced. This typically results in a more stable structure even though the forces and moments are increased.

From the results shown in section 4.5.4 it is seen that raising the boom increases the force acting on the crane, except in the 90° and 270° wind directions. This can be explained by the fact that the axis of rotation of the boom, relative to the wind changes with the angle of inclination of the boom. This results in the boom rotating about another axis relative to the wind. In the boom down position, the boom girders nearly always exert a form of shielding on one another. In the boom up and intermediate boom positions, this shielding is almost exclusively found in the 90° and 270° wind directions, quickly falling off as the wind turns. This effect can be clearly seen in figure 4.16a where the arches of the ”M” are more pronounced.

6.4. Reaction forces and stability

The reaction forces are a very important result of the force and moment calculations done. Perhaps moreso than the forces and moments since the reaction forces determine:

- Bogey brake force
- Bogey drive torque
- Tie down force
- Wheel pressure

Now it is important to reiterate that these reaction forces are instantaneous reaction forces for an infinitely stiff structure. The reaction of the structure to the applied load is not taken into account.

The reaction forces will be discussed per direction.

6.4.1. Reaction forces in x direction

The reaction forces in x direction are the lateral forces between rail and bogie. The first clear trend observed is that the maximum reaction forces in this direction in the wind tunnel are always higher than those measured at cardinal directions. As such the cardinal directions are not to be taken representative for calculation of these forces.

Comparing the maximum wind tunnel reaction forces to those found in the standards, it is found that the F.E.M. 1.004 always undercalculates the reaction force in this direction. This is a trend spotted in other sections as well.

In the boom down situation, all standards calculate a reaction force which is lower than that calculated from wind tunnel measurements. The closest is the DIN 1055 which is generally the highest of the set.

In the boom up situation, the difference between the wind tunnel measurements at the cardinal directions and the maximum forces is less pronounced. In this configuration all standards calculate reaction forces which are higher than the forces calculated from the wind tunnel tests.

In the intermediate boom configuration, we see a similar picture as in the boom down configuration where all standards undercalculate the reaction forces.

Overall it was seen that peak loads were found in the boom down configuration, and in that configuration the standards undercalculate the reaction forces. This is unwanted situation as this could lead to premature wear, cracks, or damage to the rail or bogies.

6.4.2. Reaction forces in y direction

Reaction forces in y direction are the reaction forces which are needed for calculating storm pin loads, brake loads and motor power. Depending on the application it may be worth noting that exceeding the maximum reaction force is not necessarily problematic. For the calculation of storm pins, which can fail or deform under excessive load, exceeding the maximum design load is problematic. For brakes and motors this is less problematic as the load can be spread over multiple corners to reach the same overall force.

As was the case with the reaction forces in x direction, the reaction forces calculated from the F.E.M. 1.004 are lower than the maximums found in the wind tunnel, and in some instances lower than the results from the wind tunnel cardinal directions.

6.4.3. Reaction forces in z direction

Reaction forces in z direction are the reaction forces which are needed for calculating stability, tie down forces, and bogie rail pressure, amongst other things. It is to be noted that these are instantaneous forces for an infinitely stiff frame and as such that an upwards force may not directly result in corner lift due to flex in the frame. However, if this occurs, the downwards force on the other corners will increase accordingly.

As was the case with the reaction forces in x direction, the reaction forces calculated from the F.E.M. 1.004 are lower than the maximums found in the wind tunnel, and in some instances lower than the results from the wind tunnel cardinal directions.

When comparing the boom up and intermediate boom positions no significant difference is found stability between the configurations. This is contrary to the initial expectation since the there is a 35° difference in boom inclination which leads to a significant reduction in overall height. The reduction in corner loads between the boom up and intermediate boom configurations in the standard calculations is not seen in the wind tunnel cardinal directions, which are similar or even greater in the intermediate boom configuration compared to the boom up. From this it is concluded that the intermediate boom configuration offers no advantage over the boom up situation in terms of stability or maximum pressure.

6.4.4. Computational fluid dynamics

CFD offers interesting and exciting possibilities. Whilst wind tunnel testing is expensive, CFD is comparatively cheap whilst offering a greater amount of freedom with regards to flow conditions and setup. It was found in table 5.2 that CFD can offer sufficiently accurate results. However, whilst the results in the global x direction are satisfactory, staying under 10%, forces in the other directions show greater percentual differences. Whilst the percentual differences are quite big, the absolute differences are still within the same order of magnitude. The potential causes for this will be discussed in section 6.5.

In table 5.4/5.3 it can be seen that the shielding effect windward members have on leeward members is underestimated. Standards generally only account for members which are placed directly behind each other (with up to 5° deviance), CFD implicates that there is more to shielding than just that.

Whilst the actual figures for windward elements might not correspond, there are interesting phenomenons:

- A-frame: besides the DIN 1055, no standards account for shielding effect for these members. The CFD results show that the leeward member has reduced force acting upon it, which suggests the presence of a shielding effect.
- Boom and bridge girders: The leeward members show negative forces in the CFD calculation. This is presumed to be the result of lower pressure between the members, causing a suction effect. No such effect is accounted for or mentioned in any standard, which is unsurprising since it is quite a complex effect.
- Back tie: the shielding effect supposed by the DIN 1055 is not present in the other standards or in the CFD calculations.
- Cross girder: The DIN 1055 takes shielding into account, but not sufficiently, the other standards do not.

For all items the CFD calculated drag is different than the drag calculated with standards. When looking at the theory behind the drag of members this seems unsurprising. All members in a structure influence the air around them, and as a result each other. The drag is commonly calculated for free stream members, rather than members contained in a structure.

6.5. Computational fluid dynamics differences

As noted in section 6.4.4, for directions other then those parallel to the wind, the forces calculated using the CFD model can have big relative disparities. The following aspects are to be thought to be of potential influence:

- Wind tunnel model
  - The wind tunnel model is not a perfect model. It was noted that the frame is slightly contorted and that there was play in the boom hinge.
  - The wind tunnel model is handmade. Whilst made with utmost care, there are certain manufacturing tolerances which are not present in the CFD geometry.
  - It was seen in section 5.4 that the shadow effect can be significant. Misaligned items in the construction, for example due to the above mentioned reasons, are thought to have significant impact.
  - The wind tunnel model was made from various materials (section 4.2) which have different surface roughnesses. These surface rougnesses were not taken into account in the CFD model but can have significant impact on the drag generated by a member [37].
- Wind tunnel measurements
  Whilst attention was paid during the setup of the wind tunnel testing setup, this is a potential source of error.
  - Misalignment of the turntable
    Since no alignment system was in place in the wind tunnel, it is possible that the turntable and flow direction were not perfectly aligned. When looking at the measurements for 0° wind, a lateral force component is seen. It is thought that this component is due to a slight rotation of the model with respect to the direction of air flow. Exploratory CFD runs found this plausible.
  - Unaccounted effects
    Whilst an effort was made to eliminate any bias from the testing setup from the measurements (section 4.4.2), it is possible that an unaccounted for variable was still present, although unlikely.
- CFD meshing discrepencies
  Whilst the CFD geometry is taken directly from the wind tunnel model, several differences were noted as explained in section 5.2.

- Model errors and uncertainties
  Differences between the actual flow and the mathematical model fall in this category. Simplification of a real gas to a constant density, turbulence modelling and the fact that flow equations are not solved but rather replaced with a simplified model of reality fall in this category [41].

- Discretisation and numerical errors
  The CFD flow volume was limited to less that 5 000 000 cells. The smallest cell being 1mm means that small eddys could be lost in the grid size. The smallest time step used was $1e-4$. This means that high frequency phenomenons such as vortex shedding which could occur up to 1200Hz, can not be captured. The reason for this limitation is computing power.

6.6. Qualitative measurements

The qualitative measurements revealed that windward elements can disturb airflow significantly to affect leeward elements. This disturbance reaches farther than accounted for in DIN 1055, F.E.M. 1.004, and the EN 13001-1. As seen from other measurements, merely looking at the wake effect of elements is not sufficient as the interaction of elements is equally if not more important.

An unsurprising result as well is that all elements affect one another. This makes it so that the local flow characteristics are unpredictable, which makes it harder to calculate for. This also influences the flow conditions in the wake downstream which makes calculations difficult.

6.7. Proposal for adaptation of EN 13001-2

It was shown in chapter 4 that the EN 13001-2 overestimates the wind actions on a model crane, when compared to the wind tunnel measurements in all cases. Subsequent investigation using CFD showed that the way in which members influence each other is insufficiently covered by this standard. Especially the shielding effect of windward members on leeward elements.

The proposed adaptation will focus on the shielding effect. It was noted in chapter 3 that the DIN 1055 has a more comprehensive graph for calculating the effects of shielding (figure 6.1a). The DIN 1055 covers a wider range of relative distances, up to 25 whereas the EN 13001-2 covers only up to 6 (figure 6.1b). Likewise, the shielding effect is also presumed stronger for equivalent distances, leading to an overall stronger shielding effect.

From plot 4.10 it was learned that the wind force acting on a crane is correlated with the surface area of the projected surface area. Observing the crane in the wind tunnel it was seen that vertical elements of the crane move behind each other as the wind rotates. Horizontal elements exhibit this behaviour less, only moving from each others wake at near right angles.

Combining these insights leads to the following proposal:

> *Calculation of wind loads according to EN 13001-2, with the adaption of the DIN 1055 shielding coefficients, as depicted in figure 6.1a, for all horizontal elements.*

6.7.1. Calculation example

Putting the above adaptation in practice, the calculations from section 3 is repeated with the proposed adaptation. The results are compared to the original equation and shown in table 6.2. From these results it is clear that the biggest reduction is found in the force in y-direction and corresponding moment about the x-axis. Lower reduction figures are found for the other directions.

The results of the adapted EN 13001-2 are also compared to the wind tunnel measurements. Whilst the maximum wind tunnel forces are still lower than the standard calculations, they are closer than first reported in table 4.4. This improvement is in line with the reduction found in table 6.2. Noted is that the force in the x direction is still severely overestimated. This is thought to be the case of more non-linear flow effects which were visualised with CFD in section 5.5.1.

The shielded surfaces and the shielding coefficient for the elements on which they apply are given in table 6.1. From this table it is evident that most reduction is found in the y direction due to most shielded area being in this direction. The boom and bridge girders make up a large portion of the projected area in this direction. The reduction in surface area is congruent with the reduction in force. The height of the members is in part responsible for the difference in moment.

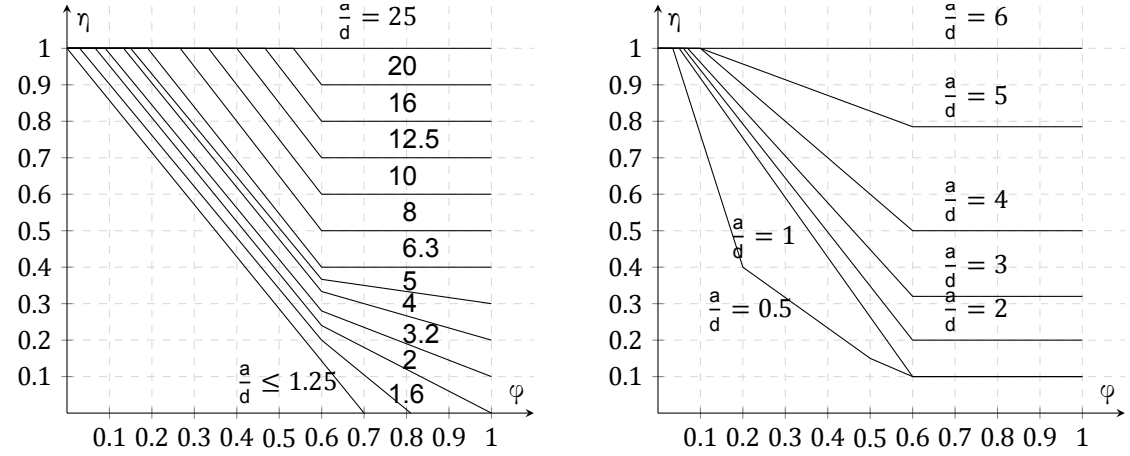

(a) Shielding coefficients according to DIN1055

(b) Shielding coefficients according to EN 13001-2

Figure 6.1: Graphs with shielding coefficients

	Effective surface [mm]			
		Side		
Member	**EN 13001-2**	**EN 13001-2 adapted**	**reduction**	**reduction %**
Cross girder starboard	3706	1853	1853	50%
Horizontal pipe above cross girder starboard	1067	1045	22	2%
Horizontal pipe above bridge girder starboard	1103	1081	22	2%
Bridge girder starboard	2701	871	1830	68%
Boom girder starboard	3404	1135	2270	67%
total	**86290**	**80258**	**5997**	**7%**
		Front		
Member	**EN 13001-2**	**EN 13001-2 adapted**	**reduction**	**reduction %**
Gantry drive	3750	3000	750	20%
Sill beam	2640	1663	977	37%
Boom cross connectors	3082	1641	1441	47%
total	**62926**	**59759**	**3168**	**5%**

Table 6.1: Effective surface area comparison between the EN 13001-2 and the adapted EN 13001-2 standards.

	EN 13001-2	**EN 13001-2 adapted**	% **reduction**
$\mathbf{F_x}$	22.49	21.13	6.04%
$\mathbf{F_y}$	32.17	29.31	8.87%
$\mathbf{M_y}$	6.39	6.08	4.86%
$\mathbf{M_x}$	10.96	9.98	8.95%

Table 6.2: EN 13001-2 vs EN 13001-2 with adapted shielding coefficients

		EN 13001-2 adapted	Wind tunnel	diff	Wind tunnel maximum	diff
Boom down	Fx	21.13	13.01	62.4%	17.86	18.3%
	Fy	29.36	22.85	28.5%	24.77	18.5%
	My	6.08	3.11	95.4%	4.15	46.6%
	Mx	10.99	7.70	42.7%	8.04	36.6%
Boom intermediate	Fx	24.67	14.73	67.5%	19.76	24.9%
	Fy	29.43	22.48	30.9%	25.89	13.7%
	My	8.32	4.59	81.1%	5.95	39.8%
	Mx	10.88	8.23	32.2%	9.30	17.0%

Table 6.3: Comparison of the adapted EN 13001-2 standard and wind tunnel measurements

7

Conclusion and recommendations

In this chapter the conclusion of the research will be presented as well as recommendations on further research and for practical implementation.

7.1. Conclusion

Cranes have a typical construction which follows the same lines. A lower structure consisting of the legs bogies, and bracing. An upper structure consisting of a bridge and boom girder, machine house, and supporting structure. This typical structure creates a typical response relationship between forces and wind angles.

At first glance the forces, moments, and reaction forces calculated with the standards are higher than those measured in the wind tunnel. However, when we look at the crane as a whole with the wind coming in at angles other than 0° and 90°, the results may change drastically.

The aerodynamic characteristics of the crane with respect to the wind angle are not captured in the standard calculations. As such, maximum forces, moments, and reaction forces were found at angles other than those used for calculation in the standards. The results from these measurements are more closely approximated by the standards than those at the cardinal directions.

This research started with the question:

"How should standards for calculating wind actions on shiptoshore cranes be adapted to achieve more accurate results compared to wind tunnel testing or computational fluid dynamics?"

This research question was answered with a proposed adaptation of the EN 13001-2 standard in section 6.7. This proposed adaptation yields a reduction in calculated force and moment, mainly in the y-direction of the crane and about the x direction of the crane. These coincidentally are the directions where the greatest load was found and where the risk for instability is greatest due to the small footprint associated with this direction.

7.2. Recommendations

From this research there are several recommendations to be made. These recommendations will be split out over the following parts and will be discussed in seperate sections:

- Adaptation of the EN 13001-2 standard
- Further research
- Wind tunnel testing
- Computational fluid dynamics
- Practical implementation

7.2.1. Adaptation of the EN 13001-2 standard

From this research it was shown that a small adaptation of the EN 13001-2 standard can improve the calculation results, bringing them closer to the actual values. This adaptation is relatively minor which allows for straightforward implementation into existing calculations.

7.2.2. Further research

Whilst this research provided many new insights, several propositions for further research can be made.

- Further research into the influence of auxiliary elements (e.g., staircases).
  Auxiliary elements such as staircases were included in the wind tunnel tests of this research. However, only rudimentary representations were used. Since the effect of these elements was already significant, further research could provide more insight in how these elements shape the flow around the main structure. This could provide new methods to reduce wind load by smarter placement of such elements.

- Investigate the relationship between several design dimensions and the characteristic aerodynamic response.
  The characteristic response which was found during the wind tunnel tests might be the result of the crane geometry. Since most STS cranes follow the same general design principle, it is thought that the response can be predicted based on the general dimension (e.g., distance between legs, length of the boom, etc.)

7.2.3. Wind tunnel testing

During the wind tunnel experimental phase of this research, several lessons were learned which can now be offered as recommendations for further research:

- Have a good wind tunnel model.
  The wind tunnel model used in this research was good but could have been better suited for this specific research. Certain elements were hard to model in 3D introducing an uncertainty. Furthermore, the forestays allowed movement which can influence the measurements. A better model would have eliminated several uncertainties.

  Auxiliary elements can have a bigger influence on wind load that common sense would dictate. Be weary of this when creating a model. Elements can be aerodynamically or geometrically scaled, this can be used to mitigate these effects.

- Be weary of Reynolds conditions.
  Due to wind tunnel limitations, the Reynolds number of the flow was different for the scaled model than for the real life crane. This induces differences between the scaled and full size versions. Also, certain effects such as vortex shedding which are Reynolds dependent could not be fully emulated. A higher velocity or bigger scale would have been beneficial as the Reynolds number would be closer to full scale conditions.

7.2.4. Computational fluid dynamics

Computational fluid dynamics were explored as a potential alternative for wind tunnel testing. Its use and potential have been shown and some recommendations can be made.

- Conduct full scale CFD analyses
  Unlike the wind tunnel, the CFD analyses can be conducted at full scale which eliminates a lot of problems related to the scaling effects.

- Conduct CFD in multiple parts
  In the previous section it was proposed that the characteristic response is geometry dependent. This can be used to the advantage to use a simplified model to quickly determine the least favourable wind angle for wind loading. Subsequent simulations can be done with more details. This results in quicker overal simulation times.

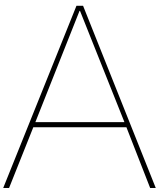

Academic Paper

Wind loading of STS cranes: Proposed improvement on EN13001-2

T.L.A. Rasch

***Abstract*—A $\frac{1}{150}$ scale model of a STS container crane was placed in a wind tunnel. Wind loading on the model was measured with six component balance with a variable wind direction under a uniform flow field. In parallel CFD simulations were performed on the same case. Results from wind tunnel tests were compared to standard calculations showing significant differences. With the aid of the CFD, the reason for this difference was investigated. With modern STS-cranes growing increasingly taller, accurate calculation of wind loads is becoming ever more important. Wind loads are calculated by standards or measured in a wind tunnel. A common finding is that wind tunnel tests result in lower wind loads compared to standards. This research investigates the relationship between standard calculations, and standard calculations and wind tunnel tests, and explores the possibility of using CFD. This research found that the EN13001-2 standard overestimates wind forces by up to 79% at right angles, however when compared to the maximum force found in the wind tunnel this difference shrinks to 30% for the same instance. A similar trend is found in the moment calculations and for all boom configurations. CFD showed promising results, with results coming within 10% for selected values. CFD offered interesting insights in how fluid flows along the crane surface, showing that the shielding effect is underestimated in all standards evaluated. From this research, it is proposed to adapt the shielding coefficients as put forward in DIN1055 for horizontal elements.**

***Index Terms*—Ship-to-shore cranes, wind actions, CFD, EN13001-2.**

I. Introduction

WIND loads on STS-cranes have become an ever increasing problem. Modern cranes top out at over 90m, and in excess of 150m with the boom in the raised position. This makes cranes fall into the ”high-rise structures” category. Cranes of this type are typically placed in coastal regions, where wind exposure is highest. Consequently, cranes can be exposed so severe storms which results in high wind loads acting on the crane. Both static and dynamic wind loads are important design considerations when designing and constructing a crane [6]. Even today, relatively simple standards are used when calculating the wind load on STS cranes, in lieu of wind tunnel testing. Wind tunnel testing is the preferred method for calculating wind actions on STS cranes since complex flow features are accounted for by the very concept of the test, flow features which are not covered in standard calculations. However, wind tunnel testing can be both time consuming and expensive, and therefore their use is limited. Standard calculations can be performed in a fraction of both the cost and time, and are therefore preferred. However, standard calculations are much more elementary and typically are conservative with the wind loads. This results in higher calculated wind loads in comparison to wind tunnel tests. With recent cranes growing taller, a need has risen to close this gap between standard calculations and wind tunnel tests.

In this study, wind tunnel tests and computational fluid dynamics are used to get new insights in the behaviour of flow around the crane structure. These insights will help to investigate the cause of the gap between standard calculations and wind tunnel tests. For this study, a $\frac{1}{150}$ scale model of a typical STS container crane was placed in a wind tunnel and the response was measured for different wind angles and configurations. This data was used to validate the existence of a gap between standards and wind tunnel measurements, and was subsequently used as validation for the computational fluid dynamics. Computational fluid dynamics were then used to visualise and study the flow around the crane to get new insights in the behaviour of wind flowing past a crane structure.

This study concludes with a proposed adjustment to the existing EN13001-2 standard for calculating wind loads, to get a more accurate result when calculating wind loads.

II. Wind tunnel testing

The wind tunnel test conducted in this study was used to examine the aerodynamic behaviour of a STS crane as well as serve as validation data for the computational fluid dynamics.

A. Wind tunnel testing setup

Wind tunnel testing was performed in the Open Jet Facility of the Delft University of Technology. A $\frac{1}{150}$ scale model was placed upon a 6-component external balance, which was then placed upon a turntable with a ±45 degree range of motion. Simulating a flat surrounding area, a table was prepared with a hole through which the model was placed.

The whole setup was placed on a height-adjustable platform which was placed in the opening of the wind tunnel. The height was adjusted so the boundary layer coming from the wind tunnel opening was cut off and a (near) uniform wind profile was applied to the crane model, with only a small boundary layer forming on the table top. The setup can be seen in figure 2. To eliminate bias from the measurement setup, runs were done without the model in place which measured the bias introduced by the measurement setup. This bias was removed from the measurements.

Measurements from the external balance were converted to a global right-handed coordinate system with the x-axis aligned towards the air flow and the z-axis aligned upwards. Measurements were also adjusted for the offset in centre of measurements to place this at the centre of the crane model. This was consolidated in a single transformation matrix in

$$\begin{bmatrix} F_{x,g} \\ F_{y,g} \\ F_{z,g} \\ M_{x,g} \\ M_{y,g} \\ M_{z,g} \end{bmatrix} = \begin{bmatrix} \cos\theta & \sin\theta & 0 & 0 & 0 & 0 \\ \sin\theta & -\cos\theta & 0 & 0 & 0 & 0 \\ 0 & 0 & -1 & 0 & 0 & 0 \\ -h_{offset}\cos\theta & h_{offset}\sin\theta & 0 & \cos\theta & \sin\theta & 0 \\ -h_{offset}\sin\theta & -h_{offset}\cos\theta & 0 & \sin\theta & -\cos\theta & 0 \\ 0 & 0 & 0 & 0 & 0 & -1 \end{bmatrix} \begin{bmatrix} F_{x,bl} \\ F_{y,bl} \\ F_{z,bl} \\ M_{x,bl} \\ M_{y,bl} \\ M_{z,bl} \end{bmatrix} \quad (1)$$

equation 1. Subsequently, measurements were transformed to the crane local coordinate system, as shown in figure 1 by use of the transformation matrix found in equation 2.

$$\begin{bmatrix} F_{x,cl} \\ F_{y,cl} \\ F_{z,cl} \\ M_{x,cl} \\ M_{y,cl} \\ M_{z,cl} \end{bmatrix} = \begin{bmatrix} \cos\theta & -\sin\theta & 0 & 0 & 0 & 0 \\ \sin\theta & \cos\theta & 0 & 0 & 0 & 0 \\ 0 & 0 & 1 & 0 & 0 & 0 \\ 0 & 0 & 0 & \cos\theta & -\sin\theta & 0 \\ 0 & 0 & 0 & \sin\theta & \cos\theta & 0 \\ 0 & 0 & 0 & 0 & 0 & 1 \end{bmatrix} \begin{bmatrix} F_{x,g} \\ F_{y,g} \\ F_{z,g} \\ M_{x,g} \\ M_{y,g} \\ M_{z,g} \end{bmatrix} \quad (2)$$

Initially a test run was performed in four different configurations at various speed to check the dependence of the drag on the Reynolds number. Based on this test, a air velocity of $21ms^{-1}$ was decided upon. It is to be noted that this yields Reynolds number in the order of magnitude of $1E3$ to $1E5$, which is 2 orders of magnitude smaller than the Reynolds numbers typically encountered on a full scale crane. The effect thereof is that drag coefficients of cylindrical objects will be typically higher. This is deemed as inconsequential for this study since as the CFD study was conducted under identical boundary conditions and no specific investigation is made into the drag coefficients on specific elements.

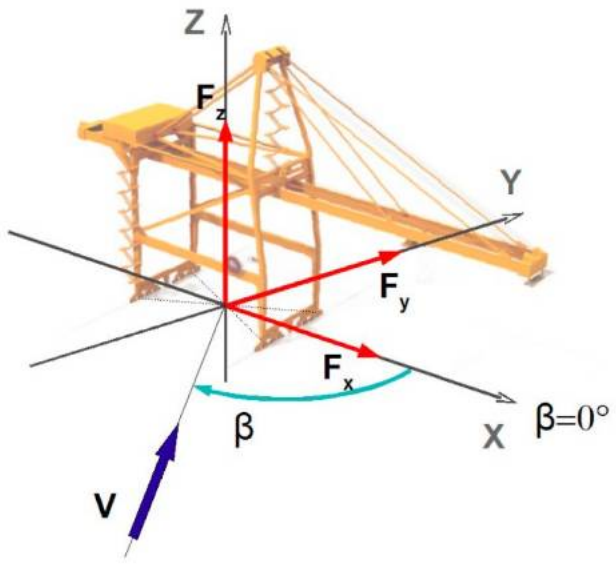

Fig. 1: Crane local coordinate system; Forces and moments

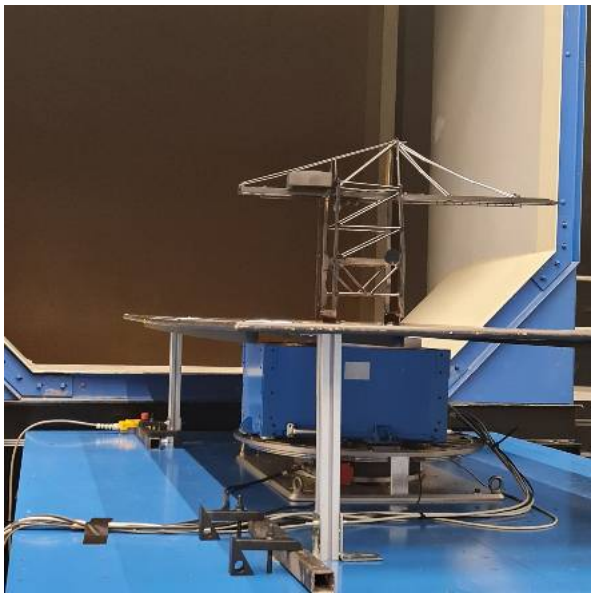

Fig. 2: Wind tunnel setup

B. Wind tunnel results

Wind tunnel results are presented as force and moment coefficients, as detailed in equation 3. The reference area A is taken as $\frac{1000}{150^2}$ and the reference length l as $\frac{80}{150}$.

$$CF_i = \frac{F_i}{q_{ref}A} \quad CM_i = \frac{M_i}{q_{ref}Al} \qquad \text{for} \qquad i = x, y, z \quad (3)$$

Results from the wind tunnel test are presented as 2 figures. Figure 3a shows the force coefficients for the x, y, and z axes. Figure 3b shows the moment coefficient about the x, y, and z axes. What is noted is that the force response in x direction and corresponding moment about the y axis show a highly dependent relationship to the wind angle. This M-shaped response is characteristic for STS cranes of this construction type [7]. It is seen that cranes experience their largest wind loads at 20-40° from the perpendicular wind angles. For this reason, results are presented for wind at right angles and the maximum values found in the wind tunnel. The difference between these values is found in table I.

When the crane is rotated through the wind, vertical members move in and out of each others wake, as is evident from the projected area. When studying the wind tunnel results, it was found that there is an apparent correlation between projected area of the crane and the horizontal force acting upon the crane. This correlation is shown in figure 4. Horizontal members stay in line with each other. This becomes evident

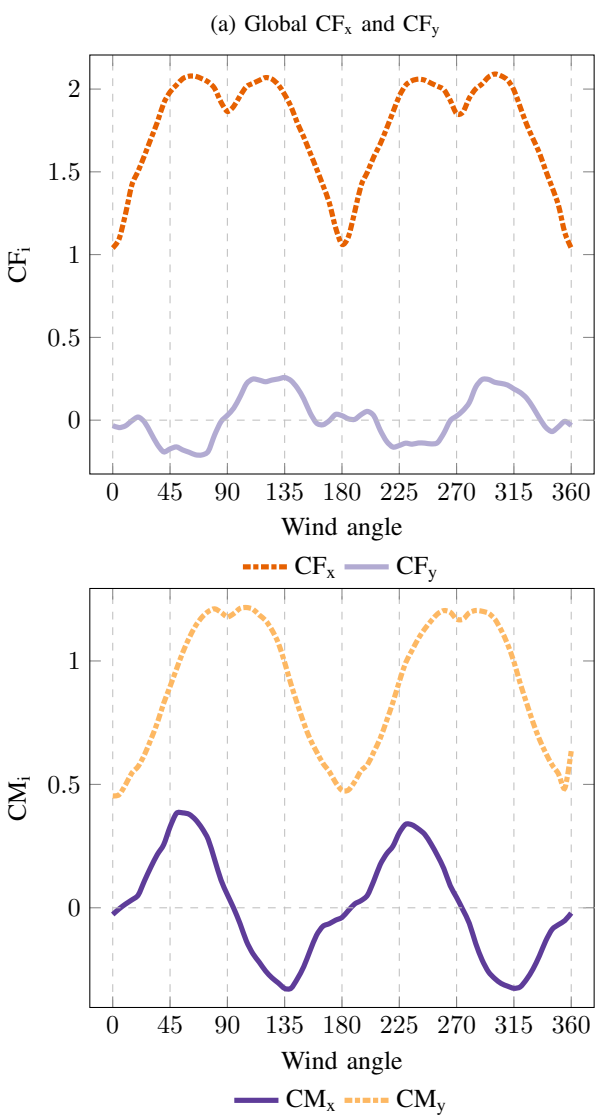

Fig. 3: Global force coefficients from wind tunnel measurements.

		Wind tunnel right angle	Wind tunnel maximum	% diff
Boom down	**Fx**	13.01	17.86	37%
	Fy	22.85	24.77	8%
	My	3.11	3.64	17%
	Mx	7.70	8.04	4%
Boom up	**Fx**	16.44	21.16	29%
	Fy	22.83	26.04	14%
	My	5.50	6.11	11%
	Mx	7.79	9.15	18%
Boom intermediate	**Fx**	14.73	19.76	34%
	Fy	22.48	25.89	15%
	My	4.59	5.32	16%
	Mx	8.23	9.30	13%

TABLE I: Wind tunnel measurements: Right angle and maximum values.

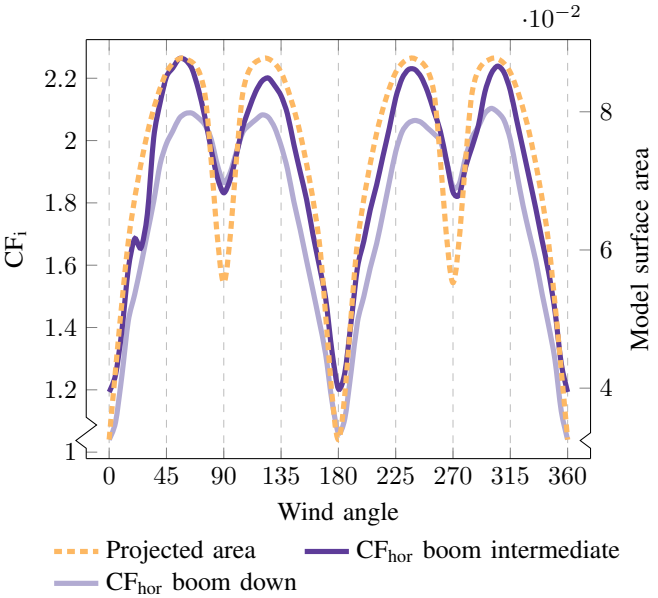

Fig. 4: Correlation between force and projected surface area

when looking at the model and evaluating the horizontal force response in the boom down and boom up situations in figure 4.

III. Standard calculation

Wind loads on the crane scale model were calculated with EN13001-2. This standard is specifically designed for the calculation of wind actions on cranes. Whilst this standard is not designed for use on scale models, it suffices in providing coefficients and methods for calculation of wind loads.

The standard typically uses a wind velocity profile which simulates an atmospheric boundary layer, for this study however a uniform velocity profile was chosen. Whilst this deviates from the standard, it does allow proper comparison between the standard calculations and the wind tunnel test. The results of the standard calculation will be presented in section III-A, along with the results from the wind tunnel test.

A. Wind tunnel compared to EN13001-2

The wind tunnel measurements are converted back from coefficients to forces for comparison sake, which is done for a standard dynamic pressure which is also used for the standard calculation. This method removes the influence of local atmospheric conditions during the wind tunnel tests. It is important that these conditions are adjusted for since it was measured that dynamic pressure in the wind tunnel could fluctuate with up to 5%.

Table II compares the wind tunnel measurements at the right angles with the standard calculations according to EN13001-2. From the table it is clear that the standard calculations overestimate the wind loads on the crane in all cases. Table III compares the maximum forces found in the wind tunnel to the EN13001-2. Whilst the differences with respect to the maximum wind load are smaller than those to the right angle, they are still significant.

		Wind tunnel right angle	EN13001-2	diff
Boom down	**Fx**	13.01	23.25	79%
	Fy	22.85	32.17	41%
	My	3.11	6.48	108%
	Mx	7.70	10.96	42%
Boom up	**Fx**	16.44	27.40	67%
	Fy	22.83	32.30	41%
	My	5.50	9.76	77%
	Mx	7.79	12.46	60%
Boom intermediate	**Fx**	14.73	26.11	77%
	Fy	22.48	32.30	44%
	My	4.59	8.45	84%
	Mx	8.23	12.06	47%

TABLE II: Comparison: Wind tunnel right angle and EN13001-2

		Wind tunnel maximum	EN13001-2	diff
Boom down	**Fx**	17.86	23.25	30%
	Fy	24.77	32.17	30%
	My	3.64	6.48	78%
	Mx	8.04	10.96	36%
Boom up	**Fx**	21.16	27.40	30%
	Fy	26.04	32.30	24%
	My	6.11	9.76	60%
	Mx	9.15	12.46	36%
Boom intermediate	**Fx**	19.76	26.11	32%
	Fy	25.89	32.30	25%
	My	5.32	8.45	59%
	Mx	9.30	12.06	30%

TABLE III: Comparison: Wind tunnel maximum and EN13001-2

IV. Computational fluid dynamics

Computational fluid dynamics is widely used in other industries [8], but relatively unused in the heavy crane industry [1, 2, 4, 5]. CFD can be an incredibly useful tool allowing for insights not previously obtainable through wind tunnel tests. CFD allows for visualisation of the flow around the crane structure, surface pressures, streamlines, per part force reports, and more. A CFD case was made to investigate the difference found between standard calculations and wind tunnel measurements. For this case, the geometry was created as digital twin of the wind tunnel. Boundary conditions were chosen equal to those of the wind tunnel. The flow domain, in figure 5 is a rectangular box with corners [-2.5, -1.0, 0.0] and [1.0, 1.0, 1.0], and the crane model placed at [0.0, 0.0, 0.0], which was believed to be sufficiently spacious to settle inflow effects, limit the blockage effects, and fully develop flow features in the wake area. Due to the computationally expensive nature, only the 0°, 60°, and 90°angles were investigated for the boom down configuration.

With the findings of section II-B, it was decided to evaluate the drag coefficient of two horizontal members, the boom and bridge girder, and two vertical members, the lower frame and A-frame members. Their reported drag coefficients for 3 wind angles are presented in table IV. Negative drag coefficients indicate that a negative pressure is exerted on the element.

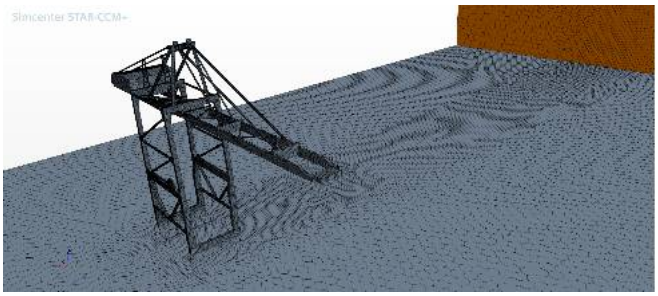

Fig. 5: CFD mesh setup

	0° wind angle	60° wind angle	90° wind angle
Boom girder SB	0.644	1.148	1.478
Boom girder PS	0.647	0.111	-0.173
Bridge girder SB	0.454	0.909	1.187
Bridge girder PS	0.458	0.120	-0.110
A-frame SB	0.902	0.949	0.946
A-frame PS	0.887	0.930	0.624
Lower frame SB	2.196	1.266	1.416
Lower frame PS	2.245	1.039	0.496

TABLE IV: Drag coefficient per part for selected vertical and horizontal members.

From flow analysis it was shown that a eddy forms between the boom elements with a negative static pressure leading to a net negative force enacted upon the member. Based on the forces presented in table IV it can be seen that the horizontal elements (i.e. the girder elements) which experience shielding effects at a wind angle of 90°, still experience significant shielding effects at 60°. Conversely, the vertical (i.e. the frame elements) which experience shielding at 90°wind angle do not experience shielding at 60°. What can also be gathered from these results is that the shielding coefficients applied to the girder according to EN13001-2, $\eta = 0.45$ & $\eta = 0.31$ for the bridge and boom girder respectively is very conservative. From the values calculated in CFD, shielding coefficients of $\eta = 0.097$ & $\eta = 0.132$ at 60° and $\eta = 0.000$ & $\eta = 0.000$ at 90°for the bridge and boom girder respectively would be accurate.

Looking at the surface pressure in figures 6a,6b, and 6c this shielding effect is clearly visible showing lower pressure on leeward elements as opposed to the windward elements. Additionally, we can look at the velocity field in figures 6d and 6e. The velocity field shows the wake effect coming from the windward elements, shielding the leeward elements. What is also noticeable is that the air velocity not only slows down around the structure, but increase in local air velocity is also found. This shows that the influence elements have on local flow conditions and the interaction between elements is more complex than portrayed by not only the EN13001-2, but also other standards [6, 7]. For this research, influence of members on local flow conditions and interaction with elementsnot in line, will not be evaluated.

Whilst the use of computational fluid dynamics has been limited in this study, it brings exciting new possibilities to the field of STS crane aerodynamics and it is highly suggested that this path is to be further pursued.

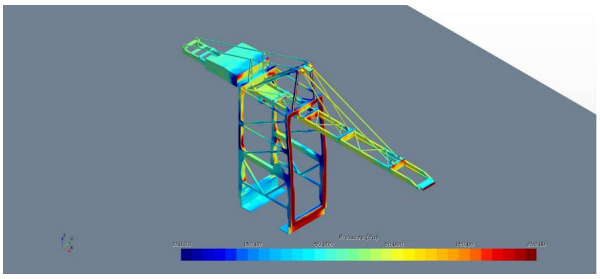

(a) Surface pressures at 0°wind angle

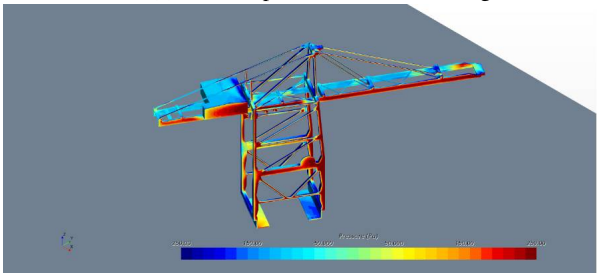

(b) Surface pressures at 60°wind angle

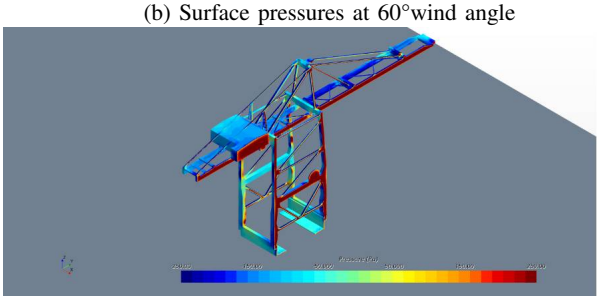

(c) Surface pressures at 90°wind angle

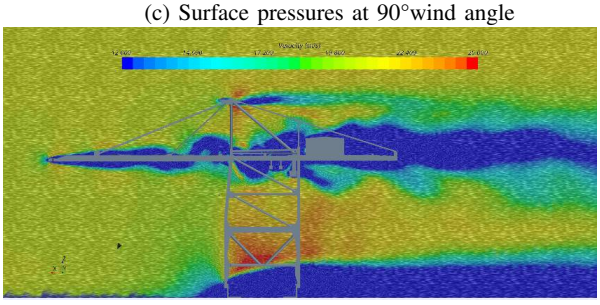

(d) Air velocities around the crane at 0°wind angle

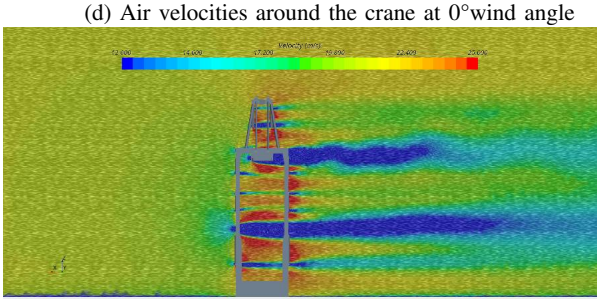

(e) Air velocities around the crane at 60°wind angle

Fig. 6: Visualisations of computational fluid dynamics results

V. Adaptation of EN13001-2

It was noted in section III that the EN13001-2 overestimates the wind load on an STS crane for all wind angles. Further investigation using computational fluid dynamics found that the shielding effect of horizontal element is underestimated in the standard. It further found that this holds true for non-cardinal wind angles. For this reason, it is suggested that more extensive shielding coefficients are to be used for horizontal elements in line, when calculating wind loads on an STS crane.

It was found that the DIN1055 [3], a German industry standard from 1986, bears many similarities to the EN13001-2 standard [7]. The manner in which the wind load is calculated specifically is very comparable to that of the EN13001-2. One area in which these two standards differ significantly is the shielding coefficients used. The DIN1055 uses a more extensive shielding coefficient chart, as seen in figure 7a when compared to the EN13001-2 shielding coefficient chart, as seen in figure 7. Therefore it is proposed that the shielding coefficients of the DIN1055 are used on horizontal elements in the crane construction, when calculating wind loads on STS cranes with the EN13001-2 standard.

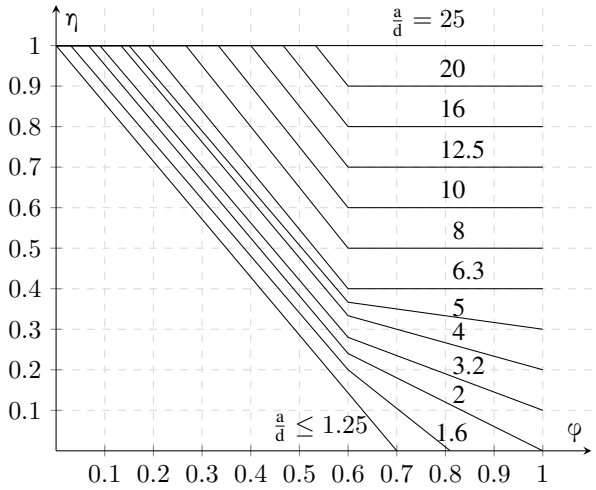

(a) Shielding coefficients according to DIN1055

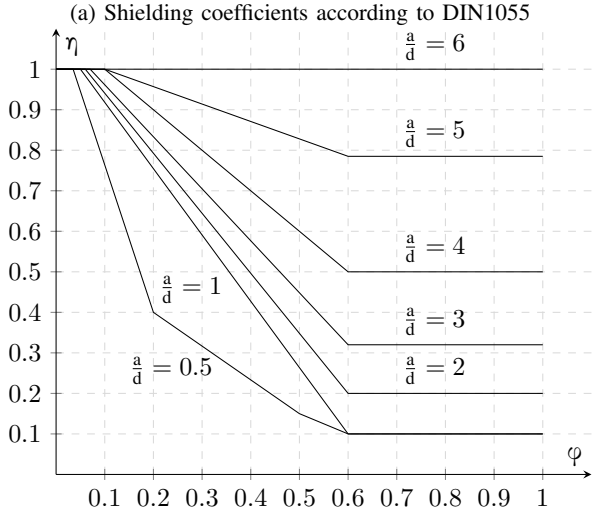

(b) Shielding coefficients according to EN13001-2

Fig. 7: Graphs with shielding coefficients

	EN13001-2	EN13001-2 adapted	% reduction
Fx	23.30	21.90	6%
Fy	32.20	29.30	9%
My	6.50	6.20	5%
Mx	11.00	10.00	9%

TABLE V: EN13001-2 vs EN13001-2 with adapted shielding coefficients

	Wind tunnel Maximum	EN13001-2 adapted	% diff
Fx	17.89	21.90	22%
Fy	24.77	29.30	18%
My	3.63	6.20	71%
Mx	8.04	10.00	24%

TABLE VI: Comparison: Wind tunnel maximum and adapted EN13001-2

Applying this adaptation and calculating the new wind loads is done and the results are presented in table V. The biggest reduction is found in the crane y direction. This is unsurprising as the boom and bridge girder are horizontal surfaces in close proximity to each other. It is seen that the wind load calculated is lowered, but still conservative when compared to the maximum values found in the wind tunnel test in table VI. Whilst the improvement is welcomed it also shows that the shielding effect is not the only effect responsible for this discrepancy.

VI. Conclusion

Through the use of wind tunnel testing combined with computational fluid dynamics multiple causes for the overestimation of wind loads through the use of standard calculations have been identified. One of these causes is believed to be the incomplete method by which shielding effects are calculated for members in line. Based on these findings, an adaption on the calculation method for calculating wind loads on STS cranes according to the EN13001-2, based on the DIN1055 has been proposed.

The new proposed method resulted in 5% to 9% lower wind loads calculated according to the standard, which makes the calculations more accurate when compared to wind tunnel testing on the same crane model.

References

[1] Soon-Kyu Kwon et al. “Flow Analysis of a Container Craine using Computation Fluid Dynamics”. In: *Korean Society of Navigation and Port Society*. Vol. 30. Spring conference. Dong-A University - Divison of Mechanical Engineering. June 2006, pp. 349–354.

[2] Soon-Kyu Kwon et al. “Wind Load Analysis of a Container Crane using the Computation Fluid Dynamics according to the change of the Boom Shape”. In: *Fall Conference of the Korean Society of Precision Engineering*. Dong-A University - Divison of Mechanical Engineering. Oct. 2006.

[3] Deutsches Institut für Normung. *DIN 1055 - part 4: Design loads for buildings - Imposed loads: Wind loads on structures unsusceptible to vibration*. Aug. 1986.

[4] Brian P. Hand. “An analysis into wind induced loading effects on a STS crane and investigation into design optimisation”. In: Dec. 2018.

[5] Teemu Kokkonen. “A computational fluid dynamics analysis of ship-to-shore crane wind coefficients”. English. Master’s thesis. Aalto University. School of Engineering, 2021, pp. 56 + 12. URL: http://urn.fi/URN:NBN:fi:aalto-202109129117.

[6] S.P. Oostlander. *Wind load on a crane*. 2012. URL: http://resolver.tudelft.nl/uuid:1bd28ce9-f115-493b-8493-bf3226aa114b.

[7] T.L.A. (Tycho) Rasch. “Wind loading of STS cranes; A deeper investigation into the aerodynamic characteristics of STS cranes”. English. Master’s thesis. Delft University of Technology, 2022, pp. 77 + 30.

[8] Jiyuan Tu, Guan-Heng Yeoh, and Chaoqun Liu. “Chapter 8 - Some Applications of CFD With Examples”. In: *Computational Fluid Dynamics (Third Edition)*. Ed. by Jiyuan Tu, Guan-Heng Yeoh, and Chaoqun Liu. Third Edition. Butterworth-Heinemann, 2018, pp. 291–367. ISBN: 978-0-08-101127-0. DOI: https://doi.org/10.1016/B978-0-08-101127-0.00008-8. URL: https://www.sciencedirect.com/science/article/pii/B9780081011270000088.

B

Crane model

Figure B.1: 3D crane geometry

(a) Detail of the apex beam digital model. Note the simplified geometry compared to the wind tunnel model.

(b) Detail of the apex beam wind tunnel model

Figure B.2: Details of the apex beam

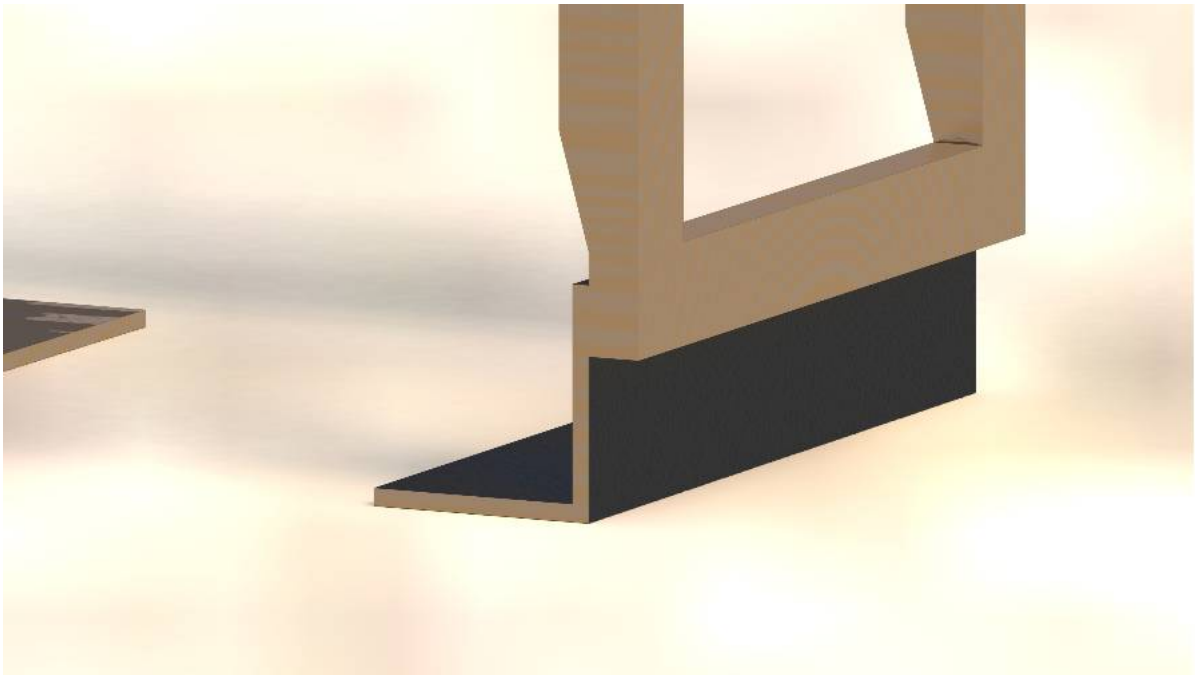

(a) Detail of the bogey digital model. Note the absence of the nuts and bolts connecting the aluminium profiles to the wooden frame.

(b) Detail of the bogey wind tunnel model

Figure B.3: Details of the bogey

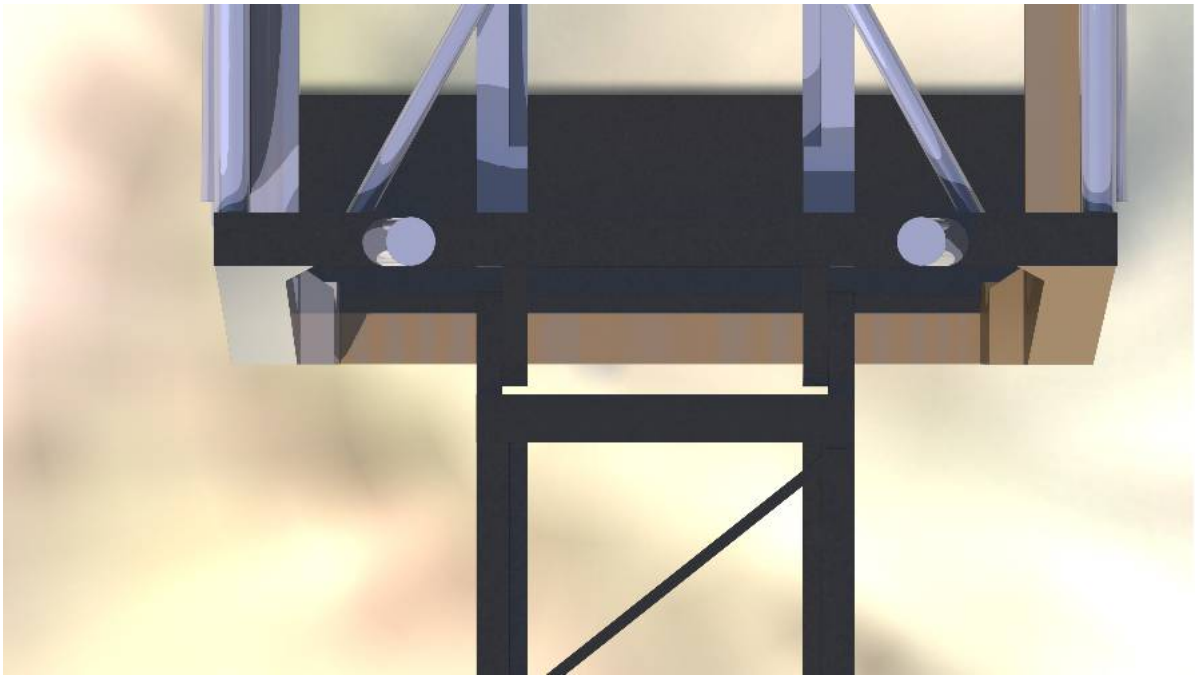

(a) Detail of the boom hinge digital model. Not the simplified geometry compared to the wind tunnel model, the absence of nuts and bolts.

(b) Detail of the boom hinge wind tunnel model

Figure B.4: Details of the boom hinge

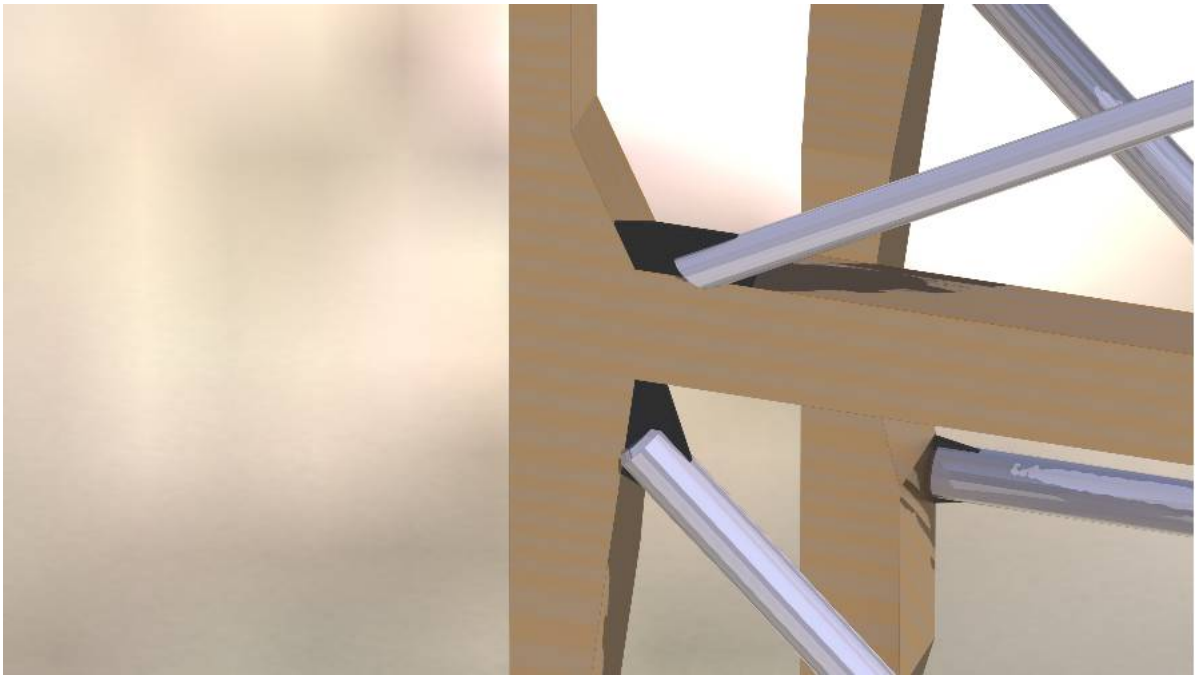

(a) Detail of the bracing digital model. Note how the geometry is simplified and incorporated into the frame to reduce edges in the geometry.

(b) Detail of the bracing wind tunnel model

Figure B.5: Details of the bracing

(a) Detail of the forestay digital model. Note how the hinges are taken out of the forestay in the digital model and the forestay is modelled as perfect rods.

(b) Detail of the forestay wind tunnel model

Figure B.6: Details of the forestay

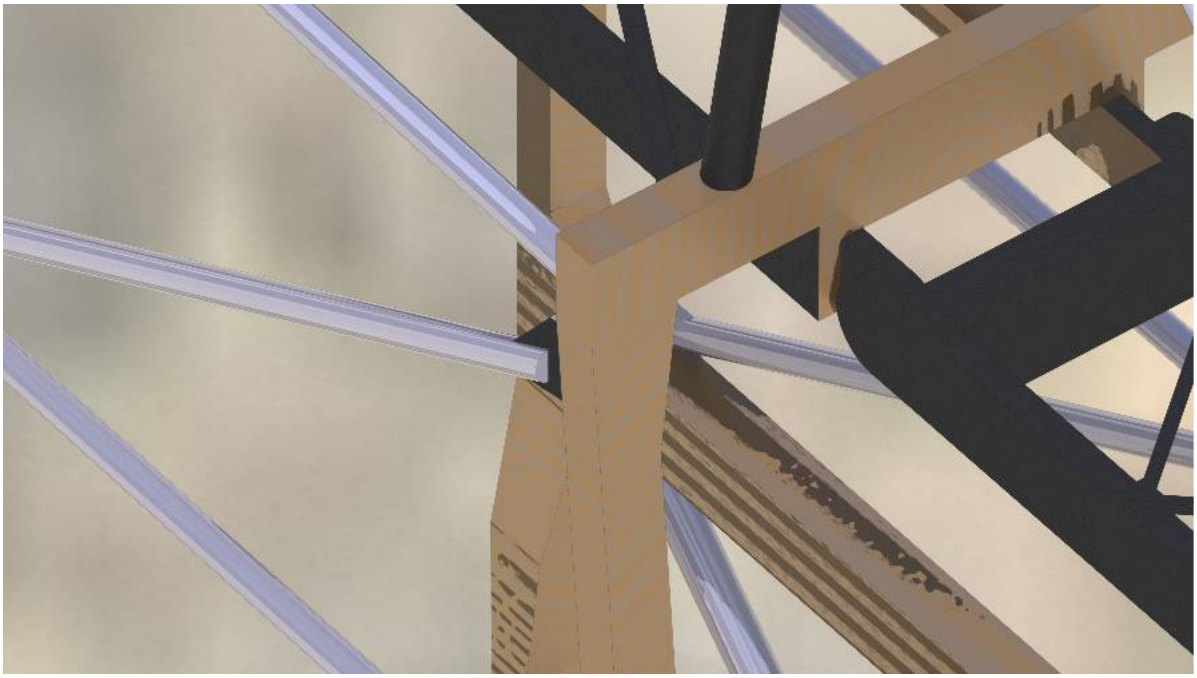

(a) Detail of the portal beam digital model. Note how the geometry is absent of screws and gaps, present in the wind tunnel model.

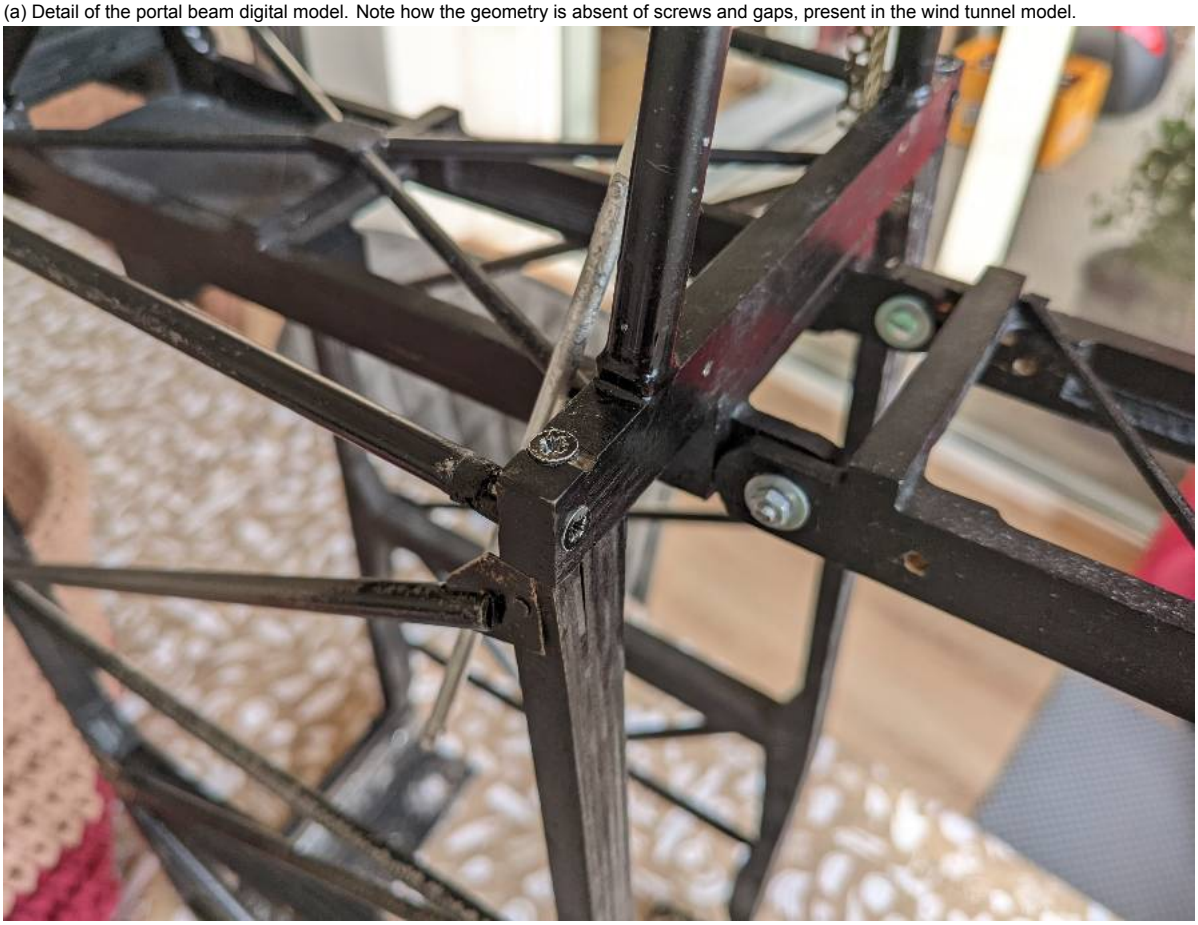

(b) Detail of the portal beam wind tunnel model

Figure B.7: Detail of the portal beam wind tunnel model

C

Simulation software and hardware

Hardware used:

- **AMD Ryzen 9 5900X 12-Core Processor** - CPU
- **Gigabyte B550 AORUS ELITE V2** - Motherboard
- **Crucial Ballistix 32GB DDR4 3800MHz CL16** - RAM (overclocked)

Software used for 3D CAD

- **SOLIDWORKS 2021**

Software used for CFD:

- **Ubuntu 21.10** - Operating system
- **Xanmod 5.17** - Kernel
- **Simcenter STAR-CCM+ v2020.3.1** - Computational fluid dynamics suite

Simulations were run under linux as tests showed significant (10% to 20%) improvement in calculation times. A custom kernel was run as it included upgrades to the memory management which also sped up calculations.

Bibliography

[1] Yousef Abu-Zidan, Priyan Mendis, and Tharaka Gunawardena. “Optimising the computational domain size in CFD simulations of tall buildings”. In: *Heliyon* 7.4 (2021), e06723. ISSN: 2405-8440. DOI: https://doi.org/10.1016/j.heliyon.2021.e06723. URL: https://www.sciencedirect.com/science/article/pii/S2405844021008264.

[2] Seong-Wook Lee et al. “Wind Load ANalysis of Container Crane Using Experimental and Analytical Methods”. In: *Fall Conference of the Korean Society of Navigation and Port Society*. Dec. 2006.

[3] Soon-Kyu Kwon et al. “Flow Analysis of a Container Craine using Computation Fluid Dynamics”. In: *Korean Society of Navigation and Port Society*. Vol. 30. Spring conference. Dong-A University - Divison of Mechanical Engineering. June 2006, pp. 349–354.

[4] Soon-Kyu Kwon et al. “Wind Load Analysis of a Container Crane using the Computation Fluid Dynamics according to the change of the Boom Shape”. In: *Fall Conference of the Korean Society of Precision Engineering*. Dong-A University - Divison of Mechanical Engineering. Oct. 2006.

[5] H.J. Alons. *OJF External Balance Documentation*. Documentation NLR-CR-2008-695. Nationaal Lucht- en Ruimtevaartlaboratorium, 2008.

[6] J.D. Anderson. *Fundamentals of Aerodynamics*. McGraw-Hill Education, 2016. ISBN: 9781259129919. URL: https://books.google.de/books?id=D1ZojgEACAAJ.

[7] Elsayed Aziz, Sven Esche, and C. Chassapis. “Online Wind Tunnel Laboratory”. In: June 2008. DOI: 10.18260/1-2--3402.

[8] Alex Mendonça Bimbato and Miguel Hiroo Hirata. “Numerical Investigation of the Drag Crisis in Flow Past a Rough Circular Cylinder”. In: 2013.

[9] Bert Blocken. “Computational Fluid Dynamics for urban physics: Importance, scales, possibilities, limitations and ten tips and tricks towards accurate and reliable simulations”. In: *Building and Environment* 91 (2015). Fifty Year Anniversary for Building and Environment, pp. 219–245. ISSN: 0360-1323. DOI: https://doi.org/10.1016/j.buildenv.2015.02.015. URL: https://www.sciencedirect.com/science/article/pii/S0360132315000724.

[10] Wouter van den Bos. *Wind loading on crane structures*. Tech. rep. Delft University of Technology - Faculty of Mechanical, Materials, Maritime Engineering; Transport Engineering, and Logistics Section, 2002.

[11] Dave Campo. *Application Guide: Wind Tunnel Testing*. 2010. URL: https://www.stratasys.com/-/media/files/education-f123/zips/wind-tunnel.pdf?la=en%5C&hash=24164CD63D57D714419987820602968D703D9F10.

[12] Brian J. Cudahy. “The containership revolution”. In: *TR News - THE INTERMODAL CONTAINER ERA: HISTORY, SECURITY, AND TRENDS, (246), pp.5-7.* 246 (Sept. 2006), pp. 5–9.

[13] TU Delft. *TU Delft Aerospace Engineering: The Open Jet Facility*. Print. Information booklet on the Open Jet Facility of the Delft University of Technology. Kluyverweg 1, 2628 HS Delft, the Netherlands.

[14] Deutsches Institut für Normung. *DIN 1055 - part 4: Design loads for buildings - Imposed loads: Wind loads on structures unsusceptible to vibration*. Aug. 1986.

[15] Sofialidis Dimitrios. *Lecture 2 Boundary Conditions & Solver Settings*. Sept. 2013. URL: https://events.prace-ri.eu/event/156/contributions/6/attachments/65/89/Fluent-Intro_14.5_L02_BoundaryConditionsSolverSettings.pdf.

[16] Sjoerd Engels. “Translation Wind Tunnel Test”. Internal document for Kalmar Netherlands use; unpublished. Dec. 2016.

[17] FEDERATION EUROPEENNE DE LA MANUTENTION. *F.E.M. 1.004: RECOMMENDATION FOR THE CALCULATION OF WIND LOADS ON CRANE STRUCTURES*. July 2000.

[18] Jörg Franke et al. “Best practice guideline for the CFD simulation of flows in the urban environment - a summary”. In: *11th Conference on Harmonisation within Atmospheric Dispersion Modelling for Regulatory Purposes, Cambridge, UK, July 2007*. Cambridge Environmental Research Consultants. 2007.

[19] H. van Ham, J.C. van Ham, and J. Rijsenbrij. *Development of Containerization: Success Through Vision, Drive and Technology*. IOS Press, 2012. ISBN: 9781614991465. URL: https://books.google.com/books?id=CgQmkTczzPwC.

[20] Brian P. Hand. “An analysis into wind induced loading effects on a STS crane and investigation into design optimisation”. In: Dec. 2018.

[21] *Hellenic Shipping News: Weekly Market Report Week 21 2021*. 2022. URL: https://www.hellenicshippingnews.com/wp-content/uploads/2021/05/WEEKLY-MARKET-REPORT-WK21.pdf.

[22] Walter de Jong. “Results wind tunnel”. Internal document for Kalmar Netherlands use; unpublished. Sept. 2013.

[23] Jong-Hoon Kang and Sang-Joon Lee. “Experimental study of wind load on a container crane located in a uniform flow and atmospheric boundary layers”. In: *Engineering Structures* 30.7 (2008), pp. 1913–1921. ISSN: 0141-0296. DOI: https://doi.org/10.1016/j.engstruct.2007.12.013. URL: https://www.sciencedirect.com/science/article/pii/S0141029607004920.

[24] Teemu Kokkonen. “A computational fluid dynamics analysis of ship-to-shore crane wind coefficients”. English. Master’s thesis. Aalto University. School of Engineering, 2021, pp. 56 + 12. URL: http://urn.fi/URN:NBN:fi:aalto-202109129117.

[25] Alberto Lago, Dario Trabucco, and Antony Wood. “Chapter 2 - Introduction”. In: *Damping Technologies for Tall Buildings*. Ed. by Alberto Lago, Dario Trabucco, and Antony Wood. Butterworth-Heinemann, 2019, pp. 7–37. ISBN: 978-0-12-815963-7. DOI: https://doi.org/10.1016/B978-0-12-815963-7.00002-6. URL: https://www.sciencedirect.com/science/article/pii/B9780128159637000026.

[26] Marc Levinson. *The Box: How the Shipping Container Made the World Smaller and the World Economy Bigger, Second Edition with a new chapter by the author*. Second with a new chapter by the author. Princeton University Press, 2016. ISBN: 9780691170817. URL: libgen.li/file.php?md5=f6fcc1a8fa61edc1941d138800c65e44.

[27] Comité Européen de Normalisation. *NEN-EN 13001-2:2021; Crane safety - General design - Part 2: Load actions*. Mar. 2021.

[28] T. Notteboom, A. Pallis, and J.P. Rodrigue. *Port Economics, Management and Policy*. Taylor & Francis, 2022. ISBN: 9781000526936. URL: https://books.google.com/books?id=o0dWEAAAQBAJ.

[29] S.P. Oostlander. *Wind load on a crane*. 2012. URL: http://resolver.tudelft.nl/uuid:1bd28ce9-f115-493b-8493-bf3226aa114b.

[30] Ronald L. Panton(auth.) *Incompressible Flow, Fourth Edition*. 4th ed. Wiley, 2013. ISBN: 9781118013434.

[31] Adam K. Prokopowicz and Jan Berg-Andreassen. “An Evaluation of Current Trends in Container Shipping Industry, Very Large Container Ships (VLCSs), and Port Capacities to Accommodate TTIP Increased Trade”. In: *Transportation Research Procedia* 14 (2016). Transport Research Arena TRA2016, pp. 2910–2919. ISSN: 2352-1465. DOI: https://doi.org/10.1016/j.trpro.2016.05.409. URL: https://www.sciencedirect.com/science/article/pii/S235214651630415X.

[32] Simon Prud’homme, Frederic Legeron, and Sébastien Langlois. “Calculation of wind forces on lattice structures made of round bars by a local approach”. In: *Engineering Structures* 156 (2018), pp. 548–555. ISSN: 0141-0296. DOI: https://doi.org/10.1016/j.engstruct.2017.11.065. URL: https://www.sciencedirect.com/science/article/pii/S0141029617337896.

[33] G Rankine et al. “COFASTRANS (Container Vessel Fast Transhipment System)”. In: 2018.

[34] Jean-Paul Rodrigue. *The Geography of Transport Systems*. Routledge, May 2020. DOI: 10.4324/9780429346323. URL: https://doi.org/10.4324/9780429346323.

[35] Siemens Digital Industries Software. *Simcenter STAR-CCM+ User Guide v.2021.1*. Version 2021.1. 2021.

[36] European Committee for Standardization. *Eurocode 1: Actions on structures , Part 1-3 General actions - Wind actions*. 2005.

[37] Tushar Surwase and D.R.Vaidya. “Study of effect of Surface Roughness on drag.” In: Apr. 2015.

[38] Yoshihide Tominaga et al. “AIJ guidelines for practical applications of CFD to pedestrian wind environment around buildings”. In: *Journal of Wind Engineering and Industrial Aerodynamics* 96.10 (2008). 4th International Symposium on Computational Wind Engineering (CWE2006), pp. 1749–1761. ISSN: 0167-6105. DOI: https://doi.org/10.1016/j.jweia.2008.02.058. URL: https://www.sciencedirect.com/science/article/pii/S0167610508000445.

[39] Jiyuan Tu, Guan-Heng Yeoh, and Chaoqun Liu. “Chapter 1 - Introduction”. In: *Computational Fluid Dynamics (Third Edition)*. Ed. by Jiyuan Tu, Guan-Heng Yeoh, and Chaoqun Liu. Third Edition. Butterworth-Heinemann, 2018, pp. 1–31. ISBN: 978-0-08-101127-0. DOI: https://doi.org/10.1016/B978-0-08-101127-0.00001-5. URL: https://www.sciencedirect.com/science/article/pii/B9780081011270000015.

[40] Jiyuan Tu, Guan-Heng Yeoh, and Chaoqun Liu. “Chapter 8 - Some Applications of CFD With Examples”. In: *Computational Fluid Dynamics (Third Edition)*. Ed. by Jiyuan Tu, Guan-Heng Yeoh, and Chaoqun Liu. Third Edition. Butterworth-Heinemann, 2018, pp. 291–367. ISBN: 978-0-08-101127-0. DOI: https://doi.org/10.1016/B978-0-08-101127-0.00008-8. URL: https://www.sciencedirect.com/science/article/pii/B9780081011270000088.

[41] European research community on flow turbulence et al. *Best practice guidelines : version 1.0, january 2000*. English. [S.l.]: [s.n.], 2000.

[42] Wei Wang, Yong Cao, and Tsubasa Okaze. “Comparison of hexahedral, tetrahedral and polyhedral cells for reproducing the wind field around an isolated building by LES”. In: *Building and Environment* 195 (2021), p. 107717. ISSN: 0360-1323. DOI: https://doi.org/10.1016/j.buildenv.2021.107717. URL: https://www.sciencedirect.com/science/article/pii/S0360132321001281.

[43] E. Willemsen. “WIND TUNNEL TESTS FOR THE NELCON SHIP-TO-SHORE CONTAINER GANTRY CRANE”. Internal document for Nelcon (now Kalmar Netherlands) use; unpublished. Feb. 2002.

[44] O. Zikanov. *Essential Computational Fluid Dynamics*. Wiley, 2019. ISBN: 9781119474623. URL: https://books.google.nl/books?id=M7ijDwAAQBAJ.